UNCLASSIFIED

AD 161323

Armed Services Technical Information Agency

ARLINGTON HALL STATION
ARLINGTON 12 VIRGINIA
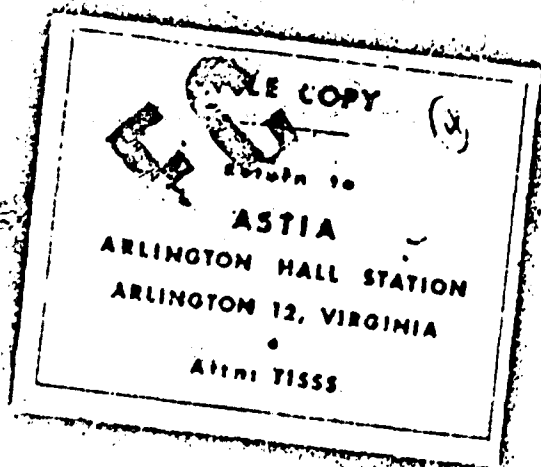
FOR
MICRO-CARD
CONTROL ONLY

1 OF 4

UNCLASSIFIED

DISCLAIMER NOTICE

THIS DOCUMENT IS BEST QUALITY
PRACTICABLE. THE COPY FURNISHED
TO DTIC CONTAINED A SIGNIFICANT
NUMBER OF PAGES WHICH DO NOT
REPRODUCE LEGIBLY.

9 April 1958
Job No. 7213

Department of the Navy
Office of Naval Research

Contract No. NONR-2292(00)
Task No. NR 094-343

AMF/TD No. 1196

A STUDY OF HIGH ENERGY LEVEL,

LOW POWER OUTPUT TURBINES

This Document Covers the Period
1 February 1957 through 31 December 1957

D. H. Silvern
Project Engineer

Dr. O. E. Balje
Principal Investigator

SUNDSTRAND TURBO

EFFECTIVE FEBRUARY 1ST, 1958, THE TURBO DIVISION OF THE
AMERICAN MACHINE AND FOUNDRY COMPANY WAS ACQUIRED BY
THE SUNDSTRAND MACHINE TOOL COMPANY. WE HAVE BEEN COM-
BINED WITH THE FORMER SUNDSTRAND-DEVER DIVISION. THE
TITLE OF THE NEW ORGANIZATION IS

THE SUNDSTRAND TURBO DIVISION

TABLE OF CONTENTS

AMF/TD No. 1196
Job No. 7213

9 April 1958
Page 2

TABLE OF CONTENTS (Cont)

1 INTRODUCTION

This report has been prepared in accordance with the requirements of ONR Contract NONR-2292(00) and contains a short discussion of the studies on low specific speed turbines performed up to December 1957. The investigations have been undertaken by the Advance Design Section of the Turbo Division of American Machine and Foundry Company with Dr. O. E. Balje acting as principal investigator, D. Silvern acting as project engineer, W. Nerenstein, H. Esten, and H. Gaveman as research engineers, and I. Friedman as mathematician.

The aim of this program was to appraise the potential of axial and terry turbines as well as drag turbines by investigating the maximum obtainable efficiency of these turbine types as function of significant design parameters and to obtain detailed design criteria for the optimum design, such as blade and channel geometries. This report, therefore, deals with the turbine performance at design point and in its present form makes no reference to the performance range and other criteria (stall torques, runaway speed) of the investigated turbine types.

The conclusions presented in this report are considered final for single stage axial turbines, but are of preliminary nature and subject to revisions for all other types due to the limited amount of experimental data, particularly on component performance, such as losses in terry buckets, influence of exhaust port configuration on performance of axial and terry turbines and influence of channel and blade geometry on drag coefficients for drag turbines.

This situation makes it evident that additional testing and analysis will be required before final conclusions on multi-staged, axial turbines, terry turbines and drag turbines can be presented.

II TECHNICAL SUMMARY

Convenient parameters for presenting performance criteria of turbines are the terms specific speed N_s and the specific diameter D_s. The significance of these parameters results from similarity considerations. Specific speed is a number which indicates the rotative speed and specific diameter is a number which indicates the rotor diameter for turbines which pass a certain amount of flow and expand a certain amount of head, i.e., develop a certain amount of power. The state of the art of designing turbo machinery can conveniently be indicated by showing lines of constant efficiency in a diagram with the coordinates specific speed and specific diameter. These parameters are, therefore, considered prime parameters. It is found that other frequently used design criteria such as pitch chord ratio, aspect ratio, and ratio of blade spacing to admitted arc are in this respect of secondary nature, meaning that optimum values of the above parameters become functions of specific speed and specific diameter.

The maximum obtainable efficiency for optimized design geometries is computed as a function of specific speed and specific diameter and is presented for all investigated turbine types in a single diagram, figure II.1. These data were partly confirmed by available test data as indicated by shadowed areas. The application of this diagram is self-explanatory when the definition of specific speed and specific diameter, as listed in figure II.1, is observed. After introducing the available head H_{ad} and the exhaust volume flow Q_3 as well as the desired rotative speed into term (I), the specific speed N_s is found. Figure II.1 then indicates the maximum obtainable efficiency for the different turbine types and the corresponding specific diameter D_s as function of N_s. Introducing the head H_{ad} and exhaust volume flow Q_3 into term II yields the required rotor diameter and term (III), the available output of the turbine. If the optimum specific diameter is too large, figure II.1 also indicates the efficiencies obtainable with smaller rotor diameters (smaller specific diameters). By multiplying the square of the rotor diameter with the factor A, listed in figure II.1 for the different turbine types, an approximate value for the overall turbine weight (rotor and casing and bearing cartridge) is found. These values have been found to give reasonable weight data, particularly for rotor diameters between 3 inches and 8 inches. Hence this diagram indicates the interrelationship between speed, efficiency rotor diameter, and turbine weight for the investigated turbine types, shows the performance characteristics in the proper perspective and clearly indicates the optimum performance regime of the different turbine designs. It reveals that axial turbines give highest efficiencies at almost all specific speeds, but require large specific diameters. For smaller specific

diameters the terry turbine becomes competitive efficiency-wise, whereas the drag turbine excels both turbine types when smaller specific diameters are desired for specific speeds below 6.

Figure II.1 also shows the optimum degrees of admission for terry and axial turbines and optimum ratio of rotor diameter to side channel depths for drag turbines as well as the optimum blade length for axial turbines, thus indicating further details of the design geometry.

The validity of this diagram is restricted to a narrow range of Reynolds numbers and blade numbers for axial and terry turbines, a narrow range of pressure ratios for drag turbines and certain values of the clearance s (expressed as clearance ratio s/D) between rotor and stator. These limiting values are listed in figure II.1 for the different turbine types together with some approximate relations for correcting the efficiency in cases where the desired design does not fall between these limits.

The conclusions, reached so far, are substantiated fairly well by test data for single stage, axial turbines. For terry turbines only incomplete test information is available, particularly test data on bucket losses. Drag turbine test data are severely lacking. The data shown for these turbine types are mainly extrapolated data, based on valid analytical arguments. These values have to be labeled "preliminary" and are subject to revision. This is particularly true for drag turbines, where the complete lack of data regarding the actual flow mechanism allows only the application of simplifying theories such as the "drag theory". Although this theory so far has been proven to allow fairly accurate predictions of performance characteristics and probably defines the main performance criteria reasonably well, the need for refined theories still exists if the full potential of this turbine type is to be exploited. By idealizing the flow pattern, D. H. Silvern developed a "dynamic theory" for these turbine types which accounts for the influence of the circulatory flow component, neglected in the drag theory. If the stipulated flow pattern can actually be established, and if secondary losses are of insignificant consequences, higher efficiencies than recorded so far appear to be obtainable with these turbine types. The present "dynamic theory" covers only the incompressible case, i.e., cases where no marked density changes occur in the peripheral channel (low pressure ratios).

A drag turbine version with component designs as stipulated by the dynamic theory is presently being prepared.

More detailed briefings on the different turbine types are presented in the individual summaries of the different sections of this report. (Sections IV-D and IV-C).

III PRESENTATION OF TURBINE DATA

In order to properly present the turbine design criteria it is advantageous to use the similarity parameters, specific speed and specific diameter. Specific speed is defined as

$$N_S = \frac{N\sqrt{Q}}{(H_{ad})^{3/4}} \qquad\qquad III,1$$

and specific diameter by

$$D_S = \frac{D(H_{ad})^{1/4}}{\sqrt{Q}} \qquad\qquad III,2$$

when Q denotes the amount of flow passing through the rotor discharge area (ft^3/sec), N the rotative speed (rpm), and H_{ad} the adiabatic head (ft) of the passing gas. These terms are derived from similarity considerations by the following arguments: The flow Q passing through a turbine is proportional to a characteristic velocity c and the through-flow area A. The area A is proportional to the square of the rotor diameter D and the characteristic velocity is proportional to the rotor tip speed u. Hence, the volume flow passing through the turbine becomes proportional to the product of rotational speed N and the cube of the rotor diameter D

$$Q \approx c \approx cD^2 \approx uD^2 \approx ND^3 \qquad\qquad III,3$$

The head H_{ad} expanded in the turbine is proportional to the square of the characteristic velocity c or tip speed u and consequently proportional to the product of the square of the rotative speed and rotor diameter

$$H_{ad} \approx c^2 \approx u^2 \approx N^2 D^2. \qquad\qquad III,4$$

Comparing the volume flow and the head of a turbine with the volume flow and head of a standard turbine (subscript "s") it follows from equation (III, 3)

$$\frac{Q}{Q_s} = \frac{ND^3}{N_s D_s^3} \qquad\qquad III,5$$

and

$$\frac{H_{ad}}{H_{ad\cdot s}} = \frac{N^2 D^2}{N_s^2 D_s^2}. \qquad\qquad III,6$$

Solving equation (III, 5) and (III, 6) for the diameter D assuming that the characteristic values of the standard turbine are unity $(Q_s = H_{ad\cdot s} = 1)$ equation (III, 1) is obtained whereas by solving equation (III, 5) and (III, 6) for the speed N, equation (III, 2) is obtained. Thus, specific speed is the rotative speed required for a turbine which handles a volume flow of unity and expands a head of unity and the specific diameter is the rotor-diameter required for this turbine. It is also evident that turbines having the same specific speed and specific diameter are similar in geometry as well as flow mechanism and, therefore, have identical characteristics, i.e., the same efficiency if Reynolds number and Mach number effects are neglected. It is to be noted that specific speed and specific diameter are truly dimensionless numbers. This becomes evident when equation (III, 4) is written in the form $g H_{ad} = N^2 D^2$ so that

$$n_s = \frac{N\sqrt{Q}}{(g H_{ad})^{3/4} 60} \qquad\qquad III/a$$

and

$$d_s = \frac{D(g H_{ad})^{1/4}}{\sqrt{Q}}. \qquad\qquad III,2a$$

For convenience and in keeping with specific speed data commonly found in the literature, the definitions given in equation (III, 1) and (III, 2) are used in this report. It is to be noted that these terms are interrelated with the quantities which determine the losses in the turbine, for example:

$$N_s = (2g)^{3/4} \frac{H_{ad}\sqrt{A_i}}{c_i} \qquad \text{III.7}$$

and

$$D_s = \frac{D}{\sqrt{A_i}} (2g)^{-1/4} \qquad \text{III.8}$$

when A_i denotes the through-flow area of a jet passing with the velocity c_i. It is also interesting to note that the product of specific speed and specific diameter is proportional to the turbine speed ratio

$$\frac{u}{c_i} = \frac{N_s D_s}{154} \qquad \text{III.9}$$

and that the product of specific speed and the cube of the specific diameter is inversely proportional to the gulp factor φ^*, or flow factor since

$$\varphi^* = \frac{Q}{ND^3} = \frac{1}{N_s D_s^3} \qquad \text{III.10}$$

both values being important design criteria. It is, therefore, possible to calculate the losses and consequently the turbine efficiency as function of specific speed and specific diameter, thus indicating that the characteristic aspects for the design of turbines are completely described by the terms specific speed and specific diameter. A diagram, therefore, which shows the efficiency as a function of these parameters is a convenient tool for expressing the present state of the art. Such diagrams are shown in figure (II.1).

Aside from being useful in calculating turbine losses the term specific speed also indicates the interrelation between the turbine HP and rotative speed since

$$N_S = \frac{N \sqrt{HP}}{(H_{ad})^{3/4}} \sqrt{\frac{550}{?\,\gamma_3}} \qquad \qquad III_{,}11$$

when γ_3 denotes the density of the gas at the exhaust port.

It is, therefore possible to express the specific speed range of turbines as a function of horsepower level, rotative speed, and exhaust condition. Introducing numerical values which are typical for accessory power units in guided missiles (by assuming a pressure ratio of 16 and exhaust densities of .04 lb/ft³) it follows that turbines delivering 5 horsepower at a rotative speed of 24,000 rpm operate at a specific speed of 3.2 and that turbines delivering 60 horsepower operating at the same speed have a specific speed of 11.1. It is apparent, therefore, that the specific speed range from 2 to 12 is of highest interest for typical APU turbines.

The absolute leaving component c_{u-3} can be expressed by

$$c_{u-3} = w_{u-3} - u_3 \qquad\qquad IV.4$$

whereby the relative leaving component w_{u-3} is a function of the relative leaving velocity w_3 and the rotor blade angle β_{b-3}

$$w_{u-3} = \gamma_R \, \psi_N c_i \sin \alpha_2 \, \frac{\cos \beta_{b-3}}{\sin \beta_{b-2}} \qquad\qquad IV.5$$

when the term $\gamma_R = {}^{w_2}\!/w_3$ denotes a velocity coefficient of the rotor. Assuming symmetrical blades, i.e., $\beta_{b-2} = \beta_{b-3}$ equation (IV. 4) takes the form

$$w_{u-3} = \gamma_R \, \psi_N c_i \sin \alpha_2 \cot \beta_{b-2} \qquad\qquad IV.6$$

Assuming additionally incidence-free inlet into the rotor blading, the angle β_{b-2} becomes interrelated with the nozzle angle α_2 and wheel speed u_2 since then

$$\cot \beta_{b-2} = \cot \alpha_2 - \frac{u/c_i}{\sin \alpha_2 \, \psi_N} \, . \qquad\qquad IV.7$$

Introducing equation (IV. 7) into equation (IV. 6) and assuming axial blading i.e., $u_2 = u_3 = u$ it follows

$$w_{u-3} = \gamma_R \left(c_i \psi_N \cos \alpha - u_2 \right) \qquad\qquad IV.8$$

Introducing equation (IV. 3), (IV. 4) and (IV. 8) into equation (IV. 2) the final equation for the force exerted by the flow on the rotor blade reads:

$$F = \frac{w}{g} \left[\psi_N c_i \cos \alpha_2 \left(1 + \gamma_R \right) - u \left(1 + \gamma_R \right) \right] \cdot \quad [LB] \quad IV.9$$

Hence, the torque of the rotor becomes

$$T = \frac{WD}{i g}\left[\gamma_N c_i \cos\alpha_2(1+\gamma_R) - u(1+\gamma_R)\right] \quad [ft\text{-}lb] \quad IV,10$$

when D denotes the rotor diameter. The head transferred into rotative power is

$$H_e = \frac{F u}{W} = \frac{c_i u\left[\cos\alpha_2 \gamma_N (1+\gamma_R) - u/c_i(1+\gamma_R)\right]}{g} \quad [ft] \quad IV,11$$

whereas the head supplied by the gas is

$$H_s = \frac{c_i^2}{2g}. \quad [ft] \quad IV,12$$

The efficiency, being the ratio of the above, two heads is then expressed by the relation

$$\gamma_h = 2\frac{u}{c_i}\left[\gamma_N \cos\alpha_2(1+\gamma_R) - \frac{u}{c_i}(1+\gamma_R)\right]. \quad IV,13$$

Equation (IV, 13) describes the hydraulic turbine efficiency for the full admission impulse turbine neglecting wheel disc friction and represents this efficiency as a function of the nozzle angle α_2, the velocity ratio u/c_i, and the velocity coefficients for the nozzle γ_N and the rotor γ_R.

For partial admission turbines, the average exit component of the rotor in peripheral direction w_{u-3} is decreased by the filling and emptying losses of the blades. These losses are sustained by the fact that a rotor channel moving into the admitted portion of the arc will at the first instance offer a larger flow area to the nozzle jet than the nozzle area thus forcing the nozzle jet to expand suddenly within the rotor channel. Hence, w_3 is smaller in this instance than the w_3 value after the channel has entered fully into the admitted arc. Analytical investigation of this aspect as reported in reference 1 and partially substantiated by test data indicate that the mean leaving velocity w_3 is decreased by a factor

$$K_F = \left(1 - \frac{t}{2x}\right) \quad IV,14$$

when t denotes the blade spacing and where a denotes the extension of the nozzle arc in the peripheral direction. Hence, the rotor velocity coefficient ψ_R has to be multiplied by the factor K_F when calculating the hydraulic efficiency of the partial admission turbines.

Another loss which has to be considered for partial admission turbines is scavenging. This loss is due to mixing of the high velocity fluid from the nozzle and the relatively stagnant fluid in that part of the rotor that is first becoming active in receiving the fluid from the nozzle. The amount of energy expanded by this loss has to be subtracted from the amount of energy transferred into rotative power. According to the analysis reported in reference 1, this energy can be represented by the head term

$$H_{lat. scav} = \frac{u^3 C f}{a \sin\alpha_2 \, 2g \, \psi_N \, c_i'} \qquad \text{IV}, 15$$

where C denotes the axial extension of the blades and f a mixing coefficient which appears to have values of about 1.4. Hence, the efficiency relation quoted in equation (IV, 13) has to be corrected by a subtractive term

$$K_m = \left(\frac{u}{c_i}\right)^3 \frac{C}{a} \frac{f}{\sin\alpha_2 \, \psi_N} \qquad \text{IV}, 15a$$

which corrects the hydraulic efficiency for the scavenging loss.

The rotative energy effective at the turbine shaft is smaller than the energy transferred into rotative power by the wheel disc friction. This loss is usually expressed in terms of horsepower loss by a relation of the form

$$L_w = \frac{u^3 d^2 \gamma K_w}{g} \qquad \left[\frac{ft \cdot lb}{lb}\right] \qquad \text{IV}, 16$$

when Υ denotes the density of the gas surrounding the wheel disc, d the disc diameter and K_W a factor representing the influence of the distance of the stationary shrouds and the influence of the Reynolds number. Usually the loss coefficient K_W is represented as function of both terms in a diagram as shown in figure (IV, 2) indicating an increase of this coefficient with decreasing Reynolds numbers and a minimum value for this coefficient for certain spacings between disc and shroud. This power loss can be transformed into a head loss by writing

$$H_W = \frac{L_W^*}{W} = \frac{K_W \Upsilon d^2 u^3}{Wg} \qquad \text{IV,17}$$

Hence, the hydraulic efficiency has to be corrected by a subtractive term of the form

$$K_W^* = \left(\frac{u}{c_i}\right)^2 \frac{u}{W} d^2 \Upsilon 2 K_W \qquad \text{IV,18}$$

when the shaft efficiency is to be calculated.

Another loss to be considered in partial admission turbines are the pumping losses caused by blade pumping in the unadmitted arc of the turbine periphery. Many imperical formulations for this loss have been presented in literature. The most pertinent appears to be the one quoted in reference 2 which expresses this loss in terms of horsepower by the relation

$$L_P^* = u^3 d^2 \frac{\Upsilon}{g} \left[\left(1 - \frac{a}{D\pi}\right) K_P \left(\frac{h_1 + h_2}{d_m}\right)^{1.5}\right] \left[\frac{ft \cdot LB}{sec}\right] \qquad \text{IV,19}$$

when h_1 denotes the blade length at inlet, h_2, the blade length at outlet, d_m the mean blade diameter, and K_P an experience factor varying from 2.9×10^{-3} for unshielded blades to about 1.4×10^{-3} for properly shielded blades. Transforming equation (IV, 19) into a head term and dividing by $\frac{c_i^2}{2g}$ the efficiency loss becomes

$$K_p^- = \frac{u}{W} 2 \left(\frac{u}{c_i}\right)^2 \gamma \left[\left(1 - \frac{a}{D\pi}\right) K_p \left(\frac{h_1 + h_2}{d_m}\right)^{1.5}\right] . \qquad IV.20$$

This term also has to be subtracted from the terms in equation (IV, 13) for calculating the shaft efficiency of partial admission turbines.

   With the above interrelation the final equation for the shaft efficiency of partial admission turbines reads:

$$\eta = 2 \frac{u}{c_i} \left[1 + \gamma_R \left(1 - \frac{r}{2a}\right)\right] \left[\gamma_N \cos\alpha_2 - \frac{u}{c_i}\right] - \left(\frac{u}{c_i}\right)^3 \frac{c}{a} \frac{\xi}{\gamma_N \sin\alpha_2}$$
$$- 2 \left(\frac{u}{c_i}\right)^2 \frac{u}{W} d^2 \gamma \left\{K_w + K_p \left(1 - \frac{a}{D\pi}\right)\left(\frac{h_1 + h_2}{d_m}\right)^{1.5}\right\} . \qquad IV.21$$

Considering now that definite interrelationships exist between the degree of admission, weight flow, etc. and specific speed and specific diameter, namely

$$\frac{t}{2u} = D_s^2 \sin\alpha_2 \gamma_N \sqrt{2g} \frac{1}{D} \frac{1}{2\xi} \qquad IV.22$$

with a denoting the blade number,

$$\frac{u d^2 \gamma}{W} = \frac{N_s D_s^3 \sqrt{2g}}{154 \xi^2} \qquad IV.23$$

with $\xi = D_s/d$ denoting the impeller diameter ratio,

$$\frac{a}{D\pi} = \frac{1}{(W/\delta) D_s^2 \gamma_N \sin\alpha_2 \sqrt{2g}} \qquad IV.24$$

$$\frac{C}{a} = \gamma_N \sin\alpha_2 \, C_s^2 \sqrt{2g} \, \frac{C}{D} \frac{h}{D}$$
 (IV.25)

$$\frac{h_1 + h_2}{d_m} = \frac{2}{\frac{D/h}{\epsilon} + \frac{1}{2}}$$
 (IV.26)

when $h_1 = h_2$ it is also evident that the efficiency can be expressed as a function of the similarity parameters - - specific speed and specific diameter. This is demonstrated by introducing equation (III.9), (IV.22), (IV.23), (IV.24), (IV.25), and (IV.26) into equation (IV.21) yielding

$$\eta = \frac{N_s D_s}{77} \left[1 + \psi_R \left(1 - D_s^2 \sin\alpha_2 \gamma_N \sqrt{2g} \frac{h}{D} \frac{1}{2z} \right) \right] \left[\gamma_N \cos\alpha_2 - \frac{N_s D_s}{154} \right]$$
$$- \frac{N_s^3 D_s^5}{(154)^3} 1.4 \sqrt{2g} \left(\frac{C}{D} \frac{h}{D} \right) - \frac{2 N_s^3 D_s^5}{(154)^3 \epsilon} \left\{ K_\nu + K_f \left(1 - \frac{1}{D_s \left(\frac{h}{D} \right) \sin\alpha_2 \gamma_N \sqrt{2g}} \right) \left(\frac{2}{\frac{D/h}{\epsilon} + \frac{1}{2}} \right)^{1.5} \right\}$$
 (IV.27)

Equation (IV.27) indicates that it is sufficient to determine the interrelationship between ψ_R, γ_N and $\frac{h}{D}$, a, ϵ, $\frac{C}{D}$ in order to calculate the maximum obtainable efficiency of all axial impulse turbine designs whereby ψ_R is a function of β_{b-2} which is related to α_2 by equation (IV.7).

The above derivations have an important meaning for the selection of the most efficient design geometry and can be enumerated as follows:

(1) The degree of admission equation (IV.24) is a function of the specific diameter. Since η max depends on Ns and Ds, the optimum degree of admission is not an independent parameter, but a function of Ns, Ds, and h/D

(2) The parameter t/a (equation IV.22) is a function of the specific diameter which again means that the optimum t/a value is a function of Ns, Ds, and h/D.

It will be shown in Section C that the above enumeration is also valid for terry turbines where the blade distance H replaces the blade heights h.

It is also important to note that the nozzle area A_N or the dimensionless parameter A_N/D^2 is related to the specific diameter since

$$D_s = \frac{\sqrt[4]{\frac{\kappa}{\kappa-1}\left[1-\left(P_3/P_1\right)^{\frac{\kappa-1}{\kappa}}\right]}}{\sqrt{A_N/D^2}\sqrt{P/P_1}\sqrt{\gamma}\sqrt{1-z\left[1-\left(P_3/P_1\right)^{\frac{\kappa-1}{\kappa}}\right]}} \qquad \text{IV,28}$$

with

$$\gamma = \sqrt{2g\frac{\kappa}{\kappa-1}\left[\left(P_1/P_2\right)^{\frac{3\kappa}{\kappa}}-\left(P_3/P_1\right)^{\frac{\kappa+1}{\kappa}}\right]} \qquad \text{IV,29}$$

Equation (IV, 29) demonstrates that A_N/D^2 changes with pressure ratio for constant Ds values meaning that the nozzle area is related to the specific diameter by the turbine pressure ratio P_1/p_3 and turbine efficiency γ.

B. Axial Turbines

1. Investigation of Losses

The information on losses published in the literature up to 1951 is critically reviewed in reference 3, which reports the following findings:

The total loss occurring in cascades can be subdivided into a number of component losses as follows:

a. Profile losses denoting that part of the total loss which is caused
   by skin friction or separation in a uniform two-dimensional flow
   across a grid.

b. Secondary losses caused by non-uniformity of the three dimensional
   flow, i.e., losses occurring mainly at the tip and hub section of
   of the cascade.

c. Leakage losses

d. Miscellaneous losses as, for example, losses caused by the wake of
   the trailing edge of the blade.

e. Reynolds number influence

a. Profile Losses

Profile losses are comparitively well documented and are found to be
mainly a function of the pitch-chord ratio S and flow turning-angle $\Delta\beta$. Figure
(IV, 3) is representative of these findings giving the profile losses for typical
nozzle blades and impulse blades, indicating that pitch-chord ratios of .5 to .9,
depending on nozzle angle α_1, are optimum for nozzles and pitch-chord ratios of
.5 to .8, depending on the blade angle β_1, are optimum for impulse blades. The
loss is expressed in these diagrams by a velocity coefficient ψ which is defined
as the ratio of actual leaving velocity c and w, respectively, and theoretical gas
velocity c_i obtainable without losses, i.e.,

$$\psi = \frac{c}{c_i} \text{ or } \frac{w}{w_i} = \sqrt{1 - \lambda} \qquad \text{IV,30}$$

when λ denotes a loss factor. It is to be noted that the optimum pitch-chord ratio
decreases with decreasing blade angles β for impulse blades.

b. Secondary Losses

Considerable uncertainty is displayed regarding numerical values for secondary losses. Since these losses are presumed to cover the influence of the flow disturbances caused by the hub and tip shroud (or tip clearance), it appears logical that these losses should depend mainly on the aspect ratio R when aspect ratio is defined as the ratio of blade heights h and chord lengths C. This thought is favored by reference 3, which states that the optimum pitch-chord ratio is independent of aspect ratio and that the sum of profile and secondary losses can be computed by adding a secondary loss factor λ_s to the profile loss factor λ_p, i.e.

$$\psi_m = \sqrt{1-(\lambda_p + \lambda_s)} \qquad \text{IV,31}$$

It is, however, pointed out in this reference that this approach is not undisputed, since some investigators quote a significant change in the optimum pitch-chord ratio with aspect ratio. This would suggest that the sum of profile and secondary losses can be obtained by modifying the loss coefficient λ_p, representing the profile losses with a secondary loss coefficient which then would depend on aspect ratio and also to some degree on the pitch-chord ratio.

For typical nozzle blades the sum of profile and secondary losses is comparatively well covered in reference 3. This information is reproduced in figure (IV,4). It is apparent from this figure that the aspect ratio has a sizeable influence on total losses, particularly the aspect ratio below unity.

Profile and Secondary Losses in Nozzle Blades.

It appears from figures (IV,3) and (IV,4) that the basic relationships governing the magnitude of the nozzle loss coefficient is fairly well established, and that ψ_N values of .95 to .96 are obtainable for most nozzle designs, and that the optimum pitch-chord ratio decreases slightly with decreasing values of α_2 rendering S values of .6 to .9 as most desirable design objectives. Actually the variation of optimum pitch-chord ratio with nozzle angle might be somewhat less, as indicated by the curve of Zweifel, reference 3, which is reproduced in figure (IV,5). The above values are independent of Mach number i.e pressure ratio, assuming that a properly diverging channel section is provided after the throat in supersonic nozzles. This is indicated by figure (IV,6) by reproducing values

from reference 9.

Profile and Secondary Losses for Impulse Rotor Blades

No conclusive values are quoted for this case. Since all indications point to an increase in secondary losses with turning angle $\Delta\beta$, it is to be assumed, that an even more pronounced influence of the aspect ratio exists in impulse blading than it does in nozzle bladings. Since the aspect ratio of the rotor is of particular significance in partial admission i.e., low specific speed turbines, a closer investigation of this aspect is warranted.

The recent literature (reference 4) contains valuable information regarding secondary losses and quotes that the secondary losses can be expressed by a loss coefficient which depends almost exclusively on the aspect ratio, and can, in a somewhat simplified form (neglecting losses caused by tip clearance effects) be expressed by

$$\lambda_s = \frac{.12}{\mathcal{R}} \qquad\qquad \text{IV,32}$$

so that the sum of profile and secondary losses, expressed by a velocity coefficient reads:

$$\Psi_m = \Psi_p \sqrt{1 - \frac{.12}{\mathcal{R}}} \qquad\qquad \text{IV,33}$$

Reference 5 assumes that the secondary losses depend, also, on pitch-chord ratio and on the ratio of blade lengths h to rotor diameter D by proposing a relation of the form

$$\lambda_s = \text{CONST} \frac{S}{\mathcal{R}(1 + h/D)} \qquad\qquad \text{IV,34}$$

without, however, quoting numerical values for the constant. This formulation in some respect is supported by test data quoted in reference 6, where the sum of profile and secondary losses is represented by a loss factor of the form

$$\lambda_m = \lambda_p + \lambda_s = \lambda_p \left(1 + \frac{K^*}{AR} \right) \qquad\qquad IV, 35$$

where the factor K^* is a function of turning angle and pitch-chord ratio, but independent of aspect ratio for $AR > 1$. A typical plot for the interrelation between K^* and pitch-chord ratio is given in figure (IV, 7) for a chamber angle of $\beta_s = 51$ degrees. Equation (IV, 35) is plotted by converting λ_m to γ_m (according to equation (IV, 31)) as a function of pitch-chord ratio for different aspect ratios in figure (IV, 8) (solid lines) indicating that the optimum pitch-chord ratio tends to decrease with decreasing aspect ratios. The dashed lines in figure (IV, 8) represent equation (IV, 33) and indicate that the optimum pitch-chord ratio is independent of aspect ratio and that the influence of the aspect ratio is considerably stronger than shown by equation (IV, 35), appearing to almost rule out aspect ratios of $AR < .4$ for efficient blade designs. The available test evidence is still insufficient to corroborate either equation. Since the difference, however, for $AR > .5$ appears to be within tolerable limits, equation (IV, 33) is selected for reasons of simplicity to represent the influence of the aspect ratio on the sum of profile and secondary losses in impulse bladings.

Conflicting information is given by the currently available literature on the optimum pitch-chord ratio for impulse blades. The most pertinent information is reproduced in figure (IV, 9), indicating that Ainley reports a tendency of decreasing optimum pitch-chord ratios with decreasing blade angles; whereas Zweifel and Howell indicate the opposite tendency. In view of this situation, it appears to be unwarranted at this time to modify equation (IV, 33), (quoted as the preferred relationship for the losses in impulse blades) by a correction factor for the pitch-chord ratio, as long as the pitch-chord ratio stays within values of .5 to .8. Since these values usually can be obtained in most turbine designs as will be shown in Section 4B (2), it is assumed that equation (IV, 33) covers the main aspect of the influence of cascade geometry on the loss coefficient, with the exception, however, of the influence of the turning angle. Reference 2 quotes data on this effect based on a large number of tests made by various investigators. They are reproduced in figure (IV, 10) where the upper line is representative of nozzle blades, the middle line for well designed impulse blades, and the lower line for sheet metal impulse blades. The upper two lines agree fairly well with later NACA investigations on gas turbine bladings. This tendency can be expressed by an approximate relation of the form

$$\psi_{\Delta\beta} = \left[1 - .228 \left(1 - \frac{\beta}{70}\right)^3\right] \qquad IV, 36$$

The influence of the flow Mach number on the losses in impulse blades was investigated in several references (references 2, 3, 7, 8, 9, and 10). These references indicate that the influence of the Mach number is comparatively small in the subsonic regime, indicating in many cases a minimum value at close to sonic velocities. For impulse blading, the influence of the Mach number seems to be more pronounced in the supersonic regime and follows a tendency as indicated in figure (IV, 11), i.e., a decrease in velocity coefficient with increasing Mach numbers. From this information, it appears that a correction factor of the form

$$\psi_{M_a} = \left[1 - .05 (M_a - 1)\right] \qquad IV, 37$$

is sufficient to express the influence of Mach number. It is interesting in this respect that the radius of curvature between throat and trailing edge at the upper blade surface is of considerable influence on the velocity coefficient in the subsonic regime as indicated in figure (IV, 12). This figure indicates that the radius should be about 5 times the blade distance, or preferably larger, in order to avoid detrimental effects of the Mach number.

Other references, (references 6, 11, and 12) report on the influence of blade curvature on profile and secondary losses for impulse blades by reporting the results of cascade measurements on four different profiles. Reference 11 indicates that a profile with a single arc curvature has a smaller velocity coefficient than profiles constructed as mathematical curves. By rounding the leading edge, the velocity coefficient is increased. The largest velocity coefficient, which is also less sensitive to Mach number than the previous profiles, was measured when the fabrication accuracy was increased from .3 millimeters to .05 millimeters. The increased accuracy gave a 2 per cent higher cascade efficiency.

In summarizing the above discussion on profile and secondary losses in impulse blades, it appears that an equation of the form

$$\psi_R = \left[1 - .228\left(1 - \tfrac{\beta}{70}\right)^3\right]\left[1 - .05(Ma - 1)\right]\left[1 - .06\tfrac{c}{h}\right] \qquad IV,38$$

is suitable for expressing the velocity coefficient in impulse blades as a function of deflection angle, Mach number, and aspect ratio.

c. Leakage Losses

Reference 5 quotes a relationship for the tip clearance loss which appears to be founded on good analytical reasoning. The derivation is based on the following considerations:

The lift experienced by the blades is assumed to be evenly distributed over the blade lengths, which means that the pressure difference between the pressure and the suction side of the profile is evenly distributed over the blade. This pressure difference causes a certain leakage flow W_ℓ over the blade tips, which can be calculated with the usual relationships. Expressing this leakage flow in the form of a leakage factor, it results for impulse blades

$$\zeta_\ell = const.\frac{W_\ell}{W} = \frac{\sqrt{c/t}}{1 + h/s} \qquad IV,39$$

whereby the constant would be expected to have values of about 1.5. Equation (IV, 39) indicates that the leakage factor depends mainly on the pitch-chord ratio and on the ratio of radial tip clearance s to radial blade lengths h. It is interesting to note that the pitch-chord ratio is of particular significance as indicated in figure (IV, 13) which shows that for equal value of s/h the leakage factor is increased by a factor of 1.4 when the pitch-chord ratio is decreased by a factor of 2. This interrelationship, however, is of importance only in cases where $s/h > .02$. Most designs can be expected to maintain $s/h < .02$ i.e. can be designed with clearances where the tip leakage loss is comparatively small. In view of this situation, it appears to be unnecessary at this time to introduce a correction factor for the tip clearance loss as long as $s/h < .02$ can be maintained.

d. Miscellaneous Losses

Some calculated data regarding the effect of trailing edge thickness on the cascade is offered in reference 3. According to this information, an equation of the form

$$\gamma_e = \sqrt{1 - \lambda_m e} \qquad \qquad IV,40$$

represents the velocity coefficient for the sum of profile losses, secondary losses, and edge losses when λ_m denotes the loss coefficient presenting profile and secondary losses and when e denotes a factor which depends on the ratio of trailing edge thickness t_e and blade pitch t and on the blade angle as indicated in figure (IV, 14). This plot shows a sizable influence of the ratio t_e/t on the loss coefficient which to some degree appears to be substantiated with test data. It means that for frequently found values of t_e/t = .04 to .05, the loss coefficient is increased (compared with t_e/t = 0) by a factor of 1.2 to 1.25. Since it is presumed for these investigations that values of t_e/t = .01 to .02 can be maintained in most cases, no correction has been introduced.

The influence of surface roughness is investigated in reference 13. The significant result is that a certain critical roughness value r_c exists. No change in loss coefficient was observed for roughness values below r_c, but a marked increased for roughness when the value was greater than r_c; namely an increase by a factor of 2 when the roughness is increased by a factor of 4.

Most investigators quote a comparatively small effect of the axial clearance between rotor and stator. As an example, a relation quoted in reference 11 is reproduced in figure (IV, 15) indicating that axial clearances up to 2 per cent of the blade length hardly effect the efficiency. It is to be expected that this relation has to be qualified since a pronounced influence of blade thickness on the clearance sensitivity will exist. It is assumed that for thick trailing edges, a small axial clearance is detrimental due to the comparatively large wake which enters the rotor blade. If the axial distance is increased, the flow pattern can straighten itself out before entering the blade, thus most likely reducing the detrimental wake effect. It is to be expected, therefore, that the optimum axial distance is to some degree a function of the thickness of nozzle blade trailing edge.

Some information is found in the literature, particularly reference 3, which indicates an inc̄ ̄ase in profile loss by oblique angles of attack at the leading, edge of the ro: ̄: blades. No detailed evaluation of these relationships has been made yet since the primary aim of this program are design considerations rather than calculations of the performance characteristics of a given turbine. It is, however, interesting to note that blunt leading edges in subsonic grids not only have a beneficial effect on the incidence losses, but also on the profile loss at zero incidence. This is demonstrated in reference 11 which indicates that a blunt edge is about 2 per cent more efficient than a sharp edge at zero incidence.

e. Reynolds Number Influence

Results of the influence of the Reynolds number on the velocity coefficient are found in reference 3. The main result is that a pronounced effect of Reynolds number exists at Reynolds number below 2×10^5. Figure (IV, 16) indicates that the profile loss, and consequently the overall loss, is almost doubled by decreasing the Reynolds number by a factor of 4. Other investigators place the critical Reynolds number at slightly lower values, namely $Re_{cr} = 10^5$. The effect of Reynolds number on the overall turbine efficiency by using the information represented in figure (IV, 16) will be discussed in more detail in Section IV, B2.

2. Performance of Single Stage Turbines

In equation (IV, 27), the efficiency of single stage turbines is quoted as a function of specific speed, specific diameter, and certain loss coefficients of the turbine nozzle and turbine rotor. The dependency of these two factors on the geometry was discussed in Section IV, B1. The main result was that the nozzle velocity coefficient can, in almost all cases, be assumed $\gamma_N = .96$ as long as pitch-chord ratios of .6 to .9 are achieved. The relation for the rotor loss coefficient is quoted in equation (IV, 38) where the assumption is made that the rotor Reynolds number is larger than 2×10^5, that the clearance ratio s/h is smaller than .02, that the critical roughness value is not exceeded, and that the trailing edge thickness ratio t_e/t is smaller than .02. Introducing the above relationship into equation (IV, 27) it results

$$\eta = \frac{N_s D_s}{77}\left\{1 + \left[1 - .228\left(1 - \frac{a}{10}\right)^3\right]\left[1 - .05(\mu_2 - 1)\right]\left[1 - .06\frac{C}{h}\right]\left[-D_s^2 \sin\alpha_2 \sqrt{.96}\frac{5}{\zeta}\frac{1}{N_s}\right]\right\} \quad \text{IV, 41}$$

$$\left[.96\cos\alpha_2 - \frac{N_s^4 D_s^3}{154}\right] - \frac{N_s^4 D_s^5}{154^3}1.4\sqrt{2g}\frac{C}{D}\frac{h}{D} - \frac{2N_s^3 D_s^5\sqrt{2g}}{154^3 \epsilon^2}\left\{K_N + K_P\left(1 - \frac{1}{D_s^2(h/D) - N_s\sqrt{.96}\sqrt{2g}}\right)\left(\frac{2}{\frac{D/h}{\zeta} + \frac{1}{\zeta}}\right)^{1.5}\right\}$$

This relation can be simplified considerably when it is assumed, as proven by sample calculations, that the members quoted in the first line of equation (IV, 41) are the most decisive values. Hence, maximum efficiencies will be obtained when the product

$$\left[1-.06\frac{C}{h}\right]\left[1-D_s^2 .96 \sin \alpha_2 \sqrt{2_g}\frac{h}{D}\frac{1}{z^2}\right] \qquad \text{IV,42}$$

yields a maximum. In referring to figure (IV, 17), which shows a typical cascade section, it is evident that the following geometrical relationships exist:

$$t = \frac{D\pi}{z} \qquad \text{IV,43}$$

and

$$C = t \ 2\sin 2\beta \qquad \text{IV,44}$$

when the radius r, is assumed to be equal to the channel width a.[*] This assumption gives reasonable channel geometries and also satisfies the optimum pitch-chord ratio relation, quoted in figure (IV, 9). Introducing these relations into equation (IV, 42) and differentiating equation (IV, 42) to find the maximum, it results that an optimum h/D value exist which follows the relation

$$\left(\frac{h}{D}\right)_{opt} = \sqrt{\frac{\sin 2\beta\pi}{4 D_s^2 \sin \alpha \sqrt{2_g}}} \qquad \text{IV,45}$$

Introducing this optimum relation into equation (IV, 41) and also replacing the value C in the second lines of equation (IV, 41) by equation (IV, 44), it follows for the maximum efficiency of single stage axial turbines

$$\eta = \frac{N_s D_s}{77}\left\{1 + \left[1 - .2\,\varepsilon\left(1 + \frac{b}{u}\right)^2\right]\left[1 - .05(n_k - 1)\right]\left[1 - \frac{24 D_s}{\varepsilon}\sqrt{\pi \sin\alpha \sin 2\beta \frac{}{\sqrt{2g}}}\right]^2\right\}$$

$$\left[.96\, a - x_2 - \frac{N_s D_s}{154}\right] - 1.4\,\frac{N_s^3 D_s^4}{2}\,\frac{(\sin\varepsilon\beta\pi)^{1.5}\,\sqrt[4]{2g}}{\sqrt{\sin\alpha_2}\,(154)^3}$$

$$- \frac{2 N_s^3 D_s^5 \sqrt{2g}}{154^3\,\varepsilon^2}\left\{K_w + K_b\left(1 - \frac{1}{D_s\sqrt{\sin\alpha_2 \sin 2\beta\,\pi\,\sqrt{2g}}\,.48}\right)\left(\frac{2}{\frac{2 D_s}{\varepsilon}\sqrt{\frac{\sin x_2\sqrt{2g}}{\sin 2\beta\pi}} + \frac{1}{2}}\right)^{1.5}\right\}$$

$$\text{IV, 46}$$

This relation now quotes the efficiency as a function of specific speed, specific diameter, nozzle angle, blade angle, and blade number, whereby it is to be observed that an interrelationship exists between the nozzle angle and blade angle (for incidence free inlet) as given in equation (IV, 7). Instead of quoting the blade number, the ratio of cutter diameter (for cutting the rotor channel) Q^* to wheel diameter, can also be introduced into equation (IV, 46), since

$$z = \frac{\pi \sin\beta}{Q^*/D}$$

$$\text{IV, 47}$$

(see figure IV, 17).

These relations indicate that the maximum obtainable efficiency becomes an exclusive function of specific speed and specific diameter, nozzle angle, and either blade number, or ratio of cutter diameter to rotor diameter. This makes it evident that other parameters such as the ratio of blade height over diameter, or the ratio of the arc of admission to blade pitch, or aspect ratio, are not primary criteria, but become functions of specific speed, specific diameter, blade number, and nozzle angle.

By selecting a specific speed, nozzle angle, and blade number and varying, for example, the specific diameter, the optimum specific diameter can be found. A typical plot is shown in figure (IV, 18), indicating that maximum efficiencies are obtained at certain specific diameters, whereby the optimum D_s value increases with decreasing specific speeds. This also means that for this maximum efficiency

certain optimum values of h/D exist whereby the optimum h/D depends mainly
on D_s, increasing with decreasing specific diameters as indicated by equation
(IV, 45). Figure (IV, 18) can now be transformed into a $N_s D_s$ diagram by show-
ing lines of constant efficiency as the function of specific speed and specific
diameter. Such a diagram is shown in figure (IV, 19) indicating at the same
time the optimum h/D values as well as optimum degrees of admission. This
plot is calculated for a nozzle angle of 16 degrees and a value of $a/D=.010$.

An inspection of this diagram reveals the following trends. The optimum
degree of admission decreases with decreasing specific speeds. In order to
obtain highest efficiencies at decreasing specific speeds, the specific diameter
has to be increased and the ratio of blade height to rotor diameter has to be
decreased. This means that turbines with low degrees of admission, i.e., low
specific speed turbines, must show comparatively large rotor diameters with
comparatively short blades. Since the ratio of cutter diameter to rotor diameter
should be minimized, it also follows that the number of blades should be maximized
which means that low specific speed turbines show best efficiences only if the
maximum possible number of blades is selected.

Full admission turbines, i.e., high specific speed turbines, show best
efficiencies at considerably smaller specific diameters and considerably larger
ratios of blade heights to rotor diameter. For the same ratio of a/D the blade
number also is smaller than in corresponding partial admission turbines. This
means that full admission turbines usually show a comparatively low number of
blades for optimum efficiency and also comparatively long blades. It becomes
evident, therefore, that only inefficient partial admission turbine designs are
obtained if the blade geometry found acceptable for full admission turbines is
adopted for partial admission turbines.

The influence of the blade number is demonstrated in figure (IV, 20) by
showing the maximum obtainable efficiency for different specific speeds as
function of specific diameter by selecting for design A, a blade number of 100
and for design B, a blade number of 42. A comparison of these curves reveals
that the smaller blade number has a considerable effect particularly at low
specific speeds. For example, it decreases the maximum obtainable efficiency
at specific speeds of 3 by 40 per cent and only by 15 per cent for specific speeds
of 30. This diagram also demonstrates that high blade numbers are desirable
for all axial turbine designs, but are of particular importance in low specific
speed turbines.

The practice of adopting the design philosophy, usually applied for full admission turbines, also to partial admission turbines, might be partly responsible for the low efficiencies quoted so far in the available literature (reference 14). The optimum data taken from reference 14 are plotted as a solid line in figure (IV, 21) by showing the maximum obtained efficiency as the function of specific speed. The dashed line in this diagram shows the efficiencies obtainable with optimized geometries and the dotted line shows the AMF/TD test results of a partial admission turbine optimized for a specific speed of 3. An inspection of these curves reveals the considerable gains which are obtainable with optimized geometries in partial admission turbines and, also, demonstrates that the considerations which led to the optimization are partly substantiated by test data.

Influence of Blade Number

It is now of interest to investigate the effect of several geometric parameters neglected so far in figure (IV, 19) on the maximum obtainable efficiency. For this purpose equation (IV, 46) has been rewritten by introducing average values for nozzle angle and blade angle, yielding an equation of the form

$$\zeta = \frac{N_S D_S}{77}\left\{ \left[1+\left(1-\frac{D_1}{2}.6\right)^{-1}\right]\left[9-\frac{N_S D_S}{154}\right] - \frac{N_S^2 D_S^4}{2\cdot10^6}\frac{6.8}{} - \frac{N_S^3 D_S^5}{10^6}\left[\left(1-\frac{1}{.6D_S}\right)\left(\frac{3}{.5+18D_S}\right)^{1.5}\left(1+\frac{K_W}{K_P}\right)\right]\right\}$$

$$\text{IV,48}$$

This equation shows that aside from specific speed and specific diameter, the ratio of specific diameter over blade number, or its equivalent, the product of specific diameter and ratio of cutter diameter over rotor diameter, emerges as additional criteria. This suggests that the influence of the blade number on efficiency could, for example, be expressed by a correction factor by writing the ratio of efficiency to base efficiency (ζ/ζ_o) and by representing this ratio as function of D_S/z. It is apparent from equation (IV, 48) that such a plot must show specific speed and specific diameter as additional parameters when an exact correction factor is to be determined. It appears possible, however, to simplify this relation by only considering the members in parenthesis in equation (IV, 48). With this assumption, the correction factor for the blade number would take the form

$$\frac{\eta}{\eta_0} = \frac{2-1.2\frac{D_s}{z}+.36\left(\frac{D_s}{z}\right)^2}{2-1.2\left(\frac{D_s}{z}\right)_0+.36\left(\frac{D_s}{z}\right)_0^2} \qquad\qquad IV, 49$$

It is evident that such a relation must be quite inaccurate at large specific
diameters since the subtractive members neglected in equation (IV, 48) increase
with increasing specific diameters and also change with specific speed. If the
influence of specific speed is neglected, it must be expected that the influence of
specific diameter is stronger than indicated in equation (IV, 49). By allowing
some inaccuracy it appears possible to account for this influence by modifying
equation (IV, 49) to the form

$$\frac{\eta}{\eta_0} = \frac{1-1.5\frac{D_s}{z}}{1-1.5\left(\frac{D_s}{z}\right)_0} = \frac{1-1.5 D_s\frac{a}{n}}{1-1.5\left(D_s\frac{a}{n}\right)_0} \qquad\qquad IV, 50$$

This relation is graphically shown in figure (IV, 22), indicating a strong influence
of the ratio of specific diameter over blade number on the obtainable efficiency,
revealing an efficiency drop of about 50 per cent for large specific diameters,
i.e., typical partial admission turbines, when only one-third of the optimum
blade number is selected. This figure at the same time also reveals that the
influence of the blade number is smaller at lower specific diameters, i.e., full
admission turbines, as discussed previously. In order to test the degree of
approximation involved in equation (IV, 50), figures (IV, 23) and (IV, 24) have
been calculated showing lines of constant efficiency as the function of specific
speed and specific diameter for a $\frac{a}{n}_D$ values of .015 and .025, (a = 66 and 40)
i.e., progressively larger than the $\frac{a}{n}_D$ (a = 100) value assumed for figure
(IV, 19). Comparing the efficiencies resulting from these diagrams with the
correction offered in figure (IV, 22), it results that the correction factor
defined by equation (IV, 50) gives fair values for specific speeds between 1 and
10, i.e., for the range which is of highest interest for partial admission

turbines as applied in accessory power units for guided missiles. Equation
(IV, 50), however, does not represent the change in optimum h/D values and
optimum degrees of admission caused by the different values of a_D. Hence,
the correction factor offered in equation (IV, 50) should only be used as a first
rough approximation. The main purpose for quoting figure (IV, 22) is to show
the high degree of sensitivity to proper blade number selection exhibited by partial
admission axial turbines.

Equation (IV, 46) quotes efficiency as a function of specific speed, specific
diameter, nozzle angle, blade angle, and blade number. It was stated in Section
B, 1 by discussing the loss sources, that Reynolds number influences have been
neglected and that equation (IV, 46) was presuming a constant Reynolds number
($Re = 2 \times 10^5$) and, furthermore, that the radial clearance is less than two per
cent of the blade height and that the trailing edge thickness is less than two per cent
of the blade pitch. It is now of interest to investigate the influence of these
parameters on the maximum obtainable efficiency.

Reynolds Number Effect

The blade Reynolds number used in figure (IV, 16) was defined by

$$ R_e = \frac{c w_2}{\nu} . \qquad\qquad IV, 51 $$

Introducing the previously defined parameters into equation (IV, 51) the Reynolds
number can also be written in the form

$$ R_e = \frac{D \pi c_0}{z \nu} \, 4 \, \psi_N \sin \alpha_2 = \frac{c_0^2 N_s}{4 \pi g \, N \nu} \pi \, 4 \, \psi_N \sin \alpha_2 \frac{D_s}{2} \qquad IV, 52 $$

revealing that the ratio of rotor diameter over blade number or for a given
specific speed, the ratio of specific diameter over blade number becomes again
a criterion. From figure (IV, 16) it appears that the blade loss coefficient Y_p
varies with Reynolds number according to the relation (approximate)

$$ Y_p = \frac{const}{\sqrt{R_e}} \qquad\qquad IV, 53 $$

whereby, the constant has a value of about 530. Considering now equation (IV, 48) and again accounting only for the members in parenthesis of this equation, the ratio of efficiency over base efficiency, after introducing equation (IV, 53) additionally, can be written in the form

$$\frac{\eta}{\eta_0} = \frac{1 + \left[1 - .6\,\frac{D_s}{z}\right]^2 \sqrt{1 - \frac{530}{\sqrt{Re}}}}{1 + \left[1 - .6\left(\frac{D_s}{z}\right)_0\right]^2 \sqrt{1 - \frac{530}{\sqrt{Re_0}}}} \qquad\qquad \text{IV,54}$$

Remembering, again, that the subtractive members in equation (IV, 48) are mainly a function of specific diameter, equation (IV, 54) has to be modified so as to yield a larger influence of specific diameter, suggesting after further simplifications, a relation of the form

$$\frac{\eta}{\eta_0} = \frac{2 - \frac{265}{\sqrt{Re}} - \frac{D_s}{z}\left(3 - \frac{265}{\sqrt{Re}}\right)}{2 - \frac{265}{\sqrt{Re_0}} - \left(\frac{D_s}{z}\right)_0\left(3 - \frac{265}{\sqrt{Re_0}}\right)} \qquad\qquad \text{IV,55}$$

This equation again indicates that the Reynolds number effect is a function of specific diameter and blade number, increasing with increasing D_s/z values. This relation is plotted in figure (IV, 25). However, the relation must be applied with discretion since, as indicated in equation (IV, 52), the Reynolds number increases with increasing D_s/z values. This means that in most cases where the Reynolds number effect is large, (large D_s/z values) the Reynolds number itself tends to be large i. e. close to the base Reynolds number, so that only small deviations from the base efficiency occur. It appears that for most cases the more conventional quotation of Reynolds number influence, namely

$$\frac{1 - \eta}{1 - \eta_0} = \sqrt[6]{\frac{Re_0}{Re}} \qquad\qquad \text{IV,56}$$

will give acceptable average values.

Leakage Effect

The influence of rim leakage on the blading efficiency was quoted in equation (IV, 39) and graphically represented in figure (IV, 13). Introducing equation (IV, 44) into equation (IV, 46), the relation for the leakage factor simplifies to

$$\frac{\xi}{\zeta} = \frac{1.5\sqrt{2\sin 2\beta}}{1 + \frac{t}{s}} \approx \frac{1.9}{1 + \frac{t}{s}} \qquad\qquad IV, 57$$

indicating that the leakage factor is almost exclusively a function of tip clearance over blade lengths. Considering, again, only the numbers in parenthesis in equation (IV, 48) and introducing equation (IV, 57) a correction factor for the leakage effect can be quoted in the form

$$\frac{\eta}{\eta_o} = \frac{1 + \left[1 - .6\frac{D_s}{z}\right]^2\left[1 - \frac{1.9}{1 + \frac{t}{s}}\right]}{1 + \left[1 - .6\left(\frac{D_s}{z}\right)_o\right]^2\left[1 - \frac{1.9}{1 + \left(\frac{t}{s}\right)_o}\right]} \cdot \qquad IV, 58$$

Considering now that the subtractive numbers in equation (IV, 48) have a strong influence at large specific diameters, a modification to the form

$$\frac{\eta}{\eta_o} = \frac{2 - \frac{2}{1 + \frac{t}{s}} - \frac{D_s}{z}\left(3 - \frac{2}{1 + \frac{t}{s}}\right)}{2 - \frac{2}{1 + \left(\frac{t}{s}\right)_o} - \left(\frac{D_s}{z}\right)_o\left(3 - \frac{2}{1 + \left(\frac{t}{s}\right)_o}\right)} \qquad IV, 59$$

is indicated which is graphically presented in figure (IV, 26), where a clearance ratio of $(s/h)_o = .02$ is used as the reference point in accordance with the assumptions discussed in Section IV, BIC. This diagram reveals a noticeable effect of the ratio D_s/s on the leakage sensitivity meaning that for equal blade numbers the ratio s/h is somewhat more important for large specific diameter

turbines (typical partial admission turbines) than for low specific diameter turbines (typical full admission turbines). It is, however, also evident by comparing figure (IV, 26) with figure (IV, 22) that the effect of specific diameter on the leakage is considerably smaller than the effect of specific diameter on the blade number.

Equation (IV, 59) gives an approximate relation for the rim clearance correction factor by expressing the rim clearance in per cent of the blade lengths. The reference value s/h is a useful parameter from an aerodynamic point of view, since s/h expresses directly the geometrical leakage, thus linking the efficiency drop to channel geometry. From a manufacturing point of view, the tip clearance ratio s/D is of more significance. By observing equation (IV, 45) which states the optimum h/D ratio as a function of specific speed, it results that the optimum blade lengths decreases with increasing specific diameters. This means that the ratio s/D becomes more sensitive to specific diameter, namely

$$\frac{\eta}{\eta_o} = \frac{2 - \frac{2}{1 + \frac{h/D}{(s/D)}} - \frac{D_s}{z}\left(3 - \frac{2}{1 + \frac{h/D}{(s/D)}}\right)}{2 - \frac{2}{1 + \frac{2 D_s}{(s/D)}} - \left(\frac{D_s}{z}\right)_o\left(3 - \frac{2}{1 + \frac{2 D_s}{(s/D)}}\right)} \qquad \text{IV, 60}$$

indicating that typical partial admission turbines are considerably more sensitive to s/D than typical full admission turbines.

Trailing Edge Thickness

The influence of this parameter on the velocity coefficient was quoted in equation (IV, 40) and graphically represented in figure (IV, 14). Introducing equation (IV, 40) into equation (IV, 46) and considering only the numbers in parenthesis in equation (IV, 46), a correction factor can be written in the form

$$\frac{\eta}{\eta_o} = \frac{1 + (1 - .05 e)\left(1 - .6 \frac{D_s}{z}\right)^2}{1 + (1 - .05 e_o)\left[1 - .6\left(\frac{D_s}{z}\right)_o\right]^2} \qquad \text{IV 61}$$

which, again, shows the influence of the parameter specific diameter over blade number. Considering that the subtractive members in equation (IV, 46) have a particularly strong influence at large specific diameters, a modification of equation (IV, 61) to the form

$$\frac{\eta}{\eta_o} = \frac{2 - .05 e - \frac{D_s}{z}\left(3 - .05 e\right)}{2 - .05 e_o - \left(\frac{D_s}{z}\right)_o\left(3 - .05 e_o\right)} \qquad \text{IV, 62}$$

is indicated.

The influence factor e in equation (IV, 62) can be approximated by the relation (see figure (IV, 14)

$$e = 1 + \left(\frac{te}{t}\right)^2 140.$$ (IV, 63)

Introducing equation (IV, 63) into equation (IV, 62) yields

$$\frac{\eta}{\eta_0} = \frac{1.95 - 7\left(\frac{te}{t}\right)^2 - \left(\frac{D_s}{2}\right)\left[2.95 - 7\left(\frac{te}{t}\right)^2\right]}{1.95 - 7\left(\frac{te}{t}\right)^2_0 - \left(\frac{D_s}{2}\right)_0\left[2.95 - 7\left(\frac{te}{t}\right)^2_0\right]}$$ (IV, 64)

revealing that the product $\frac{D_s}{2}\left(\frac{te}{t}\right)^2$ becomes the governing criterion for the correction factor for the trailing edge thickness as graphically shown in figure (IV, 27). Equation (IV, 64) indicates that a comparatively large trailing edge thickness can be tolerated at small specific diameters, i.e. in typical full admission turbines but that the sensitivity to trailing edge thickness is considerably increased at large specific diameter, i.e. partial admission turbines, again demonstrating that design trends found acceptable in full admission turbines will be found detrimental in partial admission turbine designs.

It stands to reason that the simplified relations, offered for the different correction factors can only indicate the main trends and are quoted mainly in order to indicate the most influential design parameters for the different corrections. A more accurate appraisal of the influence of the different parameters can only be obtained by calculating complete N_s-D_s diagrams for the different parameters such as different blade numbers, Reynolds numbers, tip clearance ratios, and trailing edge thicknesses. This was carried through in this report only for the influence of the blade number (figures (IV, 19), (IV, 23), and (IV, 24)). Comparing these diagrams it becomes evident that the optimum specific diameter changes considerably with blade number at small specific speeds which also causes the optimum h/D ratio to change. Similar changes will also result for tip clearance ratios and trailing edge thicknesses which are different from the base values quoted in figures (IV, 19), (IV, 23), and (IV, 24).

Since all these factors depend on the main criterion, namely $D_s/_z$, it appears possible to use figures (IV, 23) and (IV, 24) not only for showing the performance at smaller blade numbers, but also for presenting more accurately (although still approximately) the performance at larger leakage and trailing edge thickness but larger blade numbers. This consideration, in conjunction with equation (IV, 50), (IV, 59), and (IV, 64) suggests that the approximate validity of figures (IV, 23) and (IV, 24) can be extended to the combinations of values as presented in table A.

TABLE A

Fig.	$\frac{a^*}{D}$	$\frac{t_c}{t}$	$\frac{s}{h}$	Re	Fig.	$\frac{a^*}{D}$	$\frac{t_c}{t}$	$\frac{s}{h}$	Re
23	.015	.02	.02	2×10^5	24	.025	.02	.02	2×10^5
23	.014	.12	.02	2×10^5	24	.023	.12	.02	2×10^5
23	.014	.02	.08	2×10^5	24	.023	.02	.08	2×10^5
23	.014	.05	.04	2×10^5	24	.023	.05	.04	2×10^5
23	.014	.02	.02	1.7×10^5	24	.023	.02	.02	1.7×10^5

3.   Performance of Re-entry-Type Axial Turbines

It is apparent, that by considering multi-stage arrangements, the rotative speed can be decreased for the same horsepower output without impairing seriously the overall turbine efficiency. Hence, multi-stage turbines tend to have higher efficiencies at lower specific speeds than single stage turbines. By designing multi-stage turbines in the conventional fashion, greater turbine weights and increased rotor complexities are the consequence. Such a design would be unfeasible for serious consideration in small accessory power units since the simplicity inherent in single disk turbines must be retained.

An attractive way of combining the single-disk design with the multi-stage performance would be the re-entry-turbine types, whereby the first stage would be, for example, a single nozzle (partial admission) turbine, figure (IV, 28). After absorbing a part of its energy in the bucket, the jet will be collected and returned to the front side of the wheel via a return duct, and again be admitted to the turbine disk, thus expending another part of its energy (pressure-staging). This process

can be continued so that an extremely high number of stages can be combined in one disk.

It is evident that additional losses, such as filling and emptying losses, leakage losses, etc., will occur in this turbine type which are detrimental to the overall turbine efficiency. The wheel friction, however, will be smaller in the single disk turbine than in the conventional multi-disk turbine, so that the single disk turbine does not only show disadvantages, but also some aerodynamic advantages. A performance analysis of this arrangement is presented in this section for different number of stages, assuming that the rotor is shrouded at the rim.

For re-entry arrangements, the turbine efficiency, exclusive of the bearing losses may be defined as:

$$\eta = \eta_H \left[1 - L_t - L_r - L_b - L_d - L_p \right] \qquad \text{IV,65}$$

where

η = Turbine efficiency

η_H = Average stage hydraulic efficiency

L_t = Average per cent tangential leakage

L_r = Average per cent radial leakage

L_b = Blade pumping loss, per cent of available energy

L_d = Disk windage loss, per cent of available energy

L_p = Scavenging loss, per cent of available energy

For impulse blading and assuming no recovery of the exhaust energy, the average stage hydraulic efficiency can be defined
(see equation (IV, 13))

$$\eta_H = 2 \left(1 + \psi_R \right) \left(\psi_n \cos\alpha - \frac{u}{V_i} \right) \frac{u}{V_i} \qquad \text{IV,66}$$

whereby for partial admission designs ψ_{R_0} has to be modified by the factor K_F of equation (IV, 14) so that

$$\psi_R = \psi_{R_0} \left(1 - \frac{t}{2a} \right) \qquad \text{IV,67}$$

when ψ_{R-0} denotes the rotor velocity ratio for full admission designs.

The arc of admission in pressure staged turbines varies from stage to stage. An average value for γ_R can be determined for n stages by letting

$$\bar{\gamma}_R = \psi'_{R-0}\left[1 - \frac{1}{n}\left(\frac{t}{2a_1} + \frac{t}{2a_2} + \ldots + \frac{t}{2a_m}\right)\right] \qquad \text{IV,68}$$

and

$$\psi'_{R-0}$$

$$\gamma_R = \psi_{R-0}\left(1 - \frac{t}{2a_m}\right). \qquad \text{IV,69}$$

for the mth stage of the turbine. Equation (IV, 68) can be expressed as

$$\bar{\psi}_R = \psi'_{R-0}\left[1 - \frac{t}{2na_1}\sum_{1}^{n}\left(\frac{a_1}{a_m}\right)\right]. \qquad \text{IV,70}$$

With identical velocity diagrams at each stage,

$$\frac{a_1}{a_m} = \frac{\rho_m}{\rho_1} \qquad \text{IV,71}$$

thus

$$\sum_{1}^{n}\left(\frac{a_1}{a_m}\right) = \sum_{1}^{n}\left(\frac{\rho_m}{\rho_1}\right). \qquad \text{IV,72}$$

The gas density ratio in equation (IV, 72) may be approximated by (ρ_m/ρ_1). The accuracy of this approximation, is dependent upon the spec. heat ratio k, as well as the stage efficiencies. It is expected, however, that the overall accuracy of this analysis will not be too adversely affected by this approximation.

Substituting the approximation

$$\frac{P_m}{P_1} = \frac{P_m}{P_1} \qquad\qquad IV, 73$$

into equation (IV, 72), then

$$\sum_1^n \left(\frac{a_i}{a_m}\right) = \sum_1^n \left(\frac{P_m}{P_1}\right). \qquad\qquad IV, 74$$

Recognizing, now, that similar velocity triangles require

$$\frac{P_0}{P_1} = \frac{P_1}{P_2} = \frac{P_2}{P_3} = \frac{P_{m-1}}{P_m} \qquad\qquad IV, 75$$

and that

$$n\frac{P_0}{P_1} = \frac{P_0}{P_n} \qquad\qquad IV, 76$$

then

$$\frac{P_m}{P} = \left(\frac{P_0}{P_n}\right)^{\frac{1-m}{n}} \qquad\qquad IV, 77$$

substituting equation (IV, 77) into (IV, 74)

$$\sum_1^n \left(\frac{a_i}{a_m}\right) = \sum_1^n \left(\frac{P_0}{P_n}\right)^{\frac{1-m}{n}}. \qquad\qquad IV, 78$$

This final equation is a geometric series, simply evaluated to yield

$$\sum_{1}^{n} \left(\frac{\bar{u}_i}{a_m}\right) = \frac{1 - \frac{P_n}{P_0}}{1 - \left(\frac{P_n}{P_0}\right)^{Y_n}} .$$

$$\text{IV,79}$$

Applying this final expression to (IV,7'') gives the blade velocity coefficient as

$$\overline{\psi}_R = \psi'_{R-q}\left\{1 - \frac{t}{2n\,q_i}\left[\frac{1 - \frac{P_n}{P_s}}{1 - \left(\frac{P_n}{P_0}\right)^{Y_n}}\right]\right\} .$$

$$\text{IV,80}$$

     Additional losses which must be considered in the single wheel pressure staged turbine are the radial and tangential leakages. If it is considered that the turbine wheel is shrouded, then the only radial leakage is inward. The tangential leakage differs on each side of the wheel in that the upstream side has a nozzle velocity component which contributes to an increased leakage flow.

    a. Tangential Leakage

      For the mth stage, the leakage flow rate will be

$$L'_t = C_f A_{rm} V_{rm} \rho_{rm}$$

$$\text{IV,81}$$

with C_f denoting an orifice coefficient since

$$V_{rm} = V_m$$

$$\text{IV,82}$$

$$L'_{tm} = C_f C^* P_{(m-1)} h V_m (1 + \sqrt{2}) .$$

$$\text{IV,83}$$

The ratio of this leakage flow to the nozzle flow is

$$L_{tm} = \frac{A_{rm} V_{rm} \rho_{rm}}{A_m V_m \rho_m}$$

$$\text{IV,84}$$

which can be expressed as

$$L_{tm} = \frac{C_f C^* \rho_{m+1}\, h\, V_a (1 - \sqrt{2})}{A_m\, h\, \rho_m\, V_n \sin \alpha} \qquad \text{IV, 85}$$

when C^* denotes the axial clearance between rotor blading and stator blading.
Equation (IV, 85) can also be written in the form

$$L_{tm} = \frac{C_f\, C^*}{a_1 \sin \alpha} (1 + \sqrt{2}) \frac{\rho_{m+1}}{\rho_m} \frac{a_1}{a_m} \qquad \text{IV, 86}$$

which then represents the ratio of the tangential leakage to the flow of the stage.
The average leakage loss is

$$L_t = \frac{C_f\, C^*}{a_1 \sin \alpha} (1 + \sqrt{2}) \frac{\rho_{m+1}}{\rho_m} \left(\frac{1}{n}\right) \sum_1^{n-1} \left(\frac{a_1}{a_m}\right). \qquad \text{IV, 87}$$

It should be noted that the series is summed to the $(n-1)^{th}$ term since the last stage will have zero leakage. Substituting from equation (IV, 78) and letting $n = m-1$

$$L_t = \frac{C_f\, C^*}{n a_1 \sin \alpha} (1 + \sqrt{2}) \left(\frac{\rho_m}{\rho_0}\right)^{1/n} \left[\frac{\left(\frac{\rho_m}{\rho_0}\right)^{\frac{n-1}{n}} - 1}{\left(\frac{\rho_m}{\rho_0}\right)^{1/n} - 1} \right] \qquad \text{IV, 88}$$

With

$$C_f \approx 2/3 \qquad \text{IV, 89}$$

$$L_t = \frac{2(1 + \sqrt{2})\, C^*}{3\, n a_1 \sin \alpha_1} \left(\frac{\rho_m}{\rho_0}\right)^{1/n} \left[\frac{\left(\frac{\rho_m}{\rho_0}\right)^{\frac{n-1}{n}} - 1}{\left(\frac{\rho_m}{\rho_0}\right)^{1/n} - 1} \right] \qquad \text{IV, 90}$$

b. Radial Leakage

The total radial leakage must be considered lost since the amount of energy represented by this flow does not contribute in the process of generating rotative power. The only leakage which must be considered in a shrouded wheel is the leakage which occurs radially inward. The leakage flow at the mth stage can be shown as

$$L_{rm} = 2 C_i C_{um}^* \rho_{cm} V_{cm} \qquad \text{III,91}$$

when C^* again denotes the axial clearance between rotor and stator. Expressing L_{rm} as an average leakage, then

$$L_r = \frac{2 C_i C^* V_c \rho_c}{a h \sin \alpha \, V_m \rho_s} \left(\frac{m-1}{2} \right). \qquad \text{IV,92}$$

Since

$$V_n = \frac{C_i}{\sqrt{n}} \qquad \text{IV,93}$$

$$\frac{\rho}{\rho_c} \approx \frac{1}{2} \qquad \text{IV,94}$$

and assuming labyrinths

$$C_i \approx \tfrac{1}{3}$$

it follows that

$$L_r = \tfrac{1}{6} \frac{C^*}{h \sin \alpha} \frac{V_c}{C_i} \sqrt{n} \, (n-1). \qquad \text{IV,95}$$

Corresponding to the density ratio described in (IV, 94), the leakage velocity is sonic, consequently

$$\frac{V_t}{c_i} = \left\{ \frac{x-1}{(x+1)\left[1-\left(\frac{p_\eta}{p_o}\right)^{\frac{x-1}{x}}\right]} \right\}^{\frac{1}{2}}$$

IV, 96

and, therefore, the final expression for the radial leakage reads:

$$L_r = \frac{c^*\sqrt{n}\,(n-1)}{6\,h\,\sin\alpha} \left\{ \frac{x-1}{(x+1)\left[1-\left(\frac{p_\eta}{p_o}\right)^{\frac{x-1}{x}}\right]} \right\}^{\frac{1}{2}}$$

IV, 97

In accordance with reference 1, the ratio of blade scavenging loss to available work is

$$L_{p_m} = \frac{1.4\left(\frac{u}{V_m}\right)^3 w}{a_m \sin\alpha}$$

IV, 98

This average scavenging loss then becomes

$$L_p = \frac{1.4\left(\frac{u}{V_m}\right)^3 w}{a_1 \sin\alpha\,n} \sum_1^m \left(\frac{a_1}{a_m}\right)$$

IV, 99

which reduces to

$$L_p = \frac{1.4\left(\frac{u}{c_i}\right)^3 w\sqrt{n}}{a_1 \sin\alpha} \left[\frac{1-\left(\frac{p_m}{p_o}\right)}{1-\left(\frac{p_m}{p_o}\right)^{1/n}}\right]$$

IV, 100

Reference (2) gives the disk frictional windage loss as

$$L_d^* = \frac{0.06\,\rho\,d^2\,u^3}{10^6} \qquad (h_p)$$

IV, 101

and as a percentage of the total available power.

$$L_d = \frac{.0424 \, P d^2 \, u^3}{W_a \cdot \frac{c_i^2}{2g \, J}} \times 10^{-6} \qquad \text{IV,102}$$

Since

$$W_a = \rho \, c_i \, A_j \qquad \text{IV,103}$$

where A_j is the exit area of the ideal jet of a single stage machine, thus

$$L_d = 2.1 \times 10^{-3} \left(\frac{d^2}{A_j}\right)\left(\frac{u}{c_i}\right)^3 . \qquad \text{IV,104}$$

Reference (2) gives the blade pumping loss as

$$L_c^* = 1.3 \times 10^{-6} \rho \, u^3 d^2 (1-\lambda)\left(\frac{h}{D}\right)^{1.5} . \qquad \text{IV,105}$$

The symbol λ represents the ratio of the active-to-total blading, hence

$$\lambda = \frac{\sum\limits_{n} a_m}{\pi D} \qquad \text{IV,106}$$

which then reduces to

$$\lambda = \left[\frac{\left(\frac{p_1}{p_m}\right) - 1}{\left(\frac{p_o}{p_m}\right)^{1/n} - 1}\right] \frac{a_1}{\pi D} \qquad \text{IV,107}$$

Finally, the blade pumping loss expressed as a ratio of the available power reads

$$L_b = 38 \times 10^{-3} \left(\frac{D^2}{A_j}\right)\left(\frac{u}{c_i}\right)^3 \left(\frac{h}{D}\right)^{1.5}(1-\lambda)$$

IV, 108

Using the above devised relations the efficiencies obtainable with re-entry-type turbines for up to 16 stages is calculated by assuming the following values:

Stator angle   15 degrees

Number of blades   100

Minimum aspect ratio   .75

Minimum h/D ratio   .04

Axial clearance ratio c/D .001

Pressure ratio   16:1

The results are shown in figure (IV, 29) by plotting the efficiency as a function of specific diameter for different specific speeds and different stage numbers. An inspection of this diagram reveals that the efficiency can be improved 33 per cent at a specific speed of 3 when the number of stages is increased from 1 to 4 and can be improved 50 per cent at specific speeds of 1 when the stage number is increased from 1 to 8. It is also interesting to note that the optimum specific diameter decreases with increasing stage numbers for constant specific speeds, meaning that smaller rotor diameters result by multiple-staging; this compensating somewhat for the weight added by the return channels.

By plotting the maximum obtainable efficiencies as function of specific speed, a diagram as shown in figure (IV, 30) results, which also shows the efficiency gains, obtainable with multiple staging. Figure (IV, 30) also reveals that stage numbers exceeding 8 will show advantages only for specific speeds smaller than 1 revealing that the maximum stage number to be considered in typical accessory power turbines should not exceed 8.

It must be emphasized that the quoted axial clearance is an absolute pre-requisite and probably the most decisive parameter for obtaining the calculated efficiencies, in contrast to the information in figure (IV, 15) which shows the insensitivity of single stage designs to axial clearance. It stands to reason that an increase in axial clearance in pressure staged re-entry-type axial turbines must increase the leakage and consequently, "spoil" the energy con-siderably for the subsequent stages so that the merit of multiple staging is nullified at excessive axial clearances.

It is also to be noted that no reference is made to the location of the exhaust ports of the different stages and their location due to a lack of pertinent information of its influence on the performance. It is assumed that the losses incurred by the re-entry channel (and exhaust port geometry) are covered by the assumption that the absolute leaving velocity of every stage is lost entirely. This assumption is not yet substantiated by test results thus demonstrating the preliminary character of the information on re-entry-type turbines presented in this section.

A test turbine has been manufactured which allows to test different versions of re-entry arrangements. Test runs are scheduled for the month of June, and will be reported on in the next progress report.

4. Conclusions

The analysis presented in Section IV-B2 and IV-B3 allows the formu-lation of some interesting conclusions dealing with design criteria for partial admission (low specific speed) and full admission (high specific speed) turbines. Critical design parameters for low specific speed turbines are the aspect ratio, pitch chord ratio, blade height-to-diameter ratio of the rotor and the degree of admission. Investigations show that comparatively small aspect ratios are admissible in full admission turbines, i.e. high specific speed designs, but are intolerable at low specific speeds. Optimization studies indicate that the aspect ratio should increase with decreasing specific speed in order to obtain high efficiency. Another parameter which has considerable influence on the performance of low specific speed turbines is the ratio of blade height to rotor diameter. Optimum values for this parameter are primarily a function of specific diameter and specific speed, decreasing with decreasing specific speeds and increasing specific diameters.

These conclusions are in many aspects well substantiated by test data, where aspect ratios of .35 and h/d ratios of .05 gave an efficiency of only .25 per cent at specific speeds of 4, whereas aspect ratios of .75 and h/d values of .0375 indicate an efficiency of 50 per cent at the same specific speed. The difference in efficiencies of the above two designs is even more pronounced at lower specific speeds. This means that optimization of the cascade parameters is extremely critical for low specific speed turbines.

Another, but still preliminary conclusion, is that multiple staging on a single wheel, providing that small axial clearance between rotor and stator can be maintained, appears to yield appreciable improvements on turbine efficiencies for the low specific speed regime. These improvements are noticeable particularly in the low specific speed regime where a 4-stage design increases the efficiency by about 20 per cent at specific speeds of 7 whereas 8 stages improves the efficiency by about 40 per cent at specific speeds of 1.5. These investigations also indicate that an increase in the number of stages above 8 does not result in better turbine performance.

C   Terry -Type Turbines

Terry turbines are presently almost exclusively used in the low specific speed range. They are conventionally built as partial admission turbines, pre-dominately with a single nozzle admission. A typical cross section is shown in figure (IV, 31) which indicates that the jet is directed against the rim of the rotor into circular buckets. In these buckets, the jet is deflected by 180 degrees and leaves the rotor with a flow angle as prescribed by the boundaries of the bucket. These buckets fulfill the same purpose as the rotor blades in axial turbines. The difference is however, that the jet is deflected by 180 degrees instead of the more usual 120 degrees in axial-type turbines. Another difference is that the jet in the rotor has one open boundary since the rotor channel provides only three walls instead of the usual four walls found in conventional cascades In almost all other respects the working mechanism is about the same as in axial, partial admission turbines. The notations, as shown in figure (IV, 31) indicate that the two most important geometrical criteria are the nozzle angle α_2 and the blade leaving angle β_3 which usually is equal to the rotor inlet angle β_2 .

In order to analyze the performance of this turbine-type, a similar procedure, as described for axial turbines, can be applied. With this concept the head transferred into shaft power is expressed by equation (IV, 11). It appears justified to assume that the typical partial admission losses in terry-type turbines are equal in magnitude, as well as tendency, as the partial admission losses in axial turbines, so that equation (IV, 14) and (IV, 15) also become applicable In section (IV, C1) this assumption will be discussed in more detail. The head, however, lost due to blade pumping in the unadmitted part of the arc is somewhat different from equation (IV, 19) mainly because the blades in terry turbines are shrouded in a radial direction and open only at the rim. Reference 3 indicates that an equation of the form

$$ L = \frac{u^3 r\, K_w}{g} D \left[D + 5 e \frac{K_p}{K_w} \left(1 - \frac{a}{\pi D} \right) \right] \qquad \text{IV,109} $$

is applicable for expressing the wheel disc friction loss of the turbine disc and the blade pumping loss at the wheel rim where K_W denotes a loss coefficient for the wheel disc friction and K_p a loss coefficient for the pumping loss and e the wheels width. For K_W the values as given in figure (IV, 2) can be used. The discussion of drag coefficients presented in section VI-A1 makes it evident that the value K_p depends on the nozzle angle β_3 (see figure 7 in section VI, A1) and on the ratio $\frac{DN}{e}$ (see figure 6a in section VI-A1). It appears that an average value of $K_p / K_W = 3$ is suitable for most terry turbine designs.

It is therefore possible to write a relation for the efficiency of terry turbines which is similar to equation (IV, 27). By observing the notations presented in figure (IV, 31) for terry-type blading, the efficiency of terry turbines can be written in the form

$$ \eta = \frac{H_5 D_2}{77} \left[1 + \gamma_R (1 - D_3^2\cos\alpha) \frac{1}{\sqrt{N}} \sqrt{2g} \frac{1}{2e} \frac{h}{D} \right]\left[\gamma_N \cos\alpha - \frac{u_3 D_3}{154} \right] - \frac{H_5^3 D_3^3 \, 1.4 \sqrt{2g}}{(154)^3} \frac{h}{D} \frac{2e}{D} $$

$$ - \frac{2 H_5^3 D_3^5 \sqrt{2g}\, K_W}{154^3} \left\{ 1 + 5 \frac{K_p}{K_W} \frac{e}{D} \left[1 - \frac{1}{D_3^2 \left(\frac{h}{D}\right) \gamma_N \sin\alpha \sqrt{2g}} \right] \right\} \qquad \text{IV,110} $$

when r denotes the mean radius of the rotor blades, figure (IV, 31), h the axial width of the nozzle, whereby ψ_R again is a function of the rotor blade geometry and blade angle β_{4-2} which is related to the nozzle angle by equation (IV, 7) for design point operation (incidence-free inlet of nozzle jet into rotor bucket). It is evident that equation (IV, 110) is similar to equation (IV, 27) which describes the efficiency for axial turbine and that the enumeration of significant design aspects, presented in section IV-A also is valid for terry-type turbines.

1) Investigation of Losses

The largest unknown for terry turbines is the rotor loss coefficient ψ_R. It is to be expected that its value depends on the geometrical channel configuration i.e., deflection angle, radius of curvature, and blade spacing. It is not obvious that loss coefficients measured in cascades or ducts, and published in the literature, can be used as reference since a typical terry bucket has only three walls, therefore, allowing the jet to seek its own boundary at the "open" side of the channel without being forced into a given direction by a regular channel, except for the direction imposed on the flow by the blade angle β_{4-3}.

In order to investigate the ψ_R values some experimental data on typical terry-type wheels were examined. The stall torque T_{st} obtainable with the different bucket designs was measured in a test fixture as sketched in figure (IV, 32). This method can be expected to yield reasonable values since the stall torque, after assuming a reasonable nozzle coefficient, depends mainly on the rotor velocity coefficient if the nozzle and blade angle are known since

$$T_{st} = \frac{W D c_i \psi_N}{2g}\left(\cos\alpha_2 + \psi_R \cos\beta_3\right) \qquad IV,111$$

or

$$\psi_R = \frac{\dfrac{T_{st}\,2g}{W D c_i \psi_N} - \cos\alpha_2}{\cos\beta_3} \qquad IV,112$$

Since weight flow W and spouting velocity c_i are directly measured, the coefficient ψ_R is computed after introducing α_2 and β_3. It is to be noted that the angle β_3 is imposed on the bucket flow by the blades so that this value is shown from the rotor geometry.

Since the nozzle angle α_2 could be changed and since the same nozzle was used for all experiments, valid indications about the maximum obtainable velocity coefficient ψ_R for the different bucket designs could be expected. In running these experiments, the position of the rotor in regard to the nozzle was changed progressively so that the variation in stall torque with relative blade position was measured. Some typical results are shown in figure (IV, 33) where the solid line resulted for a wheel with comparatively narrow blade spacing whereas the dotted stall torques result for rotor designs with comparatively wide blade spacings. Table B gives the different geometries of the investigated rotor buckets.

TABLE B

Bucket No.	β	z	e	γ	H	t	T	R	x_{mean}	$\frac{c}{h}$	$\frac{T}{t}$	$\frac{R}{x_{mean}}$
1	31.7°	42	.45	180°	.1	.205	.015	.225	.41	3.22	.073	.55
2	24.5°	25	.45	180°	.1	.342	.101	.225	.25	3.22	.296	.9
3	31.1°	45	.45	180°	.063	.192	.07	.225	.2	3.22	.354	1.12
4	31.25°	23	.45	180°	.15	.376	.088	.235	.26	3.22	.234	.865
5	31.25°	33	.45	180°	.1	.262	.07	.225	.21	3.22	.367	1.07
6	31.25°	33	.45	120°	.1	.262	.07	.225	.21	3.22	.267	1.07
7	31.25°	35	.38	180°	.1	.248	.056	.187	.17	2.72	.226	1.1
8	31.25°	29	.62	180°	.1	.296	.104	.31	.3	4.43	.352	1.048

This table indicates that the blade angle $\beta_{b.3}$ was about 31..2 degrees, with the exception of bucket number 2, that blade number z was varied from 45 to 25; and that the wheel width e was changed from .38 inches to .62 inches whereas the rotor diameter was held constant with D = 2.75 inches. With these bucket designs the ratio e/h was changed from 2.72 to 4.43. Most of the test data were obtained at a value of e/h = 3.22.

Accounting first for the maximum stall torques (peak values in figure (IV. 33) and converting these data to ψ_R values by using equation (IV, 112) a diagram as shown in figure (IV, 34) is obtained showing $\psi_{R_{max}}$ as a function of a/t. Maximum ψ_R should be expected at a/t values of 1, 2, or 3 since only for these cases the nozzle jet fills the buckets completely. All other values of a/t mean that some of the buckets are only filled partly by the nozzle jet, thus forcing the jet to expand suddenly and creating mixing losses. This means that only ψ_R values near a/t= 1 or 2 or 3 give valid indication of maximum ψ_R values, and this only when no incidence losses occur at this condition ($\alpha_2 \approx \beta_2$) or when the incidence losses are small and can be neglected. The points of zero incidence are marked by arrows in figure (IV, 34). If it is considered that α_2 becomes larger than β_2 when a/t becomes smaller than a/t for incidence-free inlet (due to the variation of "a" with nozzle angle α) it is evident that buckets 1, 3, and 4 (particularly bucket 1) sustain incidence (separation) losses at the suction side of the blades at the optimum a/t value which means that no correct values for ψ_R are obtained for these buckets. All other buckets have incidence (separation) losses at the pressure side of the blade at optimum a/t values so that the calculated ψ_R values are not greatly falsified and most likely somewhat conservative.

With this interpretation it results from figure (IV, 34) that bucket number 5 has the highest ψ_R value (e/h = 3.22) and that e/h $\lessgtr$ 3.22 yield smaller ψ_R values. Hence it appears possible to represent this tendency in a diagram as shown in figure (IV, 35). This tendency appears reasonable for low e/h values since for e/h = 2 the turning radius would be zero, thus causing extreme turning losses. For large e/h values increasing wall friction is encountered suggesting that at some mean e/h values give smallest losses. That the optimum value occurs at e/h = 3.22 i.e. r/h = .621 is somewhat surprising since information published in the turbine literature (reference 11) on the influence of r/h in conventional channels, figure (IV, 36), would suggest larger optimum values for r/h and consequently e/h. Although a significant difference exist between a conventional cascade and a terry bucket, namely, the "open" boundary at the radius r in terry buckets, which may justify a change in optimum r/h

ratios, it has to be noted that the optimum e/h ratio shown in figure (IV, 35) is based on an exceedingly small number of test points and, therefore, not sufficiently substantiated. For lack of additional pertinent information, however, the optimum value shown in figure (IV, 35) is used in this report.

It is also interesting to plot ψ_R as a function of R/x_m for constant e/h ratios as shown in figure (IV, 37), whereby x_m is the bucket depth at the mean stream line. It is evident that the mean turning angle γ is smaller than 180 degrees when $R/x_m > 1$ so that a rapid decrease of ψ_R for $R/x_m > 1$ should be expected (since the definition of ψ_R assumes $\gamma = 180$ degrees so that $\gamma < 180$ degrees yields smaller w_{u-3} values i.e. smaller stall torques and consequently smaller ψ_R values). This tendency is reflected in figure (IV, 37), however, the regime of $R/x_m < 1$ is uncertain since the only point in this regime is bucket number 1.

It would, however, not be unreasonable to assume a decrease of ψ_R for $R/x_m < 1$ since the leaving component will tend to interfere with the incoming jet in this case as sketched in figure (IV, 38).

It is also interesting to note that a deflection of $\gamma = 120$ degrees gives no advantage as evidenced by the low ψ_R value of bucket number 6. This however, does not exclude the possibility that a $\gamma > 120 < 180$ might give optimum ψ_R values.

The above considerations dealt only with the peak stall torques obtained on the described experiments. An interesting feature is revealed when the average stall torque is considered which is obtained by integrating the curves in figure (IV, 33). These mean values are listed in table C for the different bucket designs together with the corresponding velocity coefficients and $t/2a$ values.

TABLE C

Bucket No.	α	$\psi_{R_{max}}$	a_t	$\psi_{R.average}$	$\psi_{R_{max}}(1-\frac{t}{2a})$	$\frac{\psi_{average}}{\psi_{R_{max}}(1-\frac{t}{2a})}$
1	36.5	.74	1.61	.448	.512	.875
2	36.5	.227	.97	.107	.11	.97
3	36.5	.741	1.72	.435	.525	.83
4	39	.285	.84	.082	.115	.71
5	36.5	.63	1.27	.295	.38	.78
6	36.5	.525	1.26	.262	.316	.83
7	36.5	.432	1.33	.255	.27	.945
8	36.5	.288	1.11	.13	.158	.82

Multiplying ψ_{R-max} with $(1-t/2a)$, values as listed in column 5 of table C are obtained which are in fair agreement with ψ_R values discussed before. This leads to the assumption that the difference between maximum and average (integrated) velocity coefficient is fairly well expressed by the relation $\psi_{R_{mean}} = \psi_{R_{max}}(1-t/2a)$ used in the derivation of equation (IV, 110). Since the $\psi_{R_{mean}}$ values represent the average velocity coefficient which a partial admission wheel would experience under running conditions, the above finding can be interpreted as preliminary proof that the typical partial admission losses caused by filling and emptying losses are correctly presented by equation (IV, 14) also for terry turbines. This conclusion must be considered preliminary since insufficient test data is available.

The result of the above analysis can be summarized by the conclusion that maximum turbine efficiencies result when e/h = 3.25 and R/x_m = 1. It is to be noted that no particularly detrimental effect was found for the rim blockage ratio T/t within the investigated range of T/t = .07 to .3.

This finding is preliminary and somewhat sketchy since the variation in the investigated bucket geometries was insufficient to determine the influence of the t/h ratio (corresponding to the pitch-chord ratio in axial turbines) on the rotor velocity coefficient. It is, however, assumed that this influence is of minor consequences. As shown in more detail in section C-12,

definite limits are imposed on this ratio by manufacturing considerations. These limitations appear to restrict the range of feasible t/h ratios to values which would be expected to be close to optimum.

IV-C2 Performance of Single Stage Turbines

Having found by the investigations described in section IV-C1 that bucket velocity coefficients of $\psi_R \approx .80$ to .90 can be obtained for the optimum geometry, it is now possible to introduce these values into equation (IV, 110) and to calculate the maximum obtainable efficiencies as a function of specific speed and specific diameter, when it is observed that certain definite relationships exist between the x/D value, the blade number, and the nozzle angle. This interrelationship is predicated on the necessity to avoid the undercutting of the buckets i.e., by observing that the distance b in figure (IV, 31) has to be smaller than the bucket depths x. With some simplifying assumptions the maximum allowable x/D ratio can be determined and be presented by the relation

when
$$\frac{x}{D} = \frac{\pi(\varphi - 2x^*)\sin(\beta + \alpha^*)}{360 \sin \varphi} \qquad \text{IV,113}$$

$$\sin \alpha^* = \frac{\sin \beta - \sqrt{\sin^2 \beta - \cos \beta + \%}}{2 \cos \beta} \qquad \text{IV,114}$$

and

$$\varphi = \frac{360}{z} \qquad \text{IV,115}$$

Equations (IV, 113), (IV, 114), (IV, 115) indicate that the ratio x/D is a function of blade number z, the blade angle θ, and the ratio of slot heights H to wheel diameter D. This relation is graphically presented in figure (IV, 39) by showing the maximum x/D value as a function of blade number for different blade angles and certain assumed (as suggested by manufacturing considerations) values of H/D. The right hand scale on this diagram also indicates the maximum h/D values since for the optimum geometry

$$\frac{X}{D} = 1.625 \frac{h}{D} \cdot \qquad\qquad \text{IV-116}$$

Additional lines in this diagram represent lines of constant blockage ratio $T_{/t}$ since this value is directly connected with the other values, namely

$$\frac{T}{t} = \frac{2\alpha^*}{\varphi} \cdot \qquad\qquad \text{IV,117}$$

The experimental data cover only bucket designs up to blockage ratio of $T_{/t} = .3$. It becomes evident, therefore, that only the shaded part of the diagram is directly applicable for further calculations.

Equation (IV, 110) indicates that for most cases maximum efficiencies will occur where the ratio of h/D_z becomes a minimum. This means, according to figure (IV, 39) that in all cases the maximum possible blade number should be applied. Observing now, additionally, the interrelationship between the blade angle β, nozzle angle α and specific speed and specific diameter as indicated in equation (IV, 7), and observing also that the ratio r/D is directly connected with the ratio $h/_D$, since

$$\frac{r}{D} = \frac{x + \frac{1}{2}}{D} = 2.125 \frac{h}{D} \qquad\qquad \text{IV,118}$$

it is now possible to compute the $N_s D_s$ diagram for terry-type turbines after assuming suitable suitable angles α and suitable ratios of h/D, whereby the minimum h value is determined by the smallest feasible cutter width. A typical diagram is shown in figure (IV, 40) which indicates similar tendencies as reported for axial turbines with efficiencies, however, somewhat lower than the corresponding axial turbine design. This is particularly evident at low specific speeds and large specific diameters, whereas at small specific diameters only minor differences in efficiency for terry and axial turbines exist. This deficiency

is caused by the comparatively low blade number resulting from figure (IV, 39)
for typical terry-type buckets, if a maximum blockage of .3 is not to be exceeded.
Since larger blade numbers will increase the maximum efficiency obtainable
at low specific speeds it is worthwhile to consider modifications of the terry
bucket to a form which allows larger blade numbers.

It is evident from figure (IV, 39) that larger blade numbers can be applied
if larger blockage ratios are tolerated. Since an adverse effect of blockage on
rotor velocity coefficient must be expected, it appears advantageous to consider
a terry bucket geometry which is obtained by two cuts rather than a single cut
as assumed for the relations shown in figure (IV, 39). This way the manufactur-
ing cost of the terry wheel, an important criterion for accessory power units, is
increased somewhat, but still less than the manufacturing cost of a corresponding
axial wheel. With this method a terry bucket as shown in figure (IV, 41) results
which eliminates the blockage entirely and shows a blade of almost constant
thickness. This shape suggests that such a wheel could be fabricated by a
different technique, namely, by inserting sheet metal blades into slots. This
type of bucket changes the bucket geometry from a parallel walled shape to a
converging shape. This, however, does not necessarily mean that the jet will
be accelerated first and then decelerated since due to the one open boundary the
jet can still pass through the bucket at constant velocity by merely changing its
geometrical shape. This means that equation (IV, 118) is invalidated since now
the turning radius of the jet within the bucket moves closer to the rim. Account-
ing for this in an approximated form by modifying equation (IV, 118), the blade
number for most designs can be increased by about 30 to 40 per cent without
encountering limiting cutter dimensions. This limit could probably be extended
even further if sheet metal blades, as described above, are applied. With these
assumptions, a new N_s D_s diagram for terry-type turbines has been calculated,
figure (IV, 42), which shows substantial improvement in maximum obtainable
turbine efficiencies at low specific speeds and large specific diameters, i.e.
typical partial admission designs approaching the performance of axial turbines
quoted in figure (IV, 23) i.e., axial turbines with a comparatively small
number of blades. It is to be noted that, strictly speaking, a slight change in
bucket velocity coefficient has to be expected with the different bucket geometry.
It appears, however, that this change is of minor influence since the data presented
in figure (IV, 42) have already partly been substantiated by test data, namely, in
the specific speed regime from 25 to 7 at specific diameters between 6 and 13.

Terry-type turbines are, in general, less costly from a manufacturing point of view than axial turbines, particularly if a single nozzle can be applied. It is, therefore, of interest to indicate in the $N_s D_s$ diagram the range which can be covered with such simplified designs. Figure (IV, 43) makes it evident that only for comparatively small values of f/D the nozzle jet will enter the buckets without striking over the wheel rim. From this diagram a relationship between the maximum allowable f/D value and nozzle angle can be computed which is equivalent to the maximum h/D value for round nozzles. This interrelationship reads

$$\frac{f}{D} = \cos\alpha \left[\cos\alpha + tg\alpha \sin\alpha - 1 \right] \qquad \text{IV, 119}$$

and is graphically presented in figure (IV, 44) indicating that the nozzle angle has to increase with increasing f/D values. If it is furthermore assumed that the jet diverges after leaving the nozzle with a divergence angle of 6 degrees, the safe nozzle angle is smaller from the angle α quoted in figure (IV, 44) by 6 degrees as indicated by the lower scale in figure (IV, 44). This information can now be plotted by a limiting line in the $N_s D_s$ diagram as shown by the dotted lines in figure (IV, 40) and (IV, 42) meaning that only values on this line can be covered by a single nozzle, terry-type turbine. The relation for this line reads

$$D_s = \frac{154 \times 2\pi}{\sqrt{\gamma_N} (2g)^{3/4} 2 \sin 2\alpha \ 60 \left[\cos\alpha + tg\alpha \sin\alpha - 1 \right]} \qquad \text{IV, 120}$$

indicating that single nozzle, terry-type turbines are characterized by a constant specific diameter, whereby its numerical value depends almost exclusively on the nozzle angle, decreasing with increasing nozzle angles (in contrast to single nozzle axial turbines which occur at constant $N_s D_s$ values, depending on nozzle angle due to the change in optimum h/D ratio with D_s). A numerical evaluation of equation (IV, 120) reveals that for nozzle angles of α 20 degrees, $D_s = 16.3$ and for $\alpha = 25$ degrees, $D_s = 8.4$. Since for this range of nozzle angles the maximum obtainable efficiencies vary only very little with N_s and D_s (since larger nozzle angles cause larger blade angles thus allowing larger blade numbers which compensate for the detrimental effect of increasing nozzle angles) so that

typical single nozzle terry turbines cover a specific speed range from $N_s = .6$
to 8 fairly effectively restricting, however, the maximum efficiency to or about
40 per cent as indicated in figure (IV, 42). Higher maximum efficiencies are
obtainable with multiple or oval nozzle shapes.

No data have been found regarding the influence of Reynolds number and
tip clearance on the terry turbine efficiency. It can be assumed, however, that
the influence of Reynolds number on terry turbine efficiency is similar as in
axial turbines so that equation (IV, 56) becomes applicable also for terry-type
turbines. The influence of trailing edge thickness of the nozzle should be similar
in terry-type turbines as in axial turbines so that a relation similar to the one
quoted in equation (IV, 64) should be applicable.

It is to be noted that the bucket velocity coefficients shown on figure
(IV, 34), (IV, 35), and (IV, 37) are obtained in a completely open wheel (see
figure (IV, 32). In spite of this open arrangement comparatively large velocity
coefficients are obtained, implying that the rim clearance, found somewhat
critical in axial turbines, has little, if any, influence on terry-type turbines.
This result appears reasonable since even with large gaps between rotor and
stator housing, all of the jet will pass through the terry bucket as long as the
proper nozzle angle is selected. Hence, it is assumed unnecessary to make
corrections to the shown efficiencies if the gap between rotor and stator shroud
is comparitively large.

The distance between nozzle and rotor is of similar influence in terry
turbines as found previously in axial turbines. Figure (IV, 45) shows the change
in stall torque with distance as measured in the test fixture described in
figure (IV, 32).

Due to similarity in flow mechanism, as well as performance, it is to
be expected that multiple staging as discussed in section (IV-B3) for axial turbines
will have similar beneficial effects on the performance at low specific speeds
as discussed in section (IV-B 3) for axial turbines. If the multi-stage arrange-
ment is obtained by pressure staging, the clearance between rotor and station-
ary shroud will, however, have a similar importance as in axial turbines in
contrast to single stage operation. It stands to reason that multiple staging
is somewhat easier from a manufacturing point of view in terry turbines than
in axial turbines since the return staging could easily be incorporated into the
stationary shroud without undue complications. It might even be expected that
the beneficial effect of multiple staging is somewhat better in terry turbines

The main difference for axial turbines is that partial admission (low specific speed, high specific diameter) turbines must show a comparatively short blade height for efficient operation whereby the ratio of blade height to rotor diameter must decrease with decreasing degrees of admission, i.e., decreasing specific speeds. In contrast, full admission (high specific speed, low specific diameter) turbines must show a comparatively long blade height for efficient operation. For both designs the number of blades is of particular importance, meaning that the maximum blade number should be selected for the rotor. This criterion is of some importance in full admission turbines, but of particular importance in partial admission turbines, indicating that a smaller than optimum blade number has a considerable effect on partial admission turbines, i.e., low specific speed turbines, but a comparatively small effect on the maximum obtainable efficiency in full admission turbines. This influence can conveniently be expressed by the ratio specific diameter over blade number D_s/z meaning that the efficiency decreases almost proportionally with increasing D_s/z values. This ratio also influences the effect of tip clearance on maximum obtainable efficiency in a similar fashion revealing that partial admission turbines are considerably more sensitive to increased tip clearances than full admission turbines. The same holds for the influence of the trailing edge thickness on maximum obtainable efficiencies.

Multiple staging on a single axial wheel has also been investigated for axial-type turbines, indicating that considerable gains in efficiencies can be obtained at low specific speeds by multiple staging. In these cases, however, the axial clearance between rotor and stator is of particular importance, indicating that clearance ratios of .001 must be maintained in order to obtain increased efficiencies at low specific speeds.

Terry-type turbines show a performance similar to axial-type turbines with the exception of the efficiencies obtainable at extremely low specific speeds where the axial turbine shows superiority due to the higher number of blades which can be accommodated in an axial wheel as compared to a terry wheel. In contrast to axial turbines, however, the tip clearance sensitivity in terry turbines is almost non-existent, thus accentuating the lower manufacturing cost of terry-type turbines. Since this turbine-type is particularly attractive, from a manufacturing point of view, with single (round) nozzle designs, the performance range of these arrangements was investigated and indicated in the corresponding $N_s D_s$ diagram.

All notable geometrical features considered important for the design of the different turbine types are quoted in the performance diagrams thus providing sufficient information for detailed turbine designs. This information is most complete for axial, single stage turbines, but lacking somewhat for terry turbines due to insufficient data on component performance.

V LIST OF SYMBOLS

$A\!R$	aspect ratio
a	arc of admission
a^*	cutter diameter
A	flow area
b	blade depth of terry turbine
c	absolute velocity
c_i	spouting velocity
C	chord length
C^*	axial clearance
d	disc diameter
D	rotor diameter
D_s	specific diameter
e	terry wheel width
f	scavenging coefficient, terry nozzle diameter
g	gravitational constant
h	blade height, nozzle height
H	head
K	constants
L^*	horsepower loss
L	Percentage horse power loss
N	rotative speed

LIST OF SYMBOLS

N_s	specific speed
p	pressure
Q	volume flow
r	radius in terry buckets
R_e	Reynolds number
S	pitch-chord ratio
s	tip clearance
t	pitch
u	blade speed
w	relative velocity
W	turbine weight flow
z	blade number
α	nozzle angle
β	blade angle
γ	density
$\triangle$	turning angle
ε	diameter ratio
λ	loss factor
χ	ratio of specific heats

LIST OF SYMBOLS

γ	velocity coefficient

Subscripts

F	filling and emptying
h	hydraulic
i	ideal
m	mean, meridional
N	nozzle
P	pumping
R	rotor
W	wheel disc
u	tangential
1	before nozzle
2	after nozzle
3	after rotor

VI. ANALYSIS OF DRAG TURBINES

A.   Drag Turbine Considerations Based on Drag Theory

Figure (VI, 1) shows the schematic of a drag turbine indicating that
pressurized gas enters at the inlet port, station 1, is ducted around the periphery
of the wheel and is discharged at the exit port, station 2; inlet and exit ports being
separated by a block seal (3). The flow pattern in the channel is somewhat com-
plicated, consisting of a peripheral component "c" produced by the turbine pressure
ratio, and a radial (circulatory) component c_r produced by the radial pressure
difference. In general it is assumed that these two components produce a cork-
screw-type flow pattern in the peripheral flow channel.

The drag theory offered for analyzing and calculating the performance
characteristic of drag turbines (reference 16) assumes a simplified flow pattern,
by neglecting the circulatory flow components in the drag channel, and by deal-
ing only with the peripheral components. This theory assumes that the input
head and the head transferred into shaft power depend mainly on the shear stresses τ_{fr}
between the channel flow and the stator and between the channel flow and the rotor
τ_{dr}. Thus, the input head is defined by

$$H_{IN} = \frac{\tau_{dr} a_{dr} + \tau_{fr} a_{fr}}{A_m \gamma} \qquad \qquad VI, 1$$

when

$$\tau = \frac{\gamma}{2g} V^2 \lambda \qquad \qquad VI, 2$$

denotes the shear stresses. As indicated in equation (VI, 2), a quadratic relation-
ship between shear stress and velocity v is assumed, whereby the shear velocity
for the shear stress between flow and rotor is assumed proportional to the differ-
ence in channel flow velocity c and rotor velocity u, i.e.

$$V = c - u \qquad \qquad VI, 3$$

and whereby the shear velocity for the stator is equal to the flow velocity, i.e.

$$V = c \qquad\qquad VI, 4$$

In equations (VI, 2), the drag coefficient is defined as drag coefficient per unit area.

By defining a characteristic velocity ratio

$$x = \frac{u}{c} \qquad\qquad VI, 5$$

i.e. the ratio of rotor speed to channel speed, and by defining a drag ratio

$$\delta = \frac{\lambda_{sr} a_{sr}}{\lambda_{dr} a_{dr}} \qquad\qquad VI, 6$$

i.e. the ratio of the drag forces at stator and rotor, the input head H_{in} can be presented in the form

$$q_{wd} = \frac{H_{in}}{u^2/g} = \gamma \frac{(1-x)^2 + \delta}{x^2} \qquad\qquad VI, 7$$

whereby the term

$$\gamma = \frac{\lambda_{dr} a_{dr}}{2 A_m} \qquad\qquad VI, 8$$

is defined as a geometric term denoting the ratio of the rotor frictional area a_d to through-flow area A_m times the drag coefficient at the rotor λ_{dr}.

With the above definition, the head transformed into shaft power H_{out} can be expressed by

$$q = \frac{H_{out}}{u_2^2/g} = \gamma \frac{(1-x)^2}{x} \qquad \text{VI.9}$$

so that the hydraulic efficiency follows the equation

$$z_h = \frac{q}{q_{ad}} = \frac{x}{1 + \frac{\delta}{(1-x)^2}} \qquad \text{VI.10}$$

i.e. is dependent only on the characteristic velocity ratio x and the ratio of drag coefficients δ and is independent of the geometry term γ. With the above definitions, an inter-relationship between the velocity ratio and the turbine speed ratio, defined as the ratio of tip speed to gas spouting velocity c_i, can be established which reads

$$\frac{u}{c_i} = \sqrt{\frac{x^2}{2\gamma^2[(1-x)^2 + \delta]}} \qquad \text{VI.11}$$

indicating that these two terms are inter-related by the geometry term γ and the ratio of drag coefficients δ. With equations (VI. 10) and (VI. 11), the basic characteristic of drag turbines can be plotted in terms of turbine parameters by presenting the hydraulic efficiency as a function of the turbine speed ratio as shown in figure (VI. 2). This figure makes it evident that the value of the peak efficiency depends only on the ratio of drag coefficients δ, whereas the location of this value in respect to the turbine speed ratio $\frac{u}{c_i}$ depends on the geometry term γ. This feature is expressed by plotting the hydraulic efficiency as a function of speed ratio $\frac{u}{c_i}$ times the square root of the geometry term γ.

The wheel disc friction can be accounted for by considering that the gas between the unadmitted part of the rotating disc and stator housing rotates, on the average, with half the wheel speed, thus consuming a parasitic torque of

$$T_N = \frac{\gamma}{2g}\,\lambda_w \left(\frac{1}{2}\right)^2 \dot{a}_w \frac{D}{2}.$$

VI.12

Hence, the shaft efficiency η_s can be computed from the hydraulic efficiency by a correction factor of the form

$$\frac{\eta_s}{\eta_h} = 1 - \frac{H_N}{H_{wT}} = 1 - \xi\,\frac{x^2}{(1-x)^2}$$

VI.13

whereby the term ξ represents geometrical interrelations

$$\xi = \frac{\lambda_w\, a_w}{4\lambda_{sr}\, a_{sr}}$$

VI.14

with λ_w denoting the drag coefficient for wheel disc friction and a_w denoting the wheel disc friction area.

Another important parameter which influences the performance of drag turbines is the leakage through the block seal, as well as interstage leakage caused by the static pressure decreasing gradually over the periphery thus creating cross flow leakage at opposed points of the channel. A detailed analytical treatment of the effect of leakage on turbine efficiency is given in reference 16 revealing that the ratio of leakage flow to turbine flow w_i/w is mainly proportional to the 1.5^{th} power of the ratio of clearance width h to stator channel depths H. In an approximated form the leakage ratio can be expressed by the relation

$$\frac{W_\ell}{W} = \left(\frac{h}{H}\right)^{1.5} \sqrt{\delta} \left[\frac{\pi^{1.5}\sqrt{\varepsilon}}{2\left(1-\frac{1}{\varepsilon}\right)} + 3.8\right] \qquad \text{VI,15}$$

$$= \mu^{1.5}\left(\frac{h}{D}\right)^{1.5} \sqrt{\delta} \left[\frac{\pi^{1.5}\sqrt{\varepsilon}}{2\left(1-\frac{1}{\varepsilon}\right)} + 3.8\right]$$

causing an efficiency correction factor of the form

$$\frac{\eta}{\eta_o} = \frac{1+\left(\frac{h}{D}\right)^{1.5}\mu^{1.5}\sqrt{\delta}\left[\frac{\pi^{1.5}\sqrt{\varepsilon_o}}{2\left(1-\frac{1}{\varepsilon}\right)} + 3.8\right]}{1+\left(\frac{h}{D}\right)^{1.5}\mu^{1.5}\sqrt{\delta}\left[\frac{\pi^{1.5}\sqrt{\varepsilon}}{2\left(1-\frac{1}{\varepsilon}\right)} + 3.8\right]} \cdot \qquad \text{VI,16}$$

For the weight flow passing through the drag turbine it holds

$$W = A_m \gamma_m c_m \qquad \text{VI,17}$$

which can be modified to the form

$$W = \frac{P_1}{\sqrt{RT_1}} A_m \frac{c_m}{c_L} K \qquad \text{VI,18}$$

i.e., a form similar to the weight flow term commonly used for axial and radial turbines where the factor K again is a function of the total turbine pressure ratio, increasing with increasing pressure ratios, but with numerical values which are about 50 per cent higher than the corresponding factor for axial turbines (see reference 16). It is also evident from equation (VI, 18) that the weight flow parameter, in contrast to axial and radial single stage turbines depends on the ratio of through flow velocity c_m to spouting velocity

c_i whereby this ratio is a function of the geometry term γ , the ratio of drag coefficients and the velocity ratio x since

$$\frac{c_m}{c_i}\sqrt{\gamma} = \frac{1}{\sqrt{2\left[(1-x)^2 + \delta\right]}} \qquad \text{VI.19}$$

which also can be quoted in terms of turbine speed ratio u/c_i

$$\frac{c_m}{c_i} = \frac{\frac{1}{2\gamma} - \left(\frac{u}{c_i}\right)^2}{\sqrt{\frac{1+\delta}{2\gamma} - \left(\frac{u}{c_i}\right)^2 \delta'} - \frac{u}{c_i}} \qquad \text{VI.20}$$

indicating that this parameter increases with increasing turbine velocity ratios.

The above quoted relations define the main aspects of drag turbines and demonstrate that the drag turbine performance can be presented in terms similar to the terms used in Section IV of this report, thus indicating that the same similarity parameters can be used for drag turbines, terry turbines, and axial turbines and that these terms have the same significance for the turbine-types investigated.

It is also to be noted that the above quoted relationships are valid only as long as the velocity ratio x is constant over the channel periphery, i.e., either for incompressible medii in a constant area channel or for compressible medii with a properly diverging channel.

In cases where a constant area channel is used for compressible medii the velocity ratio x changes with periphery, meaning that the efficiency changes over the periphery (see equation (VI. 10) so that the overall efficiency can be found by integrating equation (VI. 7) and (VI. 9). Evaluating this relation, a representative diagram can be plotted in a form as shown in figure (VI. 3).

by showing the hydraulic efficiency as a function of turbine velocity ratio and geometry term γ, for different density ratios, i.e., pressure ratios. This diagram indicates that for a given turbine design (constant γ value) the hydraulic efficiency decreases with increasing pressure ratios and that the peak efficiency moves to smaller turbine velocity ratios u/c_i. Selecting now, for example, a rotor drag coefficient of $\lambda_{dr} = .8$, a drag ratio of $\delta = .08$ and u value of 20, and assuming that these values are constant and independent of velocity and pressure ratio, the turbine characteristic can be represented by showing the hydraulic efficiency as a function of turbine velocity ratio u/c_i as shown in figure (VI, 4) for different pressure ratios. Additionally, by observing the influence of the wheel disc friction the efficiencies change somewhat as indicated by the dashed lines in figure (VI, 4). Accounting now, additionally, for the leakage losses, even lower efficiencies are obtained as shown in figure (VI, 4) for different clearances and pressure ratios when a wheel diameter of $D = 6$ inches is assumed. These diagrams reveal that large clearances between rotor and stator have a noticable detrimental effect on the maximum obtainable turbine efficiency, indicating that h/H values of .01 to .02 are desired for effective designs.

The above considerations make it evident that the drag theory enables the prediction of drag turbine performance in cases where the drag coefficient between flow and rotor, and the drag coefficient between flow and stator (as well as the channel geometry) are known. The drag theory, however, makes no prediction regarding the size of the drag coefficients. They must be determined experimentally.

1) Investigation of Applicable Experimental Data

An attempt is made to obtain data for the rotor drag coefficient by consulting the test data available on labyrinth seals (reference 12, 18, and 19). For this critical review, a nomenclature is selected as presented in figure (VI-5) using the same symbols as found in reference 15. This means that H denotes the stator channel depth, H' the pocket depth of the rotor, l' the blade spacing, α the blade angle against the direction of flow, s the blade thickness, and $L = D\pi$ the passage length. For arrangements which show blades on both sides of the channel, the through-flow width (equivalent to the stator channel depth for one sided blade arrangements) is denoted as 2H.

It has been found that five parameters can be defined which determine the numerical value of the drag coefficient. These parameters are:

1. The blade angle α

2. The ratio of pocket depth to stator depth $m = \dfrac{H'}{H}$

3. The blade spacing $n = \dfrac{l'}{H}$

4. The ratio of channel length to stator depth which in terms of drag channel geometry is $\mu = \dfrac{L}{H\pi} = \dfrac{D}{H}$

5. The ratio of blade thickness to stator channel depth, $^s/H$

Discussing first channel arrangements where only one side of the wall is equipped with blades, the following information has been found:

Figure (VI, 6), shows the influence of the ratio of pocket depth to channel depth and the ratio of blade spacing to channel depth on the drag coefficient λ * for blade arrangements with blade angles of α = 90 degrees, a comparatively large blade thickness (thickness ratio = 3.33 and 1.9, respectively) and μ values of 54 and 83.5, respectively, by plotting the drag coefficient as drag ratio by referring the drag coefficient to the maximum drag coefficient. This figure shows that the drag coefficient is comparatively insensitive to the ratios m and n revealing that maximum λ * values are obtained at m ratios between 1 and .5 and at n values between 4 and 18. It is to be noted that these data are obtained with comparatively large blade thicknesses and that a narrower optimum range has to be expected for smaller blade thicknesses.

Figure (VI, 6b) reveals that the insertion of blades at the surface almost doubles the resistance coefficient, λ * since for an n ratio of zero (smooth walls) the drag coefficient is only about half of the maximum value.

Figure (VI, 7) shows the influence of the channel length to channel depth ratio and the blade thickness ratio on the drag coefficient. Figure (VI, 7a) was obtained from test data on seals without blades, i.e., m - 0 whereas, figure (IV, 7b) was obtained from test data on single blades. These data show that an optimum μ value exists and that the drag coefficient is low at extremely large μ values, as well as for extremely small values, figure (VI, 7a). The blade

thickness is also a critical value as shown in figure (VI, 7b). Apparently, the blade thickness should be less than 20 per cent of the channel depth in order to obtain high drag coefficients. The data presented in figure (VI, 7b) were obtained with a single blade. It can be assumed, that for multi-bladed designs the critical blade thickness is even smaller.

In summarizing the above data, the following conclusions can be drawn:

The ratio of channel length to channel depth μ is an important criterion for the magnitude of the drag coefficient. Optimum values for this ratio appear to be between 20 and 60 for smooth labyrinth, i.e. for labyrinths without blades. A similar tendency has been found in the literature for bladed designs, although not enough test points have been found to state with certainty the optimum μ value for bladed arrangements. The insertion of blades increases the drag by factor of approximately 2 when the optimum blade spacing and optimum ratio of pocket depth to channel depth is observed. It appears likely that this factor is even larger if the optimum blade thickness ratio is observed since the factor of 2 is only correct for blade thickness ratios around 2 and 3. It appears possible to increase the difference in drag between the bladed and unbladed design by selecting smaller blade thicknesses. Differences by a factor of 4 appear to be obtainable.

Only limited information has been found on the effect of blade angle on drag coefficient for channel arrangements showing blades on one side wall. The available data show an increase in drag by a factor of about 6.3 for a Reynolds number of 10^4 when the blade angle is decreased from 90 to 40 degrees. It has to be noted, however, that the 40 degree blade test was made with extremely small thickness ratios (.041 compared to 3.2 for the 90 degree blade) and that no μ value is quoted for the 40 degree blade. It is to be expected, therefore, that the influence of the angle change might only be half of the above value, i.e. a factor of 3.15 when both blades have optimum thickness ratios. The blade spacing for the 40 degree blade was close to optimum $\ell''/H = 1.5$. The influence of this ratio on the drag coefficient in canted blades is demonstrated by the fact that the drag coefficient decreases to about 60 per cent of the previous value if the ratio of blade spacing to pocket depth is increased to 6. Comparing these data with figure (VI, 6b), it becomes apparent that the blade spacing is more critical in canted designs than for 90 degree blades. Apparently the optimum blade spacing n for 40 degree blades is closer to 1 to 1.5 as compared to 6 to 20 for the 90 degree blades.

No information was found in the literature regarding the influence of the ratio m on the drag coefficient for canted blades.

Detailed information on the influence of blade spacing n, ratio of pocket depth to channel depth m and blade angle on the drag coefficient was found in reference 20 for channel arrangements which have blades on both sides. The most significant result of these data is given in figure (VI, 8) showing the influence of the blade angle α on the drag coefficient λ^* revealing that blade angles of about 40 degrees give highest drag coefficients for this channel arrangement. This curve presents the drag coefficient for the optimum ratio of blade spacing η which changes as a function of blade angle as indicated in figure (VI, 9) revealing that larger blade spacings η are required for 90 degree blades than for 40 degree blades. This finding is in accordance with the previously quoted test data on single-sided blade rows. The data of reference 20 are somewhat different from the data quoted previously, since the drag coefficient presented in reference 20 refers only to the drag at the end of the channel. Hence, no indication of the influence of the μ- ratio can be obtained from these data. Due to the particular channel geometry selected in reference 20, the m value and n value are directly inter-related namely, m = nH/30 whereby H = 25 millimeters for the 90 degree blade and H = 20 for the 40 degree blade. Hence, the ratio of pocket depth to channel depth in all cases is proportional to the ratio of blade spacing to pocket depth, but always slightly smaller. It is interesting to note that the drag coefficient for double-sided blade rows does not decrease with increasing Reynolds numbers as found for one-sided blade rows, but is constant and in some cases even increases with increasing Reynolds numbers. The blade thickness for the double-sided channel was comparatively small, namely, blade thickness ratios of .25 to .0125. It also must be noted that the difference in drag coefficients for 90 degree blades and 40 degree blades for double-sided blade rows is the same as found previously for single-sided blade rows if the data on single-sided blade rows are referred to the same thickness ratio.

The drag coefficients determined by labyrinth tests represent combined coefficients, i.e. the sum of the rotor drag coefficient and stator drag coefficient, i.e.

$$\lambda^* = \lambda_{dr} + \lambda_{\zeta r} \qquad \qquad VI.1$$

Introducing the drag turbine nomenclature into these terms, in particular the drag ratio δ, the combined drag coefficient λ^*, found in labyrinth test data can be related to the rotor drag coefficient λ_{dr} by the relation.

$$\lambda_{dr} = \frac{\lambda^*}{1 + \delta \frac{a_{de}}{a_{fr}}}$$

$$VI, 22$$

which means that the rotor drag coefficient is smaller than the combined drag coefficient found in labyrinth data and that this difference depends on the drag ratio and on the ratio of frictional area at the blades and at the stator. The ratio of frictional areas is about unity in one sided channels, but considerably larger at double-sided blade rows. For the arrangement tested in reference 20, this ratio varies from values of $\frac{a_{de}}{a_{fr}}$ from 150 to 7.5, but varies over a considerably smaller range, namely, 100 to 50 for arrangements yielding maximum drag coefficients; λ^*.

In estigating first single-sided blade rows in more detail and remembering that the difference in drag coefficients between a smooth wall and a bladed wall with blade angles of $\alpha = 90$ degrees is equal to 4 (δ = .25), it is found that the rotor drag coefficient for this arrangement is 80 per cent of the combined drag coefficient. This would mean that numerical values of λ_{dr} = .12 to .15 result for this arrangement. According to reference 16, a δ value of .25 means drag turbine efficiencies of about 20 per cent for density ratios of 2 to 4. Available test data on drag turbines indicate that the maximum obtained efficiency for blade angles of 90 degrees and close to optimum channel geometry is about 20 per cent, thus revealing good conformity between labyrinth data and drag turbine data. By changing the blade angle to 40 degrees, the ratio of the drag coefficient at the bladed and unbladed side increases by a factor of 3 so that now the δ ratio becomes .083. This means that the rotor drag coefficient for this arrangement is 92 per cent of the combined friction coefficient yielding numerical values for the rotor drag coefficient of .4 to .42. According to reference 16, a δ value of .083 would yield drag turbine efficiencies of about 32 to 33 per cent when operating on density ratios of around 2. This value was obtained with drag turbines showing 40 degree blade angles and close to optimum channel geometry (see figures (VI, 3) and (VI, 4)) thus again demonstrating good conformity between labyrinth data and drag turbine data.

For double-sided blade rows, the combined friction coefficient reported in the literature is about four times as high as the drag coefficient for single-bladed rows. This would imply that the δ value becomes about .02 which, according to reference 16, means turbine efficiencies of about 50 per cent for expansion ratios of 2. Turbines built with such a blade arrangement (inside channels as shown in figure (VI, 5b) however, did not yield such high efficiencies.

in fact, gave only about the same efficiency as outside channels, i.e., a maximum of 34 per cent. It is conceivable that an unfavorable channel geometry was selected for the inside blade arrangement. Since reference 20 does not quote the influence of the μ value on the drag coefficient it is not possible to compare the test data on drag turbines with labyrinth data for this particular arrangement. Since double-sided blade rows show combined drag coefficients to be independent of Reynolds number, it is to be expected that small δ values for this arrangement will be obtained with comparatively large channel width (2H) implying that the optimum channel geometry for inside blade arrangements occurs at smaller μ values than for outside blades. The inside channel tested had μ values of about 20, i.e. the same μ value found close to optimum for outside channels.

Additional information on the rotor drag coefficient is obtained by analyzing the test data on drag pumps. For this purpose, the shutoff head as a function of drag pump geometry was investigated, since the shutoff head is directly related to the rotor friction coefficient by

$$\frac{H \lambda J_2}{u^2/g} = \hat{\jmath} \sim \Delta - s = \gamma - \lambda_{dr} \frac{Q_{dr}}{2 A_m} \qquad\qquad VI.23$$

In order to account properly for the slightly different channel geometries, an additional geometry factor, namely, the rim clearance factor,

$$y = \frac{s}{H} \qquad\qquad VI.24$$

is defined which represents the ratio of the rim clearance τ to the stator channel depth H. It was found that this factor has a comparatively small influence on the rotor drag coefficient as shown in figure (VI. 10), where the variation in drag coefficient is plotted as a function of the y value for different geometries, i.e. different μ values. It is evident from this diagram that the drag coefficient decreases slightly with increasing y values and that y values of about .2 or less yield maximum drag coefficients. In figure (VI. 11), the calculated rotor drag coefficients are plotted as a function of μ . These data reveal considerable scatter. This can be reduced slightly, if additionally, the other characteristic values, such as the y and m factor are considered. (No information was given in the test for the n value. It is assumed, that the n value incorporated in the

drag pumps was close to optimum). As evident from the previous discussion,
maximum drag coefficients of the rotor should be expected for m values between
1 and 3. The points denoted as squares in figure (VI, 11) refer to m values of
the quoted range. For the other points, the m value was smaller than 8. Con-
sidering now the test data with optimum m values exclusively, it is found that
these points indicate the highest rotor drag coefficients, and confirm the pre-
viously discussed trend. It is, also, to be noted that the drag coefficients
decrease with increasing μ values. i.e., reveal a tendency as found previously
in labyrinth data. It is, however. to be expected that the decrease in drag co-
efficients with increasing μ values is not quite as pronounced as apparent
from figure (VI, 11). This becomes more obvious if it is considered that large
μ values mean comparatively small channel depths. Since the leakage
increases considerably with small channel depths, assuming that the clearance
between rotor and stator is almost constant, it becomes evident that large μ
values also mean comparatively large leakage flows. The shutoff head obtained,
however, is particularly sensitive to the leakage so that for the ideal machine,
i.e. for a machine without leakage, larger shutoff heads are to be expected at
large μ values than indicated in the test data. This then in turn means that
drag coefficient for the rotor should be larger in the ideal machine than indicated
on figure (VI, 11). In this respect, it would have been better to evaluate the
performance data at the optimum pump efficiency point for determining the rotor
drag coefficient. This, however, can only be done when the efficiency is known
for this point, which was not quoted in the references (reference 20 to 25).

For blade angles $\alpha = 40$ degrees, a similar tendency has been observed
namely, a decrease in rotor drag coefficient with increasing μ values. Com-
paring these data with the data for pumps having blade angles of 90 degrees, a
difference in drag coefficients of 3.1 is found for constant μ values, thus again
confirming the labyrinth test data which show the same difference in drag co-
efficients as a function of blade angle.

Both data refer to outside channels, i.e. to arrangements where only
one side of the channel has blades. It is to be noted that the influence of the
blade angle decreases with increasing μ values meaning that for large μ
values, 90 degree blades are just about as effective as canted blades. This,
again, is in accordance with the labyrinth seal data (reference 26), which
indicates that the influence of the blade angle disappears for small channel
depths, i.e. large μ values.

In comparing the numerical values of the drag coefficient for drag turbines and labyrinth seals, it is found that the numerical value for the rotor drag coefficient in turbines is larger than found in labyrinth seals. This difference might be due to the fact that the channel is curved in drag turbines and straight in the labyrinth seals. This causes a higher turbulence level in the outer portions of the drag channel in turbines (reference 26) which might be responsible for the larger drag coefficients. Since it must be suspected that the degree of turbulence will affect the absolute size as well as the optimum blade spacing (n value) and the optimum width ratio (m value), it is assumed that a larger degree of turbulence will cause the optimum n value to be smaller in curved channels than in straight channels and will cause the drag coefficient to be less sensitive to the depth ratio in curved channels than in straight channels.

In summarizing all the above findings, the following conclusions are drawn:

Good agreement is found for the drag coefficients obtained in straight channels (labyrinth seal tests) and curved channels (drag pumps, drag turbines), which implies that the radial pressure gradient present in drag turbines is of little consequence on the drag turbine performance. The slight numerical difference in drag coefficients can be explained by the increased turbulence levels at the outer portions of a curved channel. The rotor drag coefficient is mainly a function of the ratio of channel length to channel depth, (μ value) and decreases with increasing μ values. The blade angle is of considerable influence on the drag coefficient, meaning that blade angles of 40 degrees give highest rotor drag coefficients and that the usually found blade angles of 90 degrees give drag coefficients which are only 30 per cent of the drag coefficient for the 40 degree blade. The ratio of blade spacing to stator channel depth (n value) and the ratio of pocket depth to stator channel depth (m value) are also of influence on the drag coefficient. Optimum values for these ratios depend on the blade angle and are about $n = 1$ to 1.5 and $m \approx 1$ for 40 degree blades and $m \approx 4$ to 8 and $m \approx 1$ for 90 degree blades. These values pertain to sharp blades, i.e. to blades where the blade thickness if less than 20 per cent of the stator channel depth. For larger blade thickness ratios, the optimum ratios are less pronounced. Blade thickness ratios above one decrease the rotor drag coefficient to about half its original size. The above conclusions are graphically represented in figure (VI, 12) by showing the drag coefficient for two different blade angles, 40 and 90 degrees, as a function of the μ value.

Only in one case has a discrepancy between the drag coefficient in labyrinth seals and drag turbines been found. This was the case where both rotor walls show blades as indicated in figure (VI, 5b). For this arrangement, the labyrinth seals show considerably higher friction coefficients than found in drag turbines of this arrangement. Since, however, the labyrinth seals data do not quote the μ value, it is possible that this apparent difference is caused by improper selection of channel geometries for the drag turbine, i.e. by testing the drag turbine at an adverse μ ratio. There is some evidence that the optimum μ value for inside channels is smaller than for outside channels, as indicated by the dashed line in figure (VI, 12), so that tests with smaller μ values will be required in order to clarify this point. If the labyrinth seal data can be confirmed with inside channels, drag turbine efficiencies of 50 per cent should be obtainable.

It is to be noted that in outside channels the stator wall in all cases so far, drag turbines as well as labyrinth, was smooth. It might be suspected that a wave-shaped surface in the stator channel will change the stator drag coefficient only insignificantly, but might increase the rotor drag coefficient, thus yielding higher turbine efficiencies, particularly when the wave form takes a saw tooth shape with rounded edges. No conclusive information concerning the drag coefficiencies of such a channel configuration has been found in the literature.

All labyrinth seal data were obtained in channels of constant cross-section (constant depth H). In order to obtain good drag turbine efficiencies for compressible media, a divergent stator channel is desirable, where the divergence should be of such a nature that the through flow velocity is constant over the periphery. This means that different divergence ratios are desired for different turbine pressure ratios. It is assumed that the rotor friction coefficient is affected very little by the divergence of the channel since the depth ratio m does not appear to be extremely critical.

2. Performance of Single Disc Turbines

With the relations presented in sections VIA 1 and 2 it is possible to write the efficiency of drag turbines as function of the speed ratio χ , the drag ratio δ , the leakage ratio W_ℓ/W, and the factor β (see equations III, 10) and (VI, 13)).

$$\eta = \frac{\chi \left[1 - \xi \, \frac{\chi^2}{(1-\eta)} \right]}{\left[1 + \frac{d}{(1-\chi)^2} \right] \left[1 + W_c / W \right]}$$

$$\text{VI, 25}$$

In equation (VI, 25), the ratio χ can be replaced by the similarity parameters N_s and D_s for the incompressible case, since

$$\chi = \frac{D_s^3 N_s}{19.1} \, \frac{A_m}{D^2} \, \frac{\chi_{oo}}{\delta_3}$$

$$\text{VI, 26}$$

whereby A_m / D^2 depends only on the channel geometry

$$\frac{A_m}{D^2} = \frac{1 - \frac{1}{\xi}}{\mu} + \frac{4 \varphi}{\mu^2}$$

$$\text{VI, 27}$$

with $\xi = h/\delta$. Considering now that δ is interrelated with μ by figure (VI, 12) when for λ_{fr} a frequently found value of .0675 is assumed and observing that $\lambda_W = \lambda_{fr}$ so that

$$\varphi = \frac{\delta}{4 \, \xi^2 \left(1 - \frac{1}{\xi} + \frac{4}{\mu} \right)}$$

$$\text{VI, 28}$$

it becomes apparent that the maximum obtainable efficiencies can be computed as a function of specific speed and specific diameter. By expressing the interrelation between λ_{fr} and μ in the form of an equation, it would be possible to develop an efficiency expression for drag turbines which is similar to equation (IV, 28), devised in section IV for axial and terry turbines.

Due to the preliminary character of figure (VI, 12), this step appears unadvisable at this time so that a graphical procedure was used for computing an $N_s D_s$ diagram for drag turbines for $\Gamma_1/\Gamma_3 = 1$ (incompressible case) which is shown in figure (VI, 13). Assuming additionally that figure (VI, 12) is valid for diameter ratios $\mathcal{E}$ from 1.3 to 1.8, it is possible to also show lines of constant μ - values in this diagram, thus revealing that optimum efficiencies occur for μ values of 8 to 12 as expected from figure (II, 12) for inside channels. Figure (VI, 13) indicates also that maximum efficiencies occur at specific speed of $N_s = 5$ to 15 and specific diameters of $D_s = 5$ to 2.5. These values characterize drag turbines as typical low specific speed turbines with comparatively small specific diameters, i.e. as a turbine design of low weight since for almost all investigated turbine designs, the turbine weight is proportional to the square of the rotor diameter.

Figure (IV, 13) is calculated for a comparatively low leakage characterized by assuming a small clearance ratio of $h/H = .02$. It is evident from equation (VI, 25) that the leakage is of significant influence on the turbine efficiency. By observing the relationships derived for the leakage flow equation (VI, 15) and (VI, 16), it is possible to derive a relation for a correction factor which corrects the base efficiency shown in figure (VI, 13) to the efficiency resulting for larger clearance ratios. This relation reads in an approximate form (by using average $\mathcal{E}$ and $\int$ values

$$\frac{\eta}{\eta_0} = \frac{1.0043}{1+\left(\frac{h}{H}\right)^{1.5} \mu^{1.5} 1.5} \qquad \text{VI, 29}$$

This relation indicates that the clearance ratio has a stronger influence on the efficiency at large μ-values than at small μ- values. Since large μ- values occur at large specific diameters, it becomes also evident that the detrimental influence of increased clearance ratios is stronger at large specific diameters than at small specific diameters. Since for obtaining maximum efficiencies the specific diameter has to increase with decreasing specific speeds, it is also evident that increased clearance ratios are detrimental for typical low specific speed designs. This tendency is similar to the tendency of the rim clearance influence described in section IV, on axial turbines.

Figure (VI. 13) is calculated by assuming a density change of unity and a constant area channel geometry in accordance with the d scussion presented in section VIA.1. It is to be expected that for density ratios larger than unity and properly diverging channels, figure (VI. 13) has approximate validity probably up to density ratios of 4 and possibly 10.

For constant area channels and density ratios larger than unity, lower peak efficiencies than shown in figure (VI. 13) are to be expected, according to the information presented in figure (VI. 3). Extending the information presented in this diagram to an N_sD_s diagram by a graphical procedure, figure (VI. 14) is obtained which indicates that the location for peak efficiency designs moves to smaller specific diameters without changing, however, the specific speed regime whereby the peak efficiency now decreases to values of about 19 per cent for density ratios of 10. The result then is the constant area channels operated with compressible medii give smaller optimum rotor diameters than diverging channel designs, however, the maximum efficiency decreases. In spite of this decrease in efficiency, the smaller rotor diameter will present an attractive feature for some applications due to the corresponding decrease in turbine weight so that constant channel areas for compressible medii merit considerations for applications where turbine weight and diameter are more important than efficiency. Since additionally, the original simplicity of the drag turbine design is retai .ed in constant area channels, it appears that this turbine type will show advantages in accessory power unit application for low duration.

The above discussion dealt with outside channel designs. For inside channels higher efficiencies are to be expected due to the higher λ_{dr} values quoted in figure (VI. 12). Since the higher λ_{dr} value occur at smaller μ values, the ratio of channel area over diameter will be larger for inside channels. Since the increase in rotor friction coefficient is larger than the decrease in μ value the geometry term γ will be larger for inside channels than for outside channels. This, however, does not necessarily mean that inside channels operate at smaller turbine velocity ratios u/c_i than outside channel since the optimum $u/c_i(\sqrt{\gamma})$ value increases with decreasing δ value, i.e., increasing λ_{dr} values. It is to be expected, therefore, that inside channels will show about the same optimum specific speed and specific diameter range than outside channels, with , however, higher efficiency values. No computations have been carried through for inside channels due to the speculative character of the values presented in figure (VI. 12) for inside channels. In this respect it has to be noted that in general the information

presented in figure (VI. 12) is of preliminary nature since some of the geometrical relationships affecting the drag coefficients are not yet fully explored.

3. Conclusions

Drag coefficients measured in labyrinth seals show remarkable similarity, tendency-wise as well as numerically, with drag coefficients calculated from drag turbine performance data. Since investigations on labyrinth seals cover a wider variety of geometrical shapes than the comparatively few data available on drag turbine performance, the knowledge on drag turbine characteristics can be extended by applying labyrinth data. With this assumption the complete performance range of drag turbines can be analyzed. The optimum geometry can be determined so that the $N_s D_s$ diagrams for drag turbines can be plotted. This analysis reveals that drag turbines are typical low specific speed turbines covering specific ranges of 5 to 15 with specific diameters of 5 to 2.5 with efficiencies of about 40 per cent, as peak values. The $N_s D_s$ diagram also presents additional information for the optimum geometry by quoting the ratio of rotor diameter to stator channel depths for the different specific diameters. The ratio of clearance h/H between stator and rotor and side channel depths H is a particularly influential parameter, revealing that the clearance ratio h/H, must be maintained between .01 and .02 in order to obtain peak efficiencies.

Peak efficiencies lower than 40 per cent are obtained when drag turbines of constant channel area are operated at high pressure ratios, namely about 20 per cent for $p_1/p_3 = 10$. This deficiency can be corrected by using diverging stator channels.

4. LIST OF SYMBOLS

A	drag channel area
a	frictional area
c	through flow velocity
c_i	spouting velocity
D	rotor diameter
D_s	specific diameter
d	hub diameter
g	gravitational constant
H	width of drag channel
H'	pocket depth
H_{in}	input head
H_{out}	output head
h	seal clearance
L	length of drag channel
ℓ'	blade distance
m	width ratio
N_s	specific speed
n	blade spacing
q	dimensionless head ratio

LIST OF SYMBOLS (Cont)

s	blade thickness
u	wheel speed
v	velocity
W	turbine weight flow
W_ℓ	leakage flow
χ	velocity ratio
y	rim clearance
α	blade angle
γ	density
δ	drag ratio
ϵ	diameter ratio
η_h	hydraulic efficiency
η_s	shaft efficiency
λ	drag coefficient
μ	diameter-width ratio
γ	geometry term
ζ	ratio of friction coefficients
τ	shear stress

B.   Drag Turbine Considerations Based on Dynamic Flow Theory

It is assumed for this analysis that the drag turbine (referred to in the literature as regenerate or peripheral pumps and turbines) can be associated with a flow essentially dynamic in nature, obeying the Euler equations, and that friction forces are small and can be taken into account by correction factors. This is analagous to the methods used in computing axial and radial flow machines.

It is doubtful if this theory can be applied directly to the conventional form of drag turbines, since this theory suggests a flow pattern which would be adversely affected by the conventional blading and channel geometry, meaning also that the conventional arrangement, particularly the interaction between rotor flow and stator flow in conventional designs militates against the possibility to even approximate the flow mechanism to any theoretical flow. By discussing the more significant equations of this theory and their implications and solving the basic flow equations for the assumed flow pattern a basis is established for designing blade forms and channel geometries which fulfill all the required boundary conditions. This suggests that designs can be found which have Eulerian flow and correspondingly high efficiencies. The considerations are as follows.

The fluid is introduced tangentially above a set of moving impulse turbine blades set on both sides of a disk at the periphery as shown in figure (VI, 15). The fluid goes radially inward, through the blade passages and into a vaneless passage where it circulates toroidally upward and around the circumference under the influence of the circumferential pressure gradient until it enters the blade passages again. This is repeated until the outlet is reached. Between the inlet and outlet is a seal which is shaped to maintain the boundary conditions demanded by the differential equations.

These boundary conditions were set so that the following flow characteristics exist:

1.   The velocities are circumferentially symmetrical (since the blading and passage shapes are circumferentially symmetrical).

2.   The same amount of work is taken out of each stream line.

The first equation of interest describes the variation of the tangential velocity in the free passage:

$$\Delta c_u r = \frac{\Delta P}{2 \pi W_m} V_b \qquad\qquad VI\text{-}30$$

where c_u - tangential velocity

$\frac{\Delta P}{\rho}$ - total head drop

W_m - meridional mass flow

V_o - free flow volume

This indicates that the $c_u r$ variation is independent of the passage shape, but a function only of the volume of the passage.

The second significant equation is that for the internal efficiency of the turbine, that is the efficiency which accounts only for the losses inside the turbine without inlet, exit, and wall friction losses.

$$\eta_i = \frac{U_m}{V_i} \qquad\qquad VI, 31$$

where η_i - internal efficiency

U_m - mean blade speed

V_i - mean tangential velocity in the free passage

This is the same formula arrived at from overall pressure-momentum considerations. According to the drag theory, presented in reference 16, no work can be done when this function approaches 1.0. But for this formulation, large variations in c_u can exist even if the mean velocity approaches the blade speed. This necessitates large negative velocities at the exit from the bladed portions; thus the strange shape of the block seal in figure (VI. 15).

Another significant equation shows the energy available for driving the circumferential velocity.

$$H = \Delta c_u u \left(\frac{1}{\eta_i} - 1 \right) \qquad\qquad VI, 32$$

where H = head available for circumferential losses

This indicates that all of the internal losses are available for driving the circumferential component. And, as the circumferential loss approaches zero, η_c must approach unity and v_i must approach u_m.

The analysis above determines the flow along one flow surface. Integrating point to point from this surface with the use of equation (IV, 49C), one may obtain the flow over the complete section and the design of the cross-section and blades. However, it is sufficient for this report to assume that conditions along the mean stream line represent the average conditions of the complete flow, that is, b represents the channel width. When this is done, expressions for the average efficiencies and several design criteria may be determined. It is evident that several assumptions have been made in this theory which will not be followed completely by the actual flow. This aspect merits some further discussion.

It is assumed that the pressure decreases steadily with increasing peripheral angle Δ as shown in figure (VI, 15-A). In order to simplify the representation the flow channel has been linearized in this diagram. The upper line represents the pressure at the outer radius of the side channel, whereas the lower line represents the pressure at the inner radius of the side channel; the difference between these two pressures is caused by the centrifugal field and proportional to the square of the radius ratio. This pressure pattern can be established only if an infinite number of rotor blades is assumed and if additionally the peripheral extension of the nozzle arc is infinitesimally small. In the actual case a somewhat different pressure pattern must be expected due to the finite peripheral extension of the nozzle and due to the limited number of rotor blades. In this case the pressure will be constant over the nozzle arc as indicated by the dashed line in figure (VI, 15-A). If the rotor channel is positioned in such a manner that the nozzle arc covers one blade passage entirely and if the clearance between nozzle and blade is small enough to avoid detrimental leakage, the nozzle jet will pass through the rotor channel and will again show constant pressure over the exit width of the rotor channel. The jet discharged from the rotor blades will be directed to the upper part of the side channel by the block seal, enter the second blade passage and will flow through the second blade passage due to the pressure difference existing between the outer and inner radius of the side channel. This means that the pressure pattern shows steps as indicated by the dashed lines in figure (VI,15A) whereby the peripheral extension of the steps should be approximately proportional to the blade spacing. This, then, means that a pressure gradient exists between two adjacent streamlines in the side channel. This pressure difference can not be maintained but will be modified to a more gradual decrease by a mixing process as indicated by the dotted lines in

figure (VI, 15A). It is to be noted that this gradual decrease in pressure is obtained by a process which increases the entropy and not by the dynamic action of the blades, i.e., by converting dynamic energy into shaft power. This mixing has to take place for every cycle so that for the overall process comparatively large mixing losses have to be expected.

The above described flow pattern is expected to result when one rotor channel covers the nozzle arc entirely. As soon as the rotor starts to move, a condition will exist, where two rotor channels are fed by the nozzle so that now the typical partial admission losses occur due to sudden expansion of the gas in the rotor channel. Additionally, it must be expected that the pressure at rotor exit is constant over two blade passages, which means that only a fewer number of pressure steps an occur causing the number of cycles to be smaller, so that every cycle has to show a larger pressure drop than previously if the total available pressure drop is to be utilized in the channel. This, in turn, means that the pressure gradient between two adjacent stream lines is larger, thus causing larger mixing losses.

Another aspect is revealed when the starting problem is considered. In this case the back pressure at the exit of the first blade passage can be assumed to be equal to turbine exit pressure so that a tendency will exist to expand the total available pressure in the first passage, causing the remainder of the rotor channels to receive gas which has expanded its pressure energy already. If now the rotor starts moving it is conceivable that the gas, having expanded all its energy in the first passage travels with wheel speed to the exhaust port, so that only the first passage accomplishes a conversion of dynamic energy to shaft power.

The above considerations indicate that it might be difficult to actually obtain the flow pattern stipulated in the dynamic theory, or that in order to obtain the continuously decreasing pressure pattern a considerable amount of mixing losses has to be anticipated. It is to be expected that the situation improves with increasing number of blades and decreasing peripheral extension of the nozzle arc. The above considerations also indicate that it would be inadvisable to place blades in the side channel since local fluctuations of the side channel pressure have to be expected, caused by the fact that the nozzle will feed, in most cases, two rotor passages, the position of which changes constantly.

A more optimistic approach would be to assume that with special nozzle designs the pressure at nozzle outlet is not constant, but varying with peripheral extension. If it would also be possible to design blade passages which allow the pressure at channel exit to show a pressure gradient rather than a constant value. Then the originally assumed pressure pattern could be established predominantly by dynamic flow action rather than mixing processes. In this case extremely high efficiencies should be expected for the turbine since no parasitic losses except the usual friction and turning losses would have to be considered.

Another approach would be to assume that the desired pressure gradient will eventually be established in the turbine passages and that the nozzle which originally provides a constant pressure over the nozzle exit will adjust to the gradually decreasing pressure pattern of the side channel by incurring mixing losses.

It is unlikely that further analytical arguments will give sufficient help for determining numerically the effect of the above discussed disturbances or for determining the average flow pattern actually existing in this turbine design. It may suffice to be content for the time being with the fact that a detailed mathematical treatment of drag turbines with Eulerian flow presented in section (VI, B1) indicates that the assumed flow pattern is possible from a theoretical point of view and stable for an infinite number of blades when the block seal is shaped according to the boundary conditions, i.e., has a geometrical shape as indicated in figure (VI, 15). This finding suggests that the peripheral channel should be entirely open in order to allow more flexibility for the flow pattern. It should prove therefore essential, to avoid any blading in the peripherial channel thus avoiding a rigidity in flow pattern the flow cannot adhere to. This finding also points to the desirability of providing a maximum number of rotor blades, or more precisely, to design for the largest possible ratio of nozzle arc lengths to blade spacing; a feature found essential also in partial admission axial turbines. Assuming that by these means the disturbances and secondary losses caused by the limited number of blades can be kept small, only four loss sources have to be considered for calculating the hydraulic efficiency of this turbine type. These losses are enumerated as follows:

1. Blading loss:

The blading loss in a well designed constant area turbine passage is a function of the turbine angle and the relative velocity head. Generally, a loss of 30 per cent of the relative velocity head for turning angles of less than 120 degrees is considered a conservative value, hence

$$L_b = \frac{0.3}{2}\left[(C_u - u)^2 + C_m^2\right] = 0.3\left(\frac{u^2}{2}\right)\left[\left(\frac{C_u}{u}-1\right)^2\left(1+\tan^2\beta\right)\right] \qquad \text{VI,33}$$

where β is the inlet and exit blade angle

2. Circumferential velocity loss:

The test data available for ducts indicates that the losses for 90 degree bends are on the order of one quarter of the velocity head, provided that there are no sudden expansions at the turn. A 360 degree turn would then occasion something over unity velocity head loss. A value of 1.5 would seem a conservative value, hence

$$L_c = 1.5\frac{C_m^2}{2} = 1.5\left(\frac{u^2}{2}\right)\left(\frac{C_u}{u}-1\right)^2\tan^2\beta. \qquad \text{VI,34}$$

3. Inlet and exit loss:

The inlet loss is simply the loss of the accelerating flow plus the previously discussed mixing loss at the beginning of the circumferential passage. A value of 10 per cent of the inlet velocity head is assumed for this loss. The exit loss is considerably more, since mixing and diffusion are involved. However, proper design of the exit passage will require only diffusion of the radial component. It appears that over 50 per cent of this velocity head will be lost, hence

$$L_i = 0.1\left(\frac{C_u^2}{2} + \frac{C_m^2}{2}\right) = 0.1\left(\frac{u^2}{2}\right)\left[\left(\frac{C_u^2}{u}\right) + \left(\frac{C_u}{u}-1\right)^2\right]\tan^2\beta \qquad \text{VI,35}$$

and

$$L_e = 0.5\left(\frac{C_m^2}{2}\right) = 0.5\left(\frac{u^2}{2}\right)\left[\left(\frac{C_u}{u}-1\right)^2\right]\tan^2\beta. \qquad \text{VI,36}$$

4. Tangential flow losses:

This will be a function of the friction factor and the average of the squares of the circumferential velocity multiplied by the lengths - hydraulic diameter ratio as indicated by the pipe theory. Because of the excess turbulance of this flow, the maximum tangential velocity is used here to determine the loss, hence

$$L_t = f \left(\frac{c_u^2}{2} \right) \left(\frac{2\pi r}{b_{/2}} \right) = f \left(\frac{4\pi r}{b} \right) \left(\frac{u^2}{2} \right) \left(\frac{c_u^2}{u} \right) \qquad \text{VI, 37}$$

where f = friction factor
b = channel width

For calculating the overall efficiency, the wheel disc friction loss is found in Stodola (reference 2) to be

$$L_t^* = \frac{a.c_f}{10^6} u^3 d^2 \qquad \text{VI, 38}$$

where L_t^* is in horsepower.

In terms of the variables used here the loss per pounds flow is

$$L_t = \left(\frac{U_m^2}{2} \right) \left(\frac{r_m^2}{m^2 \cdot 0} \right) \left(\frac{a}{10^6} \right) \qquad \text{VI, 39}$$

The overall efficiency is then the internal efficiency ζ_t multiplied by a factor of one minus the external losses divided by the available energy. Hence,

$$\zeta_o = \eta_i \left(1 - \frac{\Sigma L_i}{\left(\frac{\Delta P}{\rho} \right)} \right) \qquad \text{VI, 40}$$

with

$$\left(\frac{\Delta P}{\rho} \right)_o = \frac{\Delta P}{\rho} + \Sigma_e L \qquad \text{VI, 41}$$

where $\Sigma_e L$ is the sum of the external losses

so that

$$\eta_o = \eta_i \left[1 - \frac{1}{\left[\frac{\Delta P/\rho}{\Sigma_e L} + 1 \right]} \right] \qquad \text{II,42}$$

with

$$\frac{\Delta P}{\rho} = (\Delta c_u r)\left(\frac{2\pi c_a}{m}\right) = (\Delta c_u u)\left(\frac{c_a}{u_m} - 1\right)\tan\beta\left(\frac{2\pi r_m}{m}\right) \qquad \text{II,43}$$

but $\Delta c_u u = 4\left(\frac{u_m^2}{2}\right)\left(\frac{c_u}{u} - 1\right)$ for equal turbine angles so that

$$\frac{\Delta P}{\rho} = 4\left(\frac{u_m^2}{2}\right)\left(\frac{c_a}{u_m} - 1\right)^2 \tan\beta\left(\frac{2\pi r_m}{m}\right). \qquad \text{II,44}$$

The internal efficiency is defined as:

$$\eta_i = \frac{1}{\frac{\Sigma L_i}{\Delta c_u u} + 1} \times \frac{1}{\frac{\Sigma L_i}{4\left(\frac{u_m^2}{2}\right)\left(\frac{c_a}{u} - 1\right)} + 1} \qquad \text{II,45}$$

with

$$\Sigma L_i = \Delta c_u u \left(\frac{1}{\eta_i} - 1\right). \qquad \text{II,46}$$

Another important parameter is the velocity ratio.

$$\frac{u}{c_i} = \sqrt{\frac{u^2}{2\left(\frac{\Delta P}{\rho}\right)}} = \frac{1}{2\left(\frac{c_a}{u}\right)\sqrt{\tan\beta\left(\frac{2\pi r_m}{m}\right)}}. \qquad \text{II,47}$$

This factor is a familiar one and related to the similarity parameters N_s and D_s as quoted in equation (III.9). It is a measure of the energy that can be

absorbed by a given size wheel at a given rotative speed.

A summary curve resulting from the above relations is shown in
in figure (VI, 16) where u/c_i and η_o are presented as a function c_u/u and θ
for a value of $\frac{r}{m} = 4.0$. This curve indicates that highest efficiencies will
be obtained with small angles. It indicates that efficiencies of between .60
and .70 are calculated for u/c_i values as low as 0.0?. For very large enthalpy
drops at the lowest blade speeds the ratio r/m must be as large as possible,
which leads to large leakage losses. Further work is necessary to optimize these
values as a function of specific speed. It must be kept in mind that these values
are calculated on the basis of an idealized flow mechanism. Since no conclusive
evidence for actually producing this flow pattern is available, only a test of a
turbine designed according to this concept, can determine the validity of this
analysis whereby the application of flow visualization techniques will prove to be
extremely desirable.

1. Detailed derivation of dynamic flow theory for drag turbines.

The Euler equation for frictionless flow and the equation of continuity
may be written as follows in cylindrical coordinates:

$$C_r \frac{\partial C_r}{\partial r} + C_u \frac{\partial C_r}{r \partial \varphi} + C_z \frac{\partial C_r}{\partial z} - \frac{C_u^2}{r} = -\frac{\partial p}{\rho \partial r} + R$$

$$C_r \frac{\partial C_u}{\partial r} + C_u \frac{\partial C_u}{r \partial \varphi} + C_z \frac{\partial C_u}{\partial z} + \frac{C_u C_r}{r} = -\frac{\partial p}{\rho \partial \varphi} + Y$$

$$C_r \frac{\partial C_z}{\partial r} + C_u \frac{\partial C_z}{r \partial \varphi} + C_z \frac{\partial C_z}{\partial z} = -\frac{\partial p}{\rho \partial z} + Z$$

$$\frac{\partial \rho r C_r}{\partial r} + \frac{\partial \rho r C_u}{r \partial \varphi} + \frac{\partial \rho r C_z}{\partial z} = 0 \qquad \qquad \mathrm{II,48}$$

Where r, φ, z - radial, tangential, and axial coordinates

C_r, C_u, C_z - velocity component

P - pressure

ρ - density

R, Y, Z - body force components

Equations (VI. 48) may be transformed into a more convenient form, by substituting the following:

$$C_r = C_m \sin \theta$$
$$C_u = C_u$$
$$C_z = C_m \cos \theta$$
$$dr = dm \sin \theta + dn \cos \theta$$
$$d\varphi = d\varphi$$
$$dz = dm \cos \theta - dn \sin \theta$$

where

$$\theta = \tan^{-1} \frac{C_r}{C_z}$$

Thus M, n form a new coordinate system in the r-z plane which moves along with the flow in the r-z plane. c_m is then the vector perpendicular to the flow in the r-z plane. c_m is then the vector sum of $c_r + c_z$. These new equations with ρ held constant may be written as follows:

$$C_m \frac{\partial C_m}{\partial m} + C_u \frac{\partial C_m}{\partial \varphi} - \frac{C_u^2}{r} \sin \theta = -\frac{\partial P}{\rho \partial m} + M \qquad (a$$

$$\underline{VI, 49}$$

$$\frac{C_m}{r} \frac{\partial C_u r}{\partial m} + C_u \frac{\partial C_u}{\partial \varphi} = -\frac{\partial P}{\rho \partial \varphi} + Y \qquad (b)$$

$$c_m \frac{\partial \Theta}{\partial m} + c_u c_m \frac{\partial \Theta}{\partial \psi} - \frac{c_u^2}{r}\cos\Theta = -\frac{\partial P}{\partial m} + N \qquad (c)$$

$$\frac{\partial c_m r}{r \partial m} + c_m \frac{\partial \Theta}{\partial m} + \frac{\partial c_u}{\partial \psi} = 0 \qquad (d)$$

II,49

In the above equations, it must be remembered that r is no longer a coordinate, but rather some function of m and n as determined by the stream line. These four equations have seven unknowns - c_m, c_u, Q, M, Y, N, and P. In the free space the body forces are zero so that the flow is defined by the flow equations in four unknowns. In the bladed section the body forces are perpendicular to the blade surface and the flow is parallel to them, so that two more equations are given:

$$\frac{c_u - u}{c_m} = -\frac{M}{Y} = f(m, n) \qquad II,50$$

A seventh equations defining N, can be written if the blades are continuous surfaces.

One of the boundary conditions establishes axial symmetry of the blade passage. Since assuming that c_m, Θ, and c_u are independent of Y fulfills this boundary condition, let us assume this and determine if the other boundary conditions can be met. The equations then reduce to:

$$c_m \frac{\partial c_m}{\partial m} - \frac{c_u^2}{r}\sin\Theta = -\frac{\partial P}{\partial m} + M \qquad II,51$$

$$\frac{c_m}{r} \frac{\partial c_u r}{\partial m} = -\frac{\partial P}{\partial \psi} + Y \qquad II,52$$

$$c_m^2 \frac{\partial \Theta}{\partial m} - \frac{c_u^2}{r}\cos\Theta = -\frac{\partial P}{\partial m} + N \qquad II,53$$

$$\frac{\partial c_m r}{r \partial m} + c_m \frac{\partial \Theta}{\partial m} = 0 \qquad II,54$$

Another simplication results if the equations are written in terms of the distance between two closely spaced stream lines (b).

$$\Delta\theta = \frac{\partial\theta}{\partial n} b$$

$$\Delta\theta = \frac{\Delta b}{\Delta m}$$
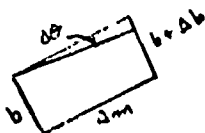
$$\frac{\partial b}{b\,\partial m} = \frac{\partial\theta}{\partial n}$$

Substituting this result in equation (VI, 54) allows immediate integration.

$$\frac{\partial c_m r}{r\,\partial m} - \frac{c_m}{b}\frac{\partial b}{\partial m} = 0 \qquad\qquad\qquad VI, 55$$

$$2\pi\rho c_m r b = W_m \qquad\qquad\qquad VI, 56$$

where W_m is now equal to the total flow in the particular stream tube. This is equivalent to stating that an average value of the variables can be used for the whole stream tube. This is shown as the "donut-shaped" section in figure (VI, 17). At some point in the section is a seal and the fluid is introduced on one side of the seal and removed on the other. However, care must be taken in the inlet and outlet seal to assure that the boundary conditions are maintained.

Substitution of equation (VI, 56) in equation (VI, 52) allows immediate integration with $Y = 0$ in the free space:

$$\frac{\partial c_u r}{\partial m}\,dm = \frac{\partial P}{\rho\,\partial\varphi}\left(\frac{2\pi P r b\,dm}{W_m}\right) \qquad\qquad\qquad VI, 57$$

It will be noticed that none of the variables in this equation is a function of φ, so that this may be written

$$dm\,\frac{\partial c_u r}{\partial m} = \frac{\Delta P}{2\pi W_m}\left(2\pi r\,b\,dm\right) \qquad\qquad\qquad VI, 58$$

where ΔP is the total pressure drop in the machine, constant at each radial position.

It is interesting to note that the bracketed value on the right side of the above equation is simply the differential volume of the stream tube under consideration. Thus integrating:

$$\Delta C_u r = \frac{\Delta P}{2 \pi W_m} V_b \qquad\qquad \text{VI.59}$$

where V_b = volume enclosed in the vaneless section as shown in figure (VI, 17)

The same process may be used to determine the blade forces in the rotor:

$$\frac{C_m}{r} \frac{\partial C_u r}{\partial m} = - \frac{\partial P}{\rho \partial \varphi} + Y$$

where Y is the blade force represented by a body force assuming an infinite number of rotor blades - thus

$$Y = \frac{\delta F}{\rho b r d \varphi d m}$$

where δF is the differential blade force

$$\frac{W_m}{2 \pi r} \frac{\partial C_u r}{\partial m} dm\, d\varphi + \frac{\partial P}{\partial \varphi} b d\varphi dm = \delta F.$$

Multiplying by r to obtain the differential torque (δT)

$$\frac{W_m}{2 \pi} \frac{\partial C_u r}{\partial m} dm\, d\varphi + \frac{\partial P}{\partial \varphi} r d\varphi dm = \delta T.$$

Since $C_u r$ is independent of φ and ΔP independent of m from considerations of boundary conditons:

$$W_m \Delta(C_u r) + \int \Delta P(r\, b dm) = T$$

But

$$-\int \Delta p r\, b\, dm$$

     is equal to the torque on the blades passing through the block seal between the inlet and outlet passages

$$T_o = W_m \Delta C_u r$$

$$W_R = W_m \Delta c_{uu}$$

The overall internal efficiency is then:

$$\eta_i = \frac{W_R}{W_a \, \Delta p}$$

$$\mathrm{VI.60}$$

W_a = flow through the machine

$$\eta_i = \frac{W_m \Delta c_{uu}}{\rho V_1 A_1 \, \Delta p}$$

V_1 = average tangential velocity

A_1 = tangential flow area

Substituting from equation (VI.59)

$$\eta_i = \frac{W_m \Delta c_{uu}}{2\pi W_m \Delta u \, r_m A_1} \cdot V_o = \frac{W_r}{V_1} \cdot \frac{U_m}{V_1} \qquad \mathrm{VI.61}$$

where r_m is the mean radius of V_b.

    This, of course, is the same formulation for efficiency which is obtained by the drag theory. Now attempts will be made to formulate the equation which determines what the value of c_m must be. To do this, the meridional pressure rise in the vaneless section less the pressure drop in the bladed section, must be determined. This difference is the driving force which overcomes the losses in the rotor blades and the frictional losses due to meridional velocity.

$$c_m \frac{\partial c_m}{\partial m} - \frac{c_u^2}{r} \sin \theta = -\frac{\partial p}{\rho \, \partial m} + M$$

but from equation (VI, 50)

$$M = -Yf = -Y \frac{c_u - u}{c_m}$$

then

$$-\frac{\partial P}{\rho \partial m} = c_m \frac{\partial c_m}{\partial m} + \left[\frac{c_m}{r} \frac{\partial c_u r}{\partial m} \right] \frac{c_u - u}{c_m} - \frac{c_u^2}{r} \sin\theta + f \frac{\partial P}{\rho \partial \varphi}$$

$$= c_m \frac{\partial c_m}{\partial m} + \frac{c_u - u}{r} \left[r \frac{\partial c_u}{\partial m} + c_u \sin\theta \right] \frac{c_u^2}{r} \sin\theta + f \frac{\partial P}{\rho \partial \varphi}$$

$$-\frac{\partial P}{\rho \partial m} = \frac{\partial c_m^2}{2 \partial m} + \frac{\partial c_u^2}{2 \partial m} - \frac{u c_u \sin\theta}{r} - \frac{u \partial c_u}{\partial m} + f \frac{\partial P}{\rho \partial \varphi}$$

integrating with respect to m

$$-\frac{\Delta P r}{\rho} = \frac{\Delta c_m^2}{2} + \frac{\Delta c_u^2}{2} - \Delta u c_u + \frac{\partial P}{\rho \partial \varphi} \int f \, dm.$$

But the integral of

$$f \, dm = \Delta Y = 0$$

$$\frac{\Delta P r}{\rho} = \Delta c_u c_u - \frac{\Delta c_m^2}{2} - \frac{\Delta c_u^2}{2}.$$

Integrating this equation in the vaneless section with M = 0

$$\int -\frac{\partial P}{\rho \partial m} \, dm = \int c_m \frac{\partial c_m}{\partial m} \, dm - \int \frac{c_u^2}{r} \, dr$$

integrating the last term in parts

$$-\frac{(\Delta P)s}{\rho} = \frac{\Delta c_m^2}{2} + \frac{\Delta c_u^2}{2} - \int \frac{c_u}{r} \, d(c_u r).$$

   Substituting equation (VI-58) for d (c_u r) and realizing the remaining integral is the area averaged tangential velocity

$$\int \frac{c_u}{r} d(c_u r) = \frac{\Delta P}{W_m} \int c_u \, b \, dm$$

$$= \frac{\Delta P}{W_m} V_1 A_1$$

But

$$\Delta c_{ur} = \frac{\Delta P}{2\pi W_m} V_b$$

$$\int \frac{c_u}{g} d(c_{ur}) = \Delta c_{ur} \left\{ \left(\frac{2\pi A_1}{V_b} \right) V_1 \right\}$$

and

Then

$$\frac{2\pi A_1}{V_b} = \frac{1}{r_m} \cdot$$

$$\frac{\Delta P}{P} = \frac{V_1 \Delta c_{ur}}{r_m} - \frac{\Delta c_m^2}{2} - \frac{\Delta c_u^2}{2} \cdot$$

Then the head difference between the rotor and stator:

$$H = \Delta c_{uu} \left[\frac{V_1}{U_m} - 1 \right]$$

or

$$H = \Delta c_{uu} \left[\frac{1}{R_1} - 1 \right]$$

$$\text{VI},62$$

Thus all of the energy lost is available for overcoming the frictional losses in circumferential flow, and if these losses are zero, u must equal V_1 and the internal efficiency becomes 100 per cent.

2.   CONCLUSIONS

By stipulating an idealized flow pattern in a drag turbine, a
dynamic theory for the turbine action is derived. This theory indicates that the
shape of the block seal, which is of negligible importance in the drag theory, is
essential for generating the stipulated flow pattern and should have a different
form than presently used. This theory also indicates that typical impulse blades
for the rotor should show higher efficiencies than the presently used straight-edged
blades; however, the conclusions suffer from a lack of pertinent test information
regarding the magnitude of secondary losses in the prescribed flow mechanism.
If they can be assumed to be of minor consequence and if the presumed flow pat-
tern can be established, comparatively high efficiencies are to be expected from
the design geometry stipulated by the dynamic flow theory. A final conclusion,
therefore, will have to await further testing.

3. LIST OF SYMBOLS AND SUBSCRIPTS

Symbols

A	- area	- ft^2
C	- absolute velocity	- ft/sec
d	- diameter	- ft.
Ds	- specific diameter	-
g	- gravity	- ft/sec^2
H	- head	- ft.
h	- blade height	- ft.
k, K	- constants	-
L	- loss	-
m	- meridional coordinate	- ft.
n	- normal coordinate	- ft.
N	- rotative speed	- RPM
Ns	- specific speed	-
p	- pressure	- lbs/ft^2
Q	- volume flow	- ft^3/sec
r	- radial coordinate	- ft
Re	- reynolds number	-
u	- blade speed	- ft/sec

Symbols (Cont)

v	-	velocity	- ft/sec
w	-	relative velocity	- ft/sec
z	-	axial coordinate	- ft
α	-	nozzle angle	
β	-	blade angle	
γ	-	turning angle	
η	-	efficiency	
λ	-	loss factor	
ρ	-	density	- lb/ft^3
ψ	-	velocity coefficient	
t	-	tangential coordinate	
θ	-	meridional angle	

Subscripts

b	-	blade
c	-	sonic, critical
d	-	disk
e	-	exit
H	-	hydraulic

Subscripts (Cont)

i   - ideal, internal, inlet

j   - jet

L   - loss

m   - main, meridional, mean

p   - pumping

r   - radial

s   - secondary

t   - tangential

u   - tangential

z   - axial

C. SUMMARY

The performance of drag turbines has been analyzed by two different theories, the drag theory and the dynamic theory. The drag theory, in contrast to the dynamic theory, considers only the peripheral component as the main criterion for the performance. On this basis, critical velocity ratios are established and the design geometry required for obtaining highest efficiencies. By using the drag coefficients obtained by labyrinth tests the optimum design geometry can be specified in considerable detail whereby it was found that blade angles of 40 degrees, a ratio of rotor diameter to side channel depths between 8 and 12, and a ratio of clearance between rotor and stator and side channel depths of .01 to .02 are essential prerequisites for highest efficiencies. The evaluation of the performance in terms of specific speed and specific diameter yielded an N_s D_s diagram for drag tu.bines indicating that maximum efficiencies are obtained at low specific speeds, namely, between specific speeds of 5 and 15 with specific diameters between 5 and 2.5, i.e., values which are considerably lower than the corresponding optimum specific diameters for axial and terry-type turbines for the same specific speed regime. The maximum efficiency, however, of drag turbines is less than that of axial turbines, particularly axial turbines with large blade numbers, yielding maximum values of only .37 to .40, depending on the clearance ratio. These maximum values appear to be obtainable for a variety of pressure ratios, however, for large expansion ratios a divergent stator channel must be applied. If a constant area channel is applied for high expansion ratios, the maximum obtainable efficiency decreases significantly. Since the required optimum specific diameter decreases at the same time, this design offers the advantage of reduced manufacturing costs and yielding smaller diameters than the corresponding design with diverging channels. The calculated data have been partially substantiated by test evidence. For outside channel arrangements it appears that higher efficiencies than tested so far with inside channels are obtainable. Test confirmation of this aspect is still lacking.

The dynamic flow theory stipulates an Eulerian flow, requiring different block seal forms and blade shapes than tested so far in drag turbines. In treating the Eulerian flow equations, it was necessary to ide ize t.e flow pattern and to assume an infinite number of blades. If it can be assumed that this simplification is of minor consequence, a considerable improvement in drag turbine efficiencies should be obtainable for block seal designs and blade forms specified by the dynamic theory. The argument, however, that the limited number of blades has a more serious effect on flow pattern and efficiency than commonly assumed for conventional designs, cannot be entirely refuted by analytical arguments alone so that test

evidence will be necessary before a final evaluation of the validity of the dynamic
theory, and a more accurate appraisal of its limitation, can be presented.

The limited test information available on drag turbine performance
and the somewhat speculative character inherent in both theories indicates that
the presented information is of preliminary nature and must be substantiated by
test data before a final acceptance is justified.

Tests on drag turbines with diverging channels of inside and outside
designs as well as tests on constant channel turbines with inside arrangement
designed in accordance with the drag theory, are scheduled for the near future.
It is intended to test these designs over a variety of pressure ratios.

A turbine designed in accordance with the dynamic theory is also being
prepared for testing. This design will be tested at low pressure ratios only,
since the dynamic theory in its present form is valid only by assuming negligible
density change in the flow channels.

VII LIST OF REFERENCES

1. A. H. Stenning - Design of Turbines for High-Energy Fuel, Low-Power
   Output Application; Mit Dynamic Analysis and Control Laboratory Report
   No. 79, 1953.

2. A. Stodola - Steam and Gas-Turbines Translated by L. C. Lowenstein.
   Peter Smith, New York, 1945.

3. An Examination of the Flow and Pressure Losses in Blade Rows of Axial
   Flow Turbines
   P. G. Ainley and G. C. R. Mathieson - ARC Technical Report R & N No. 2891,
   1955.

4. Results of Systematic Investigations on Secondary Flow Losses in Cascades.
   Part III
   Institute of Fluid Mechanics, Engineering University, Braunschweig, Germany
   Report No. 54132a.

5. Neue Allgemeine Theorie Der Mehrstufigen Axialen Turbomaschine
   Dr. Walter Traupel - Leeman & Company, Zurich.

6. Untersuchungen Über Die Dreidimensionale Strömung Durch Axiale Schaufel-
   gitter Mit Zylindrischen Schaufeln
   H. Schäffer, Forschung No. 1, 1955.

7. Untersuchungen An Turbinenschaufelgittern
   E. Olderin - Forschung No. 2, 1953.

8. Flow of Gases Through Turbine Lattices
   M. E. Deich - NACA TM 1393, 1953.

9. Reaction Tests for Turbine Nozzles for Subsonic Velocities
   H. Kraft - Trans. of ASME October, 1949, V. 71, No. 7.

10. Reaction Tests of Turbine Nozzles for Supersonic Velocities
    J. H. Keenan - Trans. of ASME October 1949, V. 71, No. 7.

11. Strömungsmaschinen
    C. Pfleiderer - Springer, 1952.

AMF/TD No. 1196
Job No. 7213

9 April 1958
Page 110

12. Report of the Grid-Meeting in Braunschweig
   A. Planid - October, 1945.

13. Einflussder Oberflächenrauhigkeit Auf Die Strömungsverluste in Ebenen Schaufelgittern
   L. Speidel - Forschung No. 5, 1954.

14. Partial Admission, Low Aspect Ratios and Supersonic Speeds in Small Turbines
   G. Olson - Doctors Thesis, MIT, January, 1956.

15. G. Fluegel - Die Dampfturbinen (Steam Turbines)
   J. A. Barth, Leipzig 1931.

16. O. E. Balje - Drag Turbine Performance; ASME Transactions - Volume 79 No. 6, August 1957.

17. K. Trutnowsky - Beruehrungsfreie Dichtungen VDI Verlag, 1943.

18. C. Pfleiderer - Die Kreisel-Pumpen
   Springer Verlag, 1955

19. H. Schlichting - Boundary Layer Theory
   McGraw-Hill, 1955

20. E. Gruenagel - Kanten Widerstand von Schaufelreihen
   Forschung 1938, Page 187 to 196.

21. H. W. Iversen - Performance of the Periphery Pump; ASME Transactions, 1955.

22. W. A. Wilson
   M. A. Santello
   S. A. Oelrich - A Theory of the Fluid Dynamic Mechanism of Regenerative Pumps; ASME Transactions, 1955.

23. Y. Senoo - A Comparison of Regenerative Pump Theories Supported by New Performance Data; ASME Transactions, 1956.

24. M. Engels - Untersuchungen an Ringpumpen
    Doctors Thesis, University Hanover, 1940.

25. K. A. Schmidt - Ueber Luftansaugende Kreisel-Pumpen
    Doctors Thesis, University Hanover, 1931.

26. K. Trutnowsky - Konstruktion 1954, Page 386 to 394.

27. S. Eskinazi
    Hsuan Yeh - An Investigation on Fully Developed Turbulent Flows in a
    Curved Channel Institute of Aeronautical Science January, 1956.

VIII LIST OF FIGURES

TURBINE TYPE	SYMBOL	A	PRESSURE RATIO	GEOMETRY	$R_e = \frac{uD}{\nu}$	α
AXIAL	——	40	→30	$\frac{t}{h}=.02$ $\frac{e}{D}=.015$	$\frac{te}{t}=.02$ 2×10^5 TO 6×10^6	$16°$
TERRY	----	40	→ 30	$\frac{e}{h}=3.25$	2×10^5 TO 6×10^6	$20°$
DRAG	— ·· —	35 TO 45	— 4	$\frac{D}{d}=1.4$ $\frac{h}{H}=.02$	—	—

AXIAL TURBINES

BLADE NUMBER CORRECTION

$$\frac{\eta}{\eta_o}=\frac{1-1.50_s\frac{e}{h}}{1-15(0_s\frac{e}{h})_o}$$

REYNOLD NUMBER CORRECTION

$$\frac{1-\eta}{1-\eta_o}=\sqrt{\frac{Re_o}{Re}}$$

RIM CLEARANCE CORRECTION

$$\frac{\eta}{\eta_o}=\frac{2-\frac{2}{1+h/s}-\frac{\Omega}{s}(3-\frac{2}{1+h/s})}{2-\frac{2}{1+(h/s)_o}-(\frac{\Omega}{s})_o[3-\frac{2}{1+(h/s)_o}]}$$

DRAG TURBINES

AXIAL CLEARANCE CORRECTN

$$\frac{\eta}{\eta_o}=\frac{1.0043}{1+(\frac{h}{D})^{-1}(\frac{D}{H})^{.5}}$$

TRAILING EDGE CORRECTN

$$\frac{\eta}{\eta_o}=\frac{1.95-7(\frac{te}{t})^2-\frac{D}{t}[2.95-7(\frac{te}{t})]}{1.95-7(\frac{te}{t})^2-(\frac{D}{t})_o[2.95-7(\frac{te}{t})_o]}$$

$$N_s=\frac{N\sqrt{Q_3}}{H_{ad}^{3/4}} \quad (I)$$

$$D_s=\frac{D\,H_{ad}^{1/4}}{\sqrt{Q_3}} \quad (II)$$

$$HP=\frac{\eta\,H_{ad}\,Q_3\,\gamma_3}{550} \quad (III)$$

N = RPM
Q = VOLUME FLOW AT TURBINE EXHAUST [FT³/SEC]
H_{ad} = EXPANSION HEAD [FT-LB/LB]

D = ROTOR DIAMETER [FT]

$\gamma_3=\frac{P_3}{RT_3}$ = GAS DENSITY AT EXHAUST [LB/FT³]

AXIAL   TERRY   DRAG
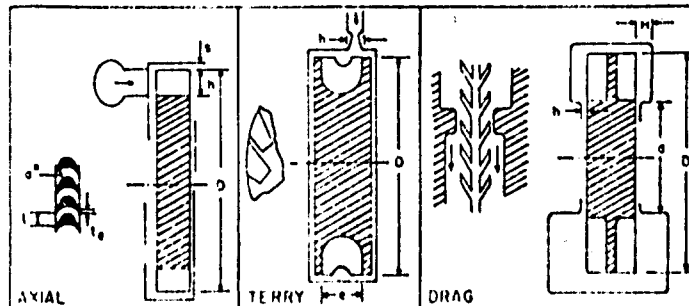
$N_s\ D_s$ DIAGRAM FOR ALL TURBINES
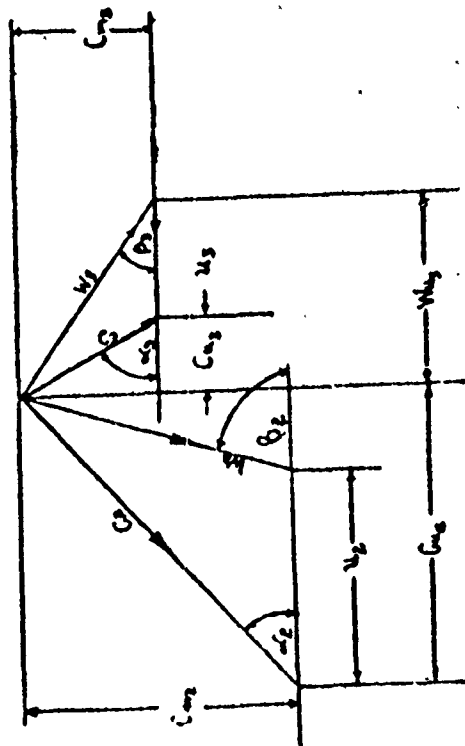
FIGURE IV, 1

TURBINE VELOCITY TRIANGLES

RESISTANCE COEFFICIENT FOR WHEEL DISC FRICTION LOSSES AS FUNCTION OF REYNOLDS NUMBER AND SPACING. FIGURE IV 2
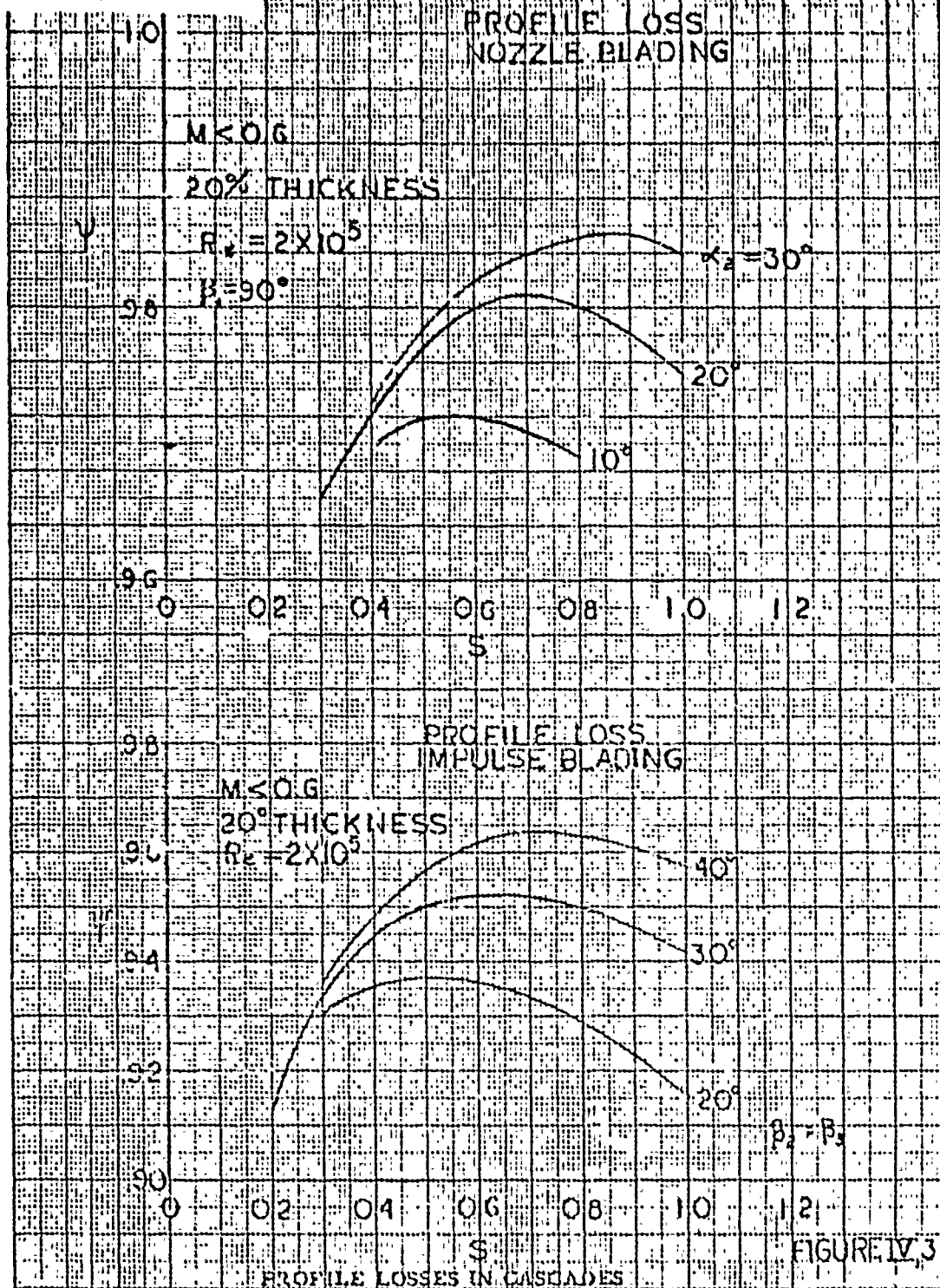
PROFILE LOSS
NOZZLE BLADING

$M \leq 0.6$

20% THICKNESS

$R_e = 2 \times 10^5$

$\beta = 90°$

$\alpha_2 = 30°$

20°

10°

PROFILE LOSS
IMPULSE BLADING

$M \leq 0.6$

20° THICKNESS

$R_e = 2 \times 10^5$

40°

30°

20°

$\beta_2 = \beta_3$

FIGURE IV.3

PROFILE LOSSES IN CASCADES

April 1948
Lab. 119

FIGURE IX,4

SUM OF PROFILE LOSSES AND SECONDARY LOSSES FOR NOZZLES

FIGURE IV.5 — OPTIMUM PITCH/CHORD RATIO FOR NOZZLES
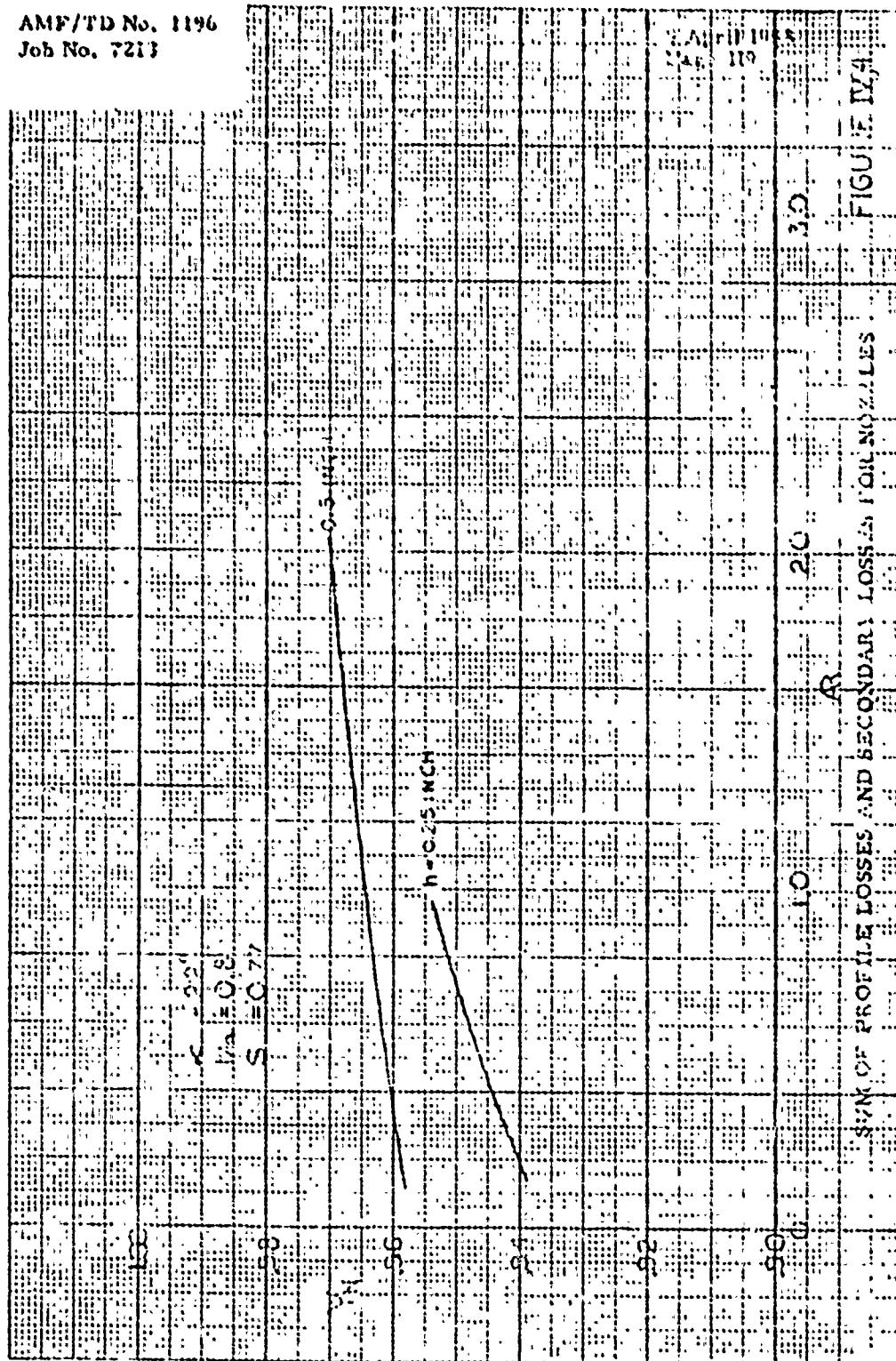
AMF/TD No. 1196
Job No. 2213
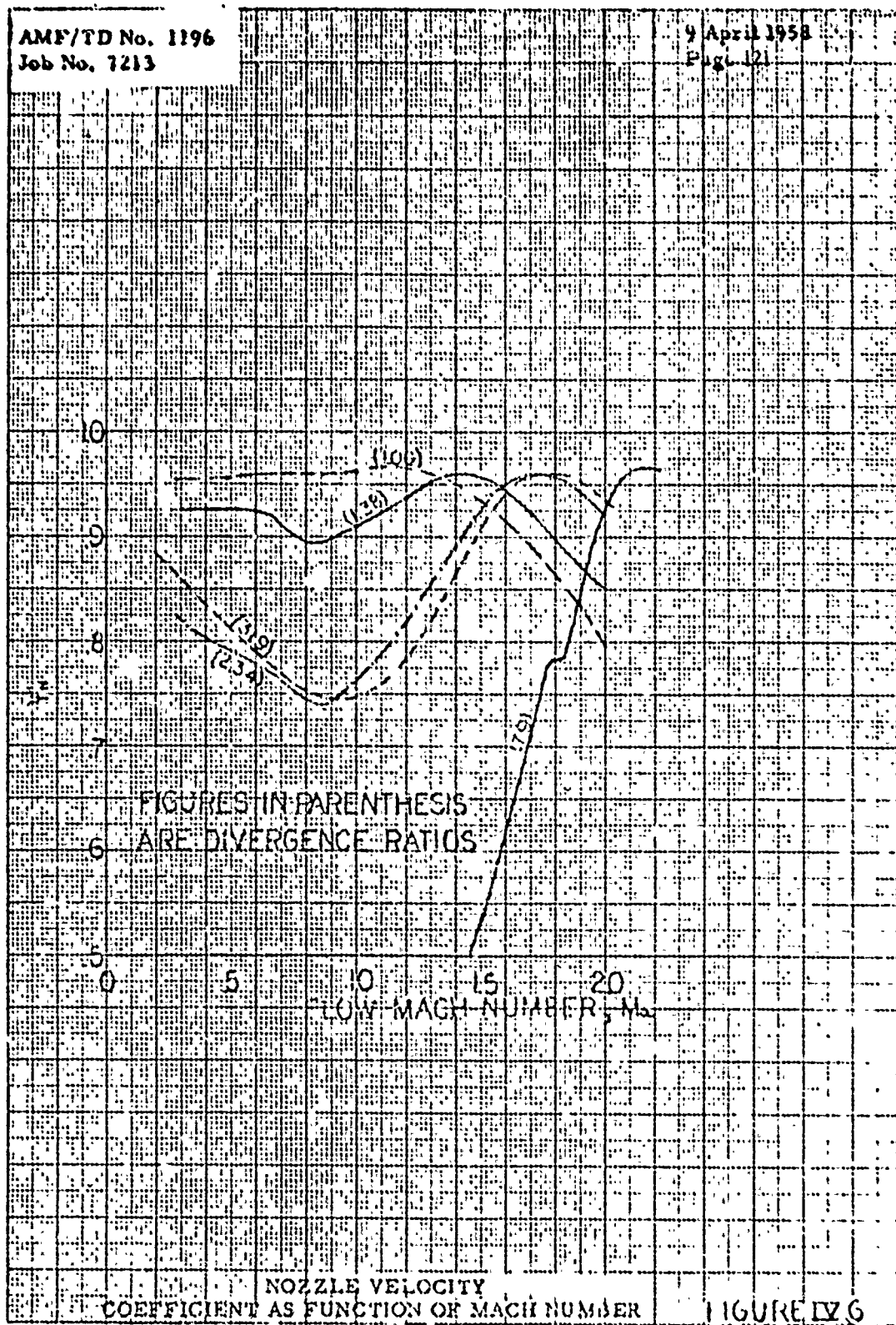
9 April 1958
Page 120

ACCORDING TO AINLEY
HOWELL AND CARTER
ZWEIFEL

FIGURES IN PARENTHESIS
ARE DIVERGENCE RATIOS

(1.00)

(1.28)

(1.18)

(2.34)

(1.9)

FLOW MACH NUMBER, M

NOZZLE VELOCITY
COEFFICIENT AS FUNCTION OF MACH NUMBER
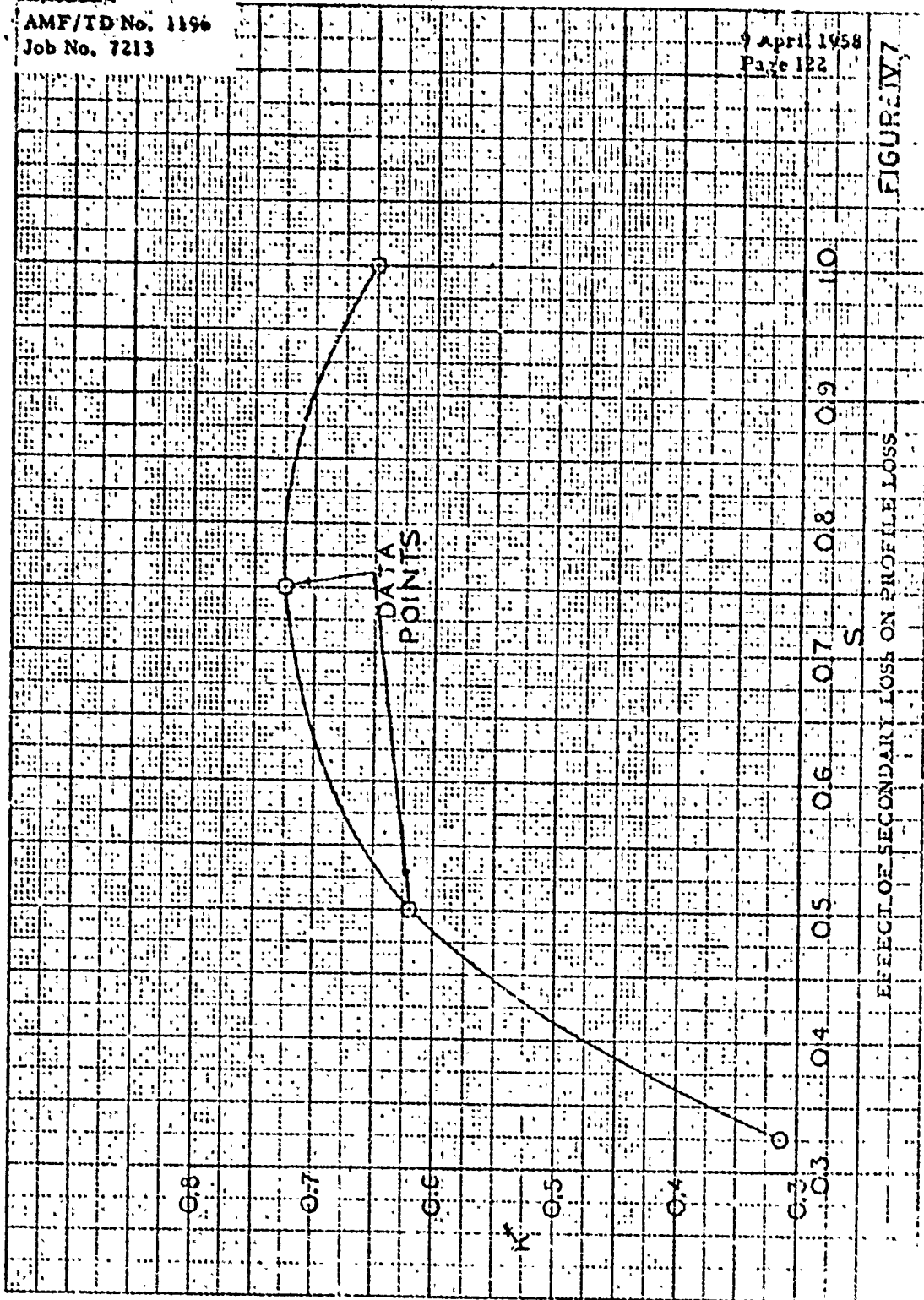
FIGURE IV 6

FIGURE IV-7

EFFECT OF SECONDARY LOSS ON PROFILE LOSS

DATA POINTS

EQUATION II, 35
EQUATION II, 33

1.00
0.50
0.30
0.40
0.20
0.40
0.20
$N = 0.20$

Y_{mc}

1.0
0.9
0.8
0.7
0.6
0.5

S

0.2 0.4 0.6 0.8 1.0
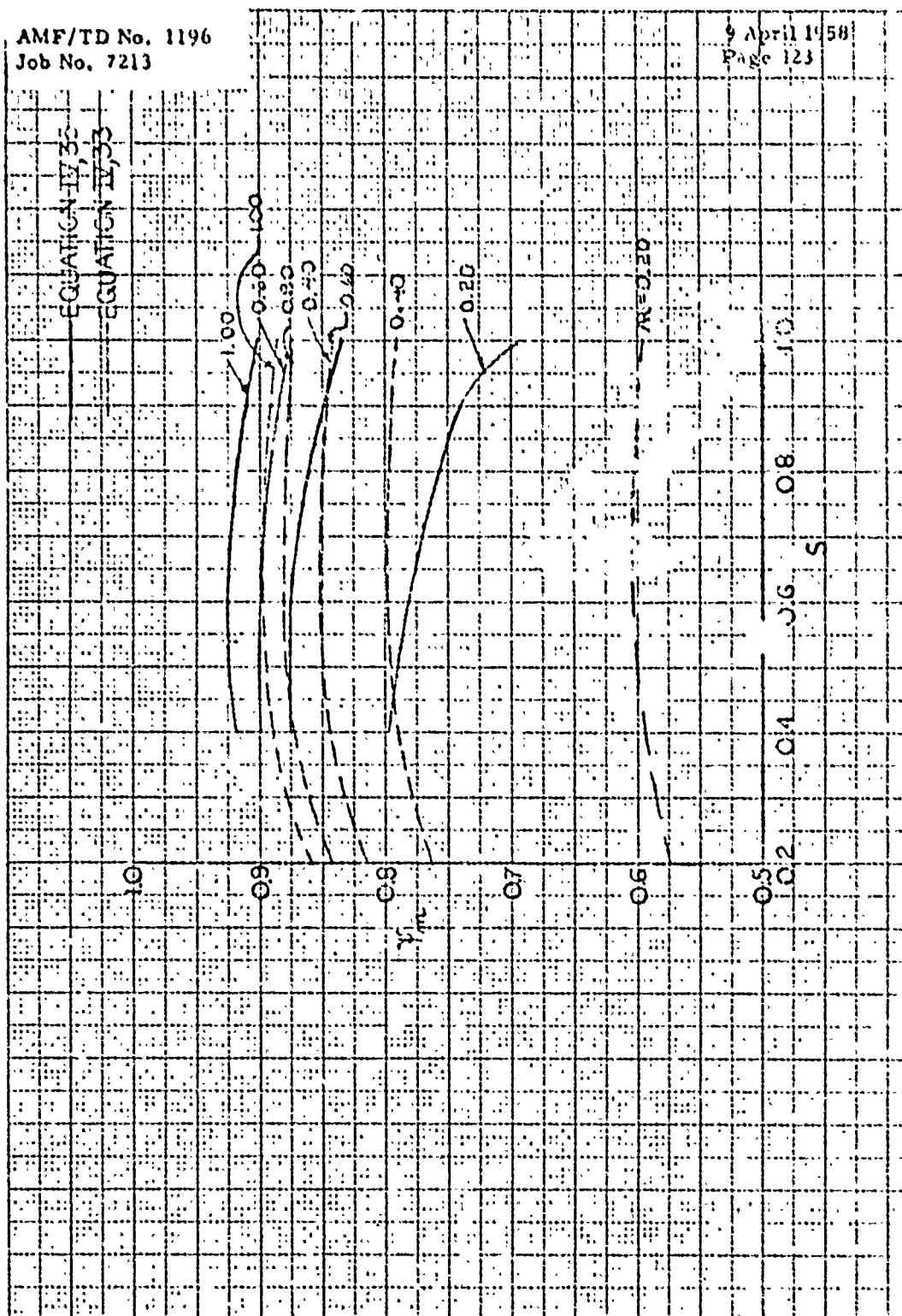
AMF/TD No. 1196
Job No. 7213

9 April 1958
Page 124

FIGURE 79

ACCORDING TO AINLEY
HOWE, AND CARTER
ZWEIFEL

$\beta_2 + \beta_3$

OPTIMUM PITCH CORD RATIO FOR IMPULSE BLADING

PITCH/CHORD

VELOCITY COEFFICIENTS FOR IMPULSE BLADING
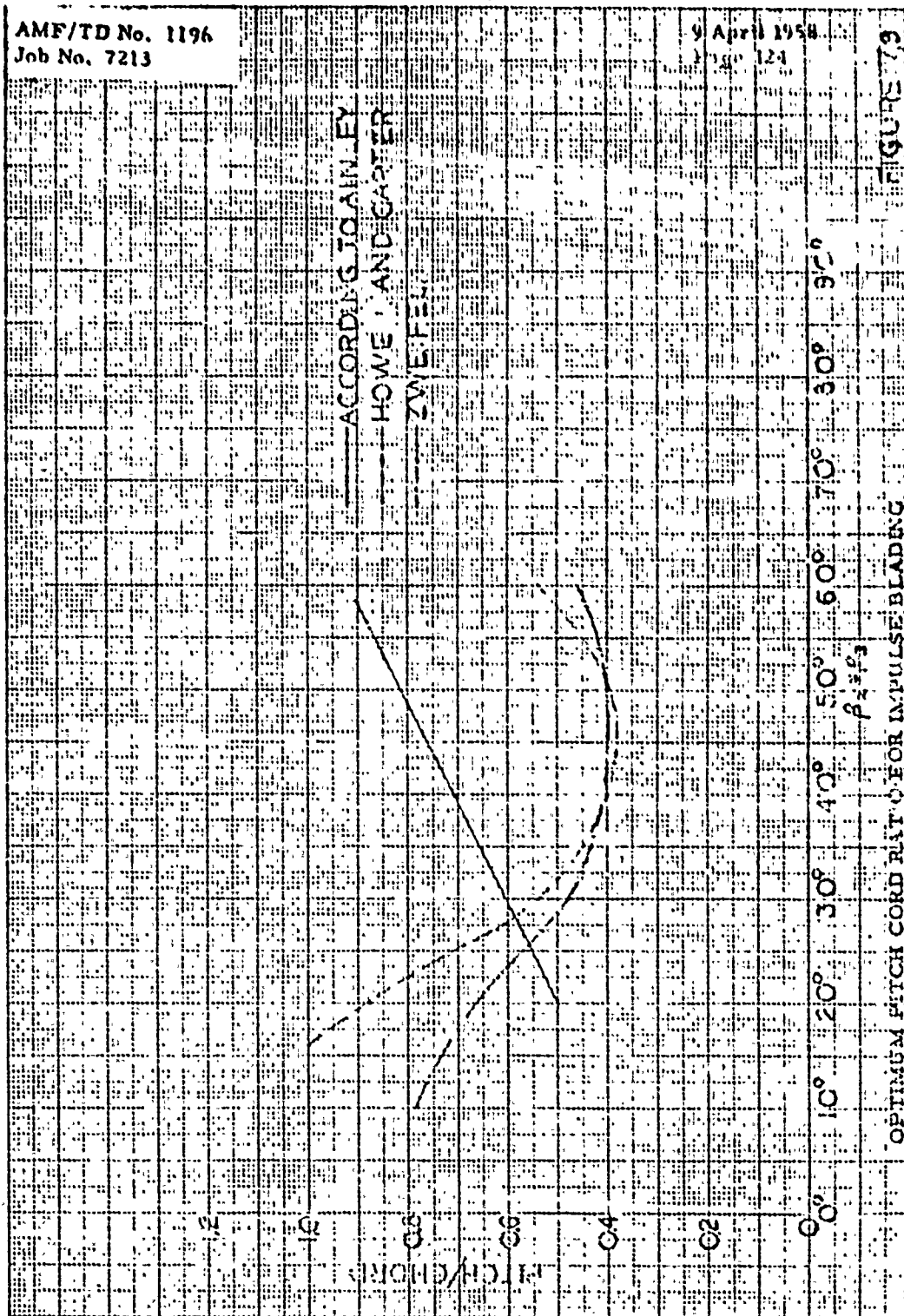
FIGURE 79

AMF/TD No. 1196
Job No. 7213

9 April 1956

IMPULSE BLADES

NOZZLE BLADES

SHEET METAL IMPULSE BLADES
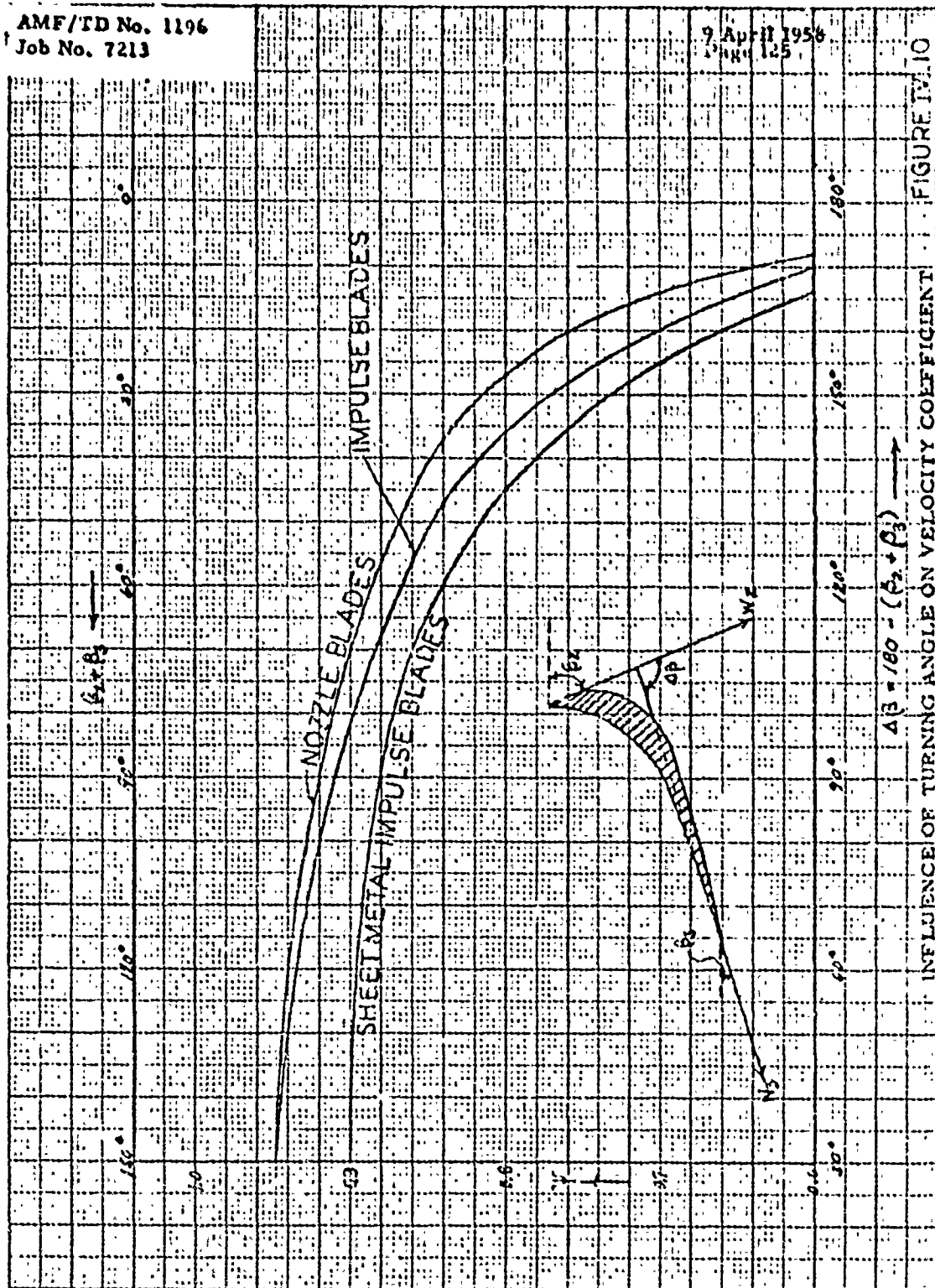
$\Delta\beta = 180 - (\beta_2 + \beta_3)$

INFLUENCE OF TURNING ANGLE ON VELOCITY COEFFICIENT — FIGURE IV.10

IMPULSE BLADES

INLET ANGLE — β_1

INLET MACH NUMBER — Ma
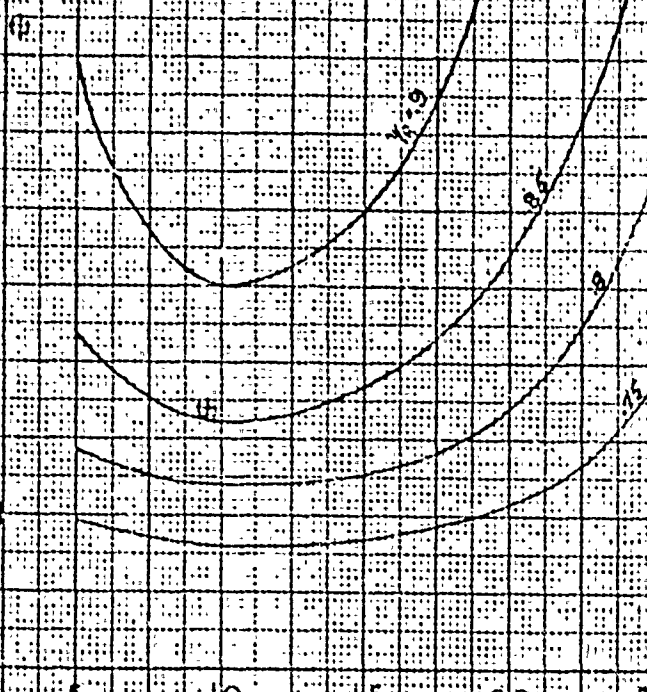
INFLUENCE OF MACH NUMBER ON LOSSES IN IMPULSE BLADINGS   FIGURE IV.11

$R_e = 2 \times 10^5$

1.0

0.9

0.8

0.7

$M_2 = 0.6$

λ (WHEN $M_2 = 0.5$)

t/e

TRAILING EDGE

BLADE THROAT

MEAN RADIUS OF CURVATURE OF $eqn = e = \dfrac{t^2}{8z}$

INFLUENCE OF RADIUS BETWEEN AND LEAVING EDGE ON BLADE LOSSES

FIGURE IV 12

INFLUENCE OF CLEARANCE ON BLADE LOSSES — FIGURE IV13

AMF/TD No. 1196
Job No. 7213

9 April 1958

FIGURE IV-14

INFLUENCE OF TRAILING EDGE THICKNESS ON BLADE LOSSES

t/c
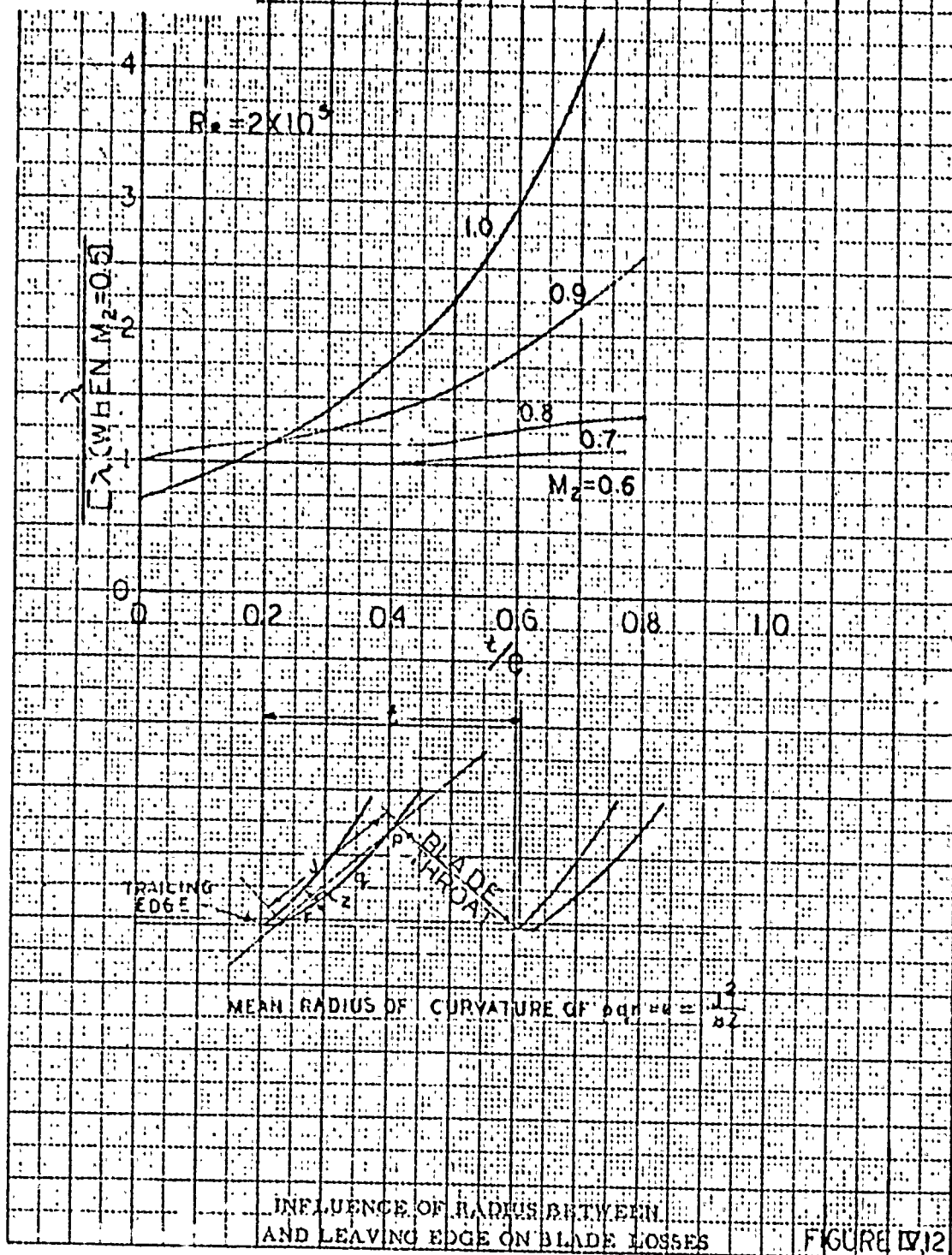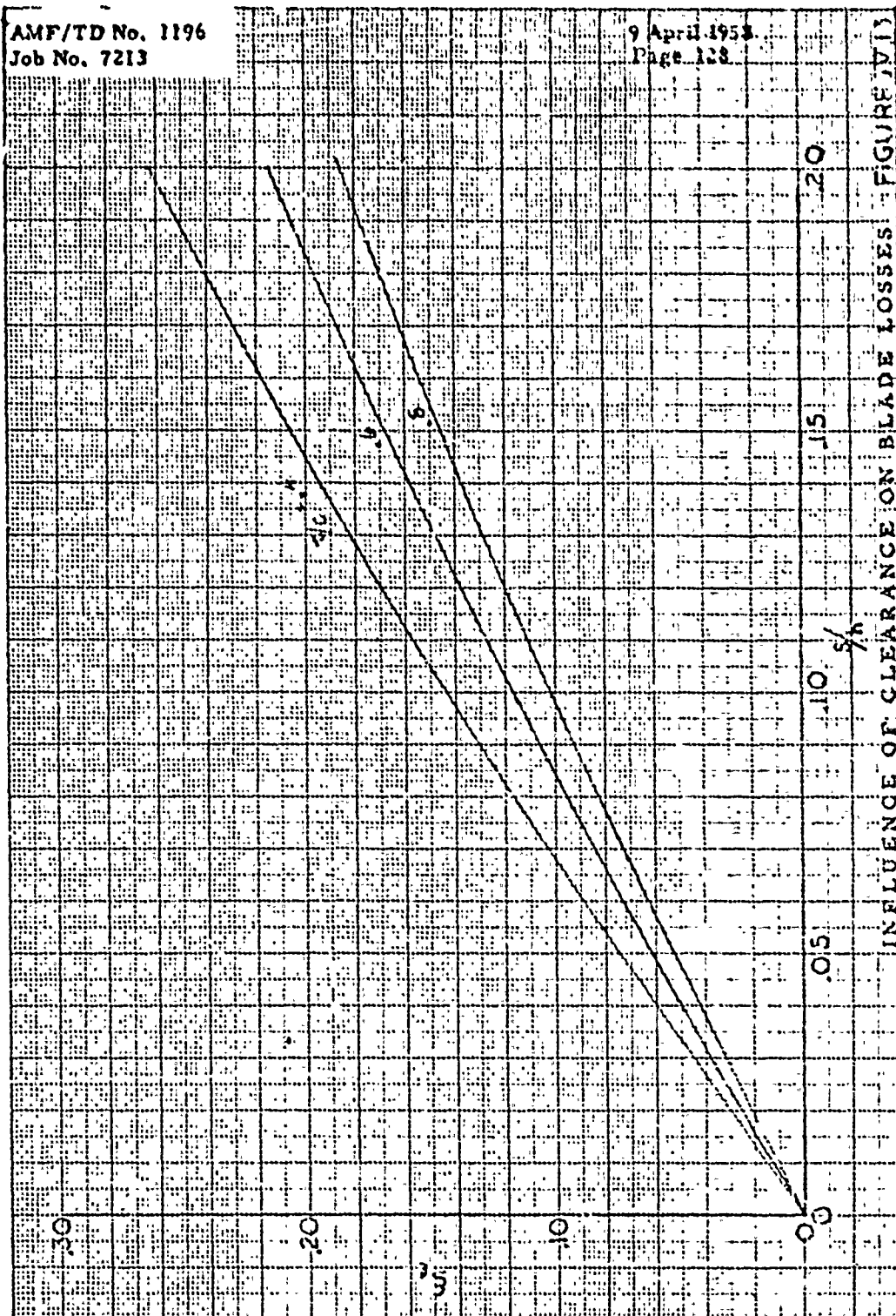
EUGENE DIETZGEN CO.
MADE IN U. S. A.

NO. 340 .20 DIETZGEN GRAPH PAPER
20 X 20 PER INCH
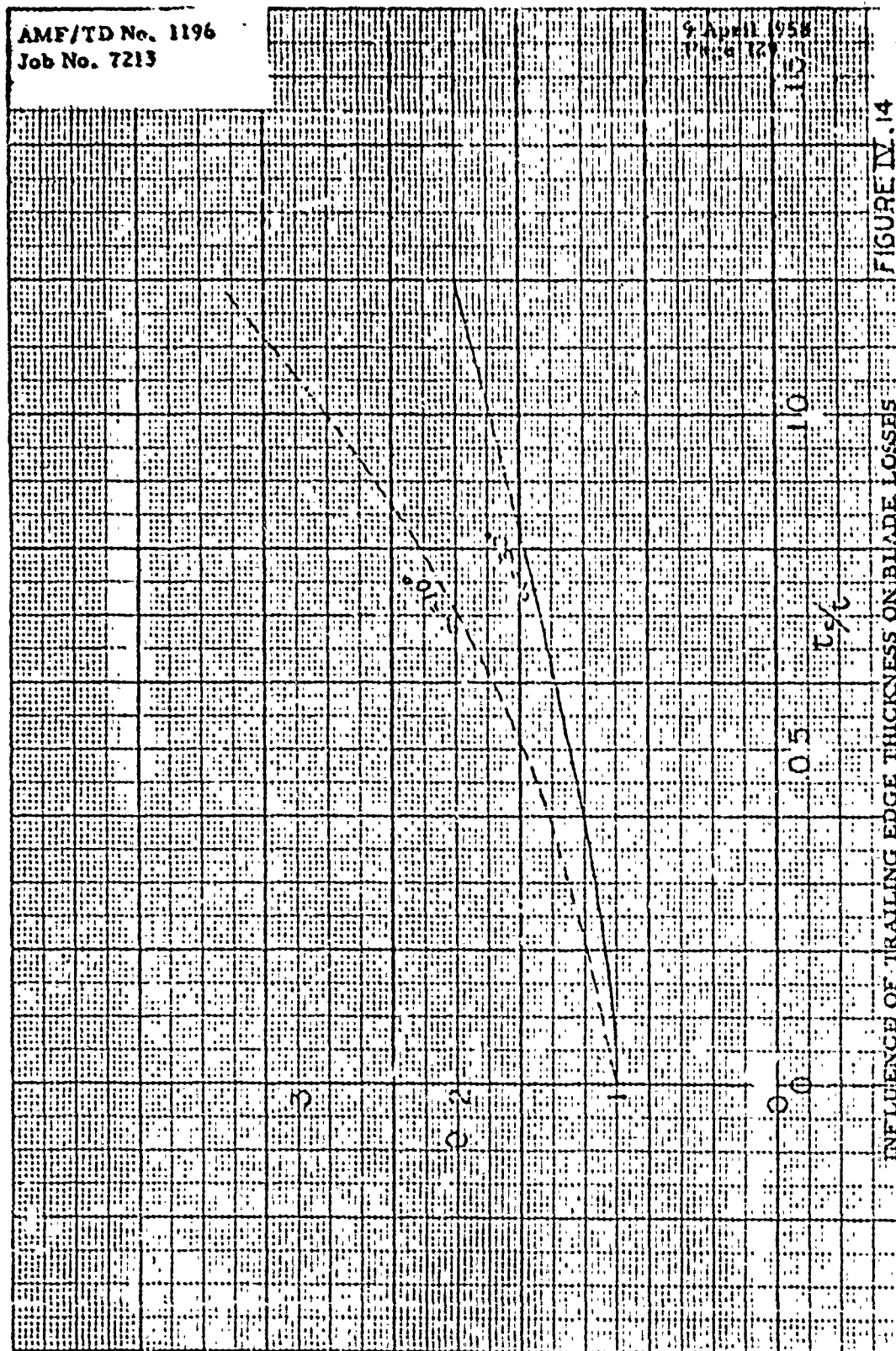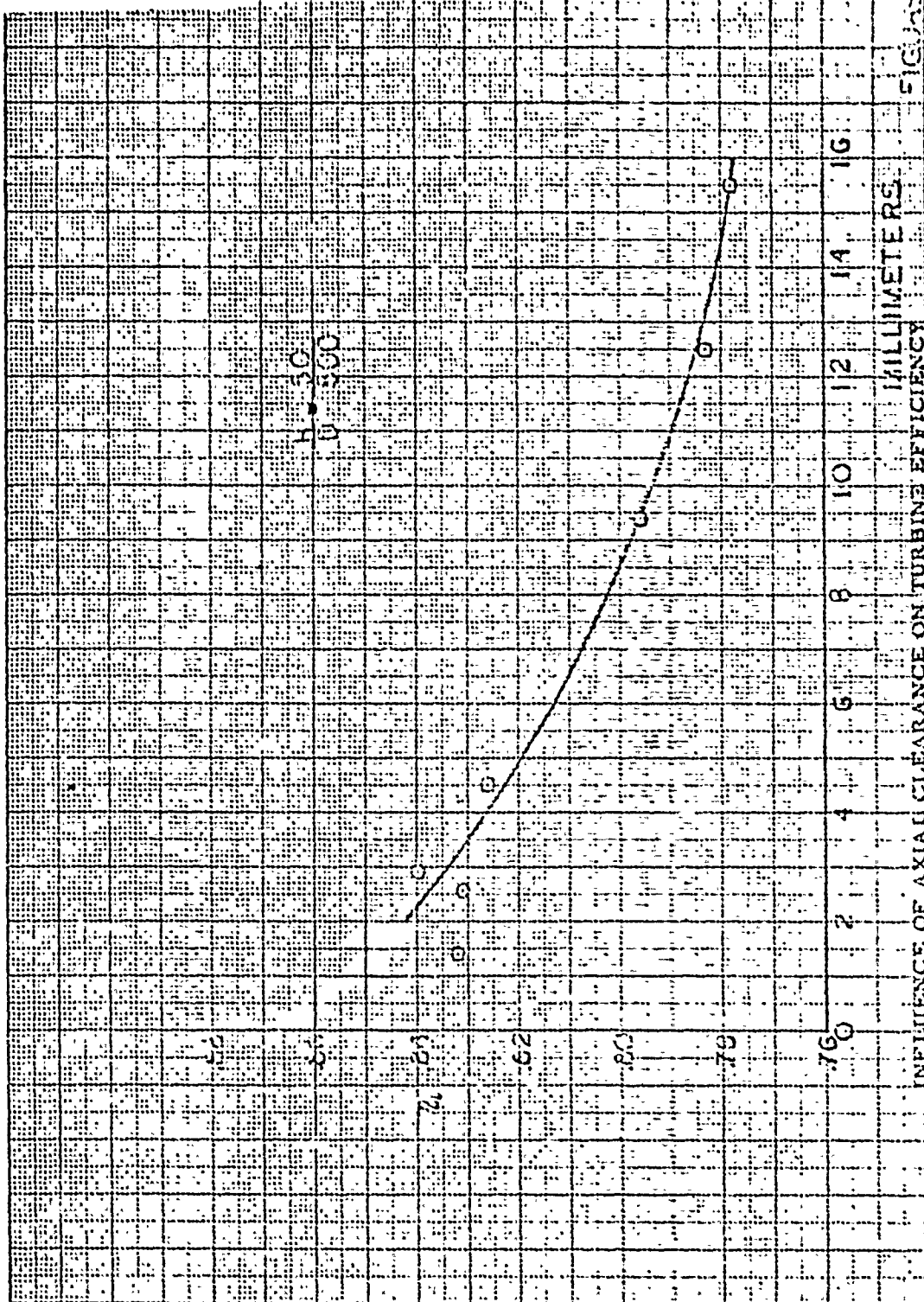
INFLUENCE OF AXIAL CLEARANCE ON TURBINE EFFICIENCY

SUGGESTED MEAN CURVE
FOR TURBINE BLADES

PROFILE LOSS AT $R_e = 2 \times 10^5$

PROFILE LOSS

REYNOLDS NUMBER $\times 10^5$

AMF/TD No. 1196
Job No. 7213

9 April 1958
Page 191
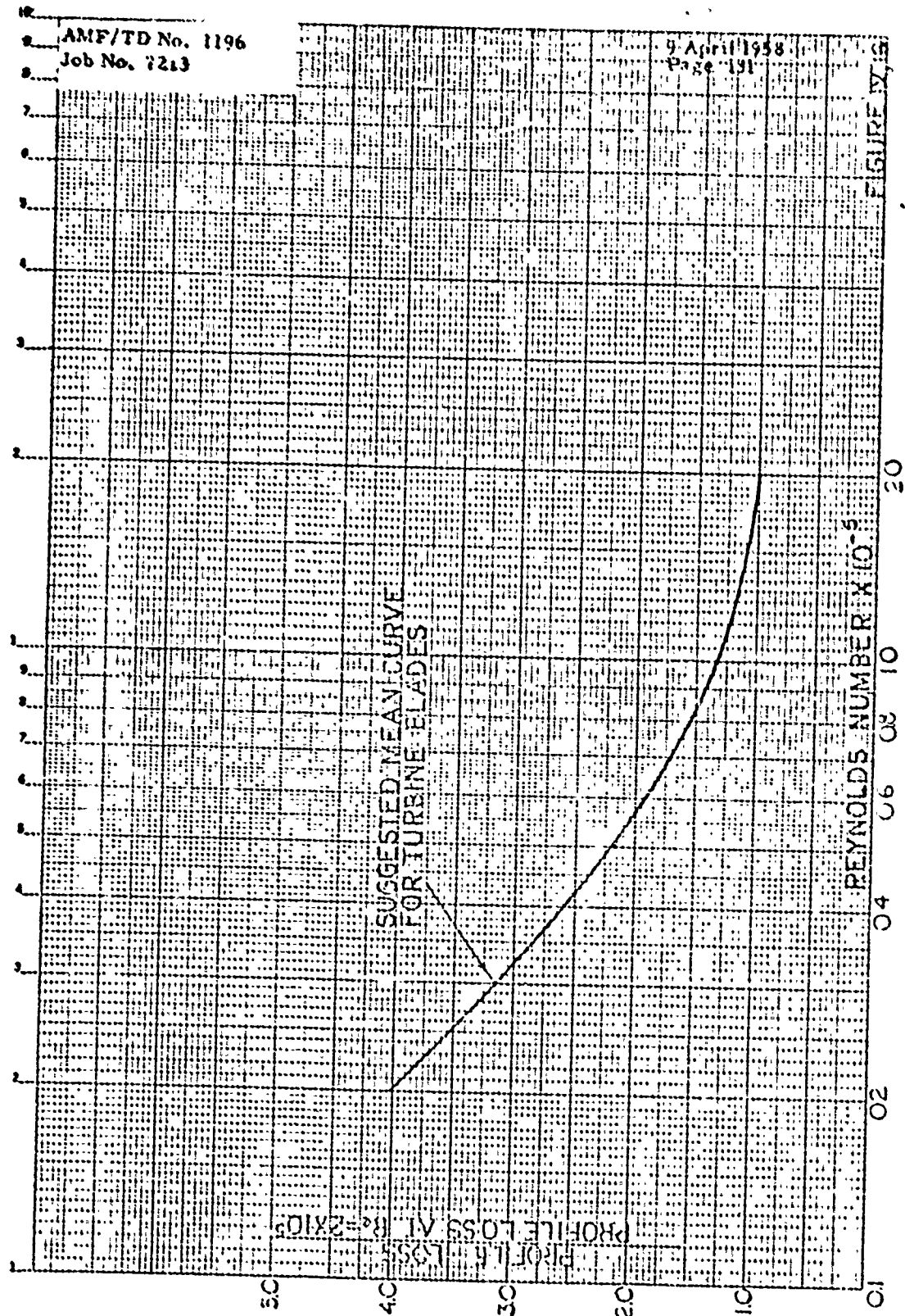
FIGURE IV
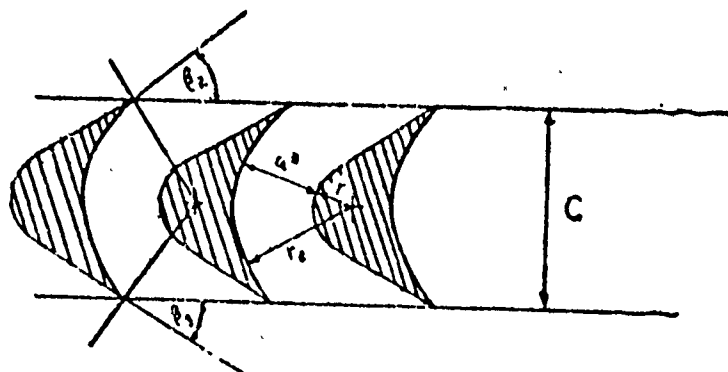
NOTATIONS FOR ROTOR CHANNEL   FIGURE IV,17

EFFICIENCY OF AXIAL PARTIAL ADMISSION TURBINES AS A FUNCTION OF SPECIFIC DIAMETER FOR DIFFERENT SPECIFIC SPEEDS

FIGURE IV,18

AMF/TD No. 1196
Job No. 7213

9 April 1958
Page 133

FIG. 03 DIAGRAM FOR AXIAL INTAKE WITH INFINITE HUB RATIO

N_s

C_s
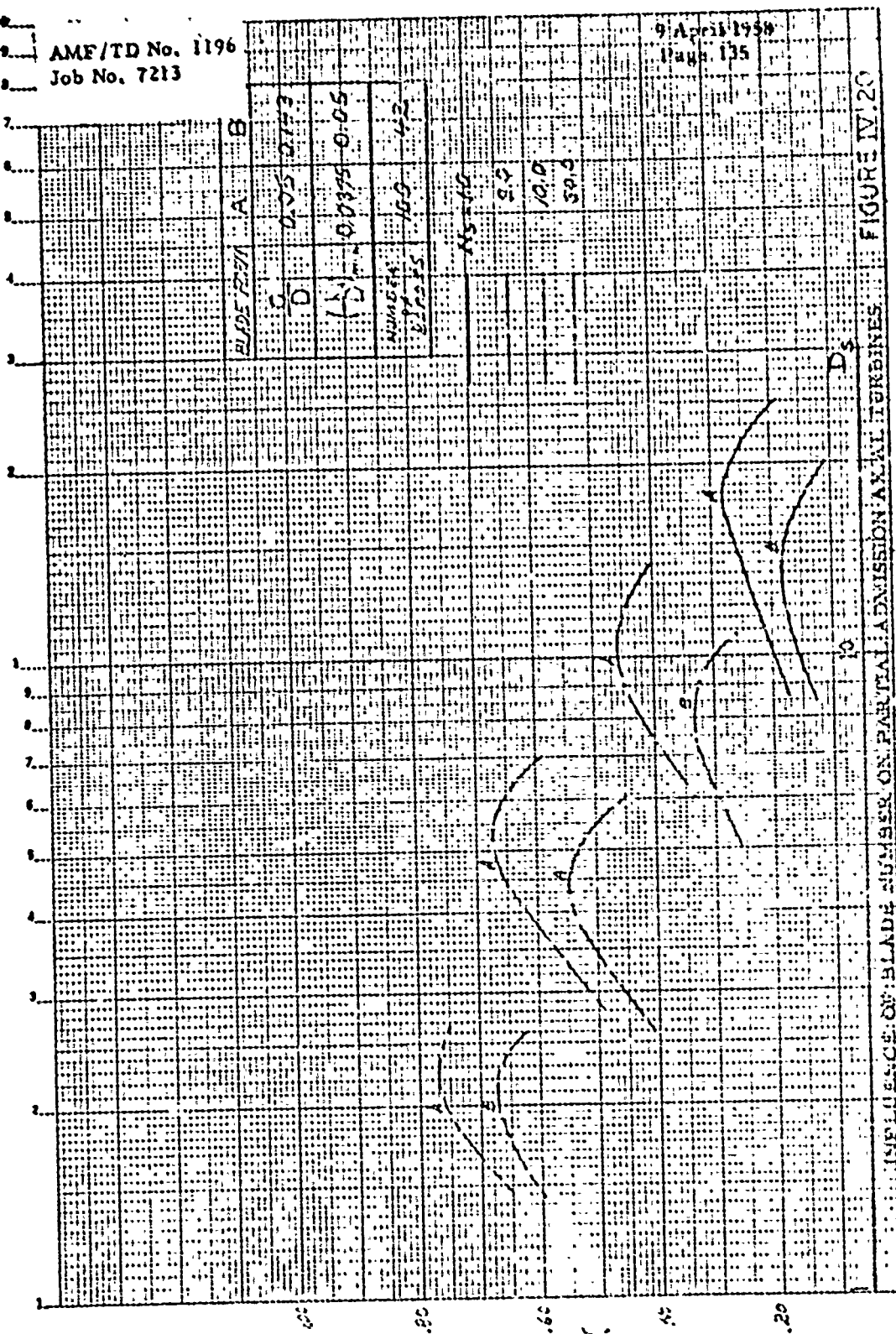
INFLUENCE OF BLADE NUMBER ON PARTIAL ADMISSION AXIAL TURBINES — FIGURE IV.20

AMF/TD No. 1196
Job No. 7213

9 April 1958
Page 135

AMF/TD No. 1196
Job No. 7213

April 1953
Page 136

Ns

REFERENCE 14

CALCULATED FOR OPTIMUM GEOMETRY
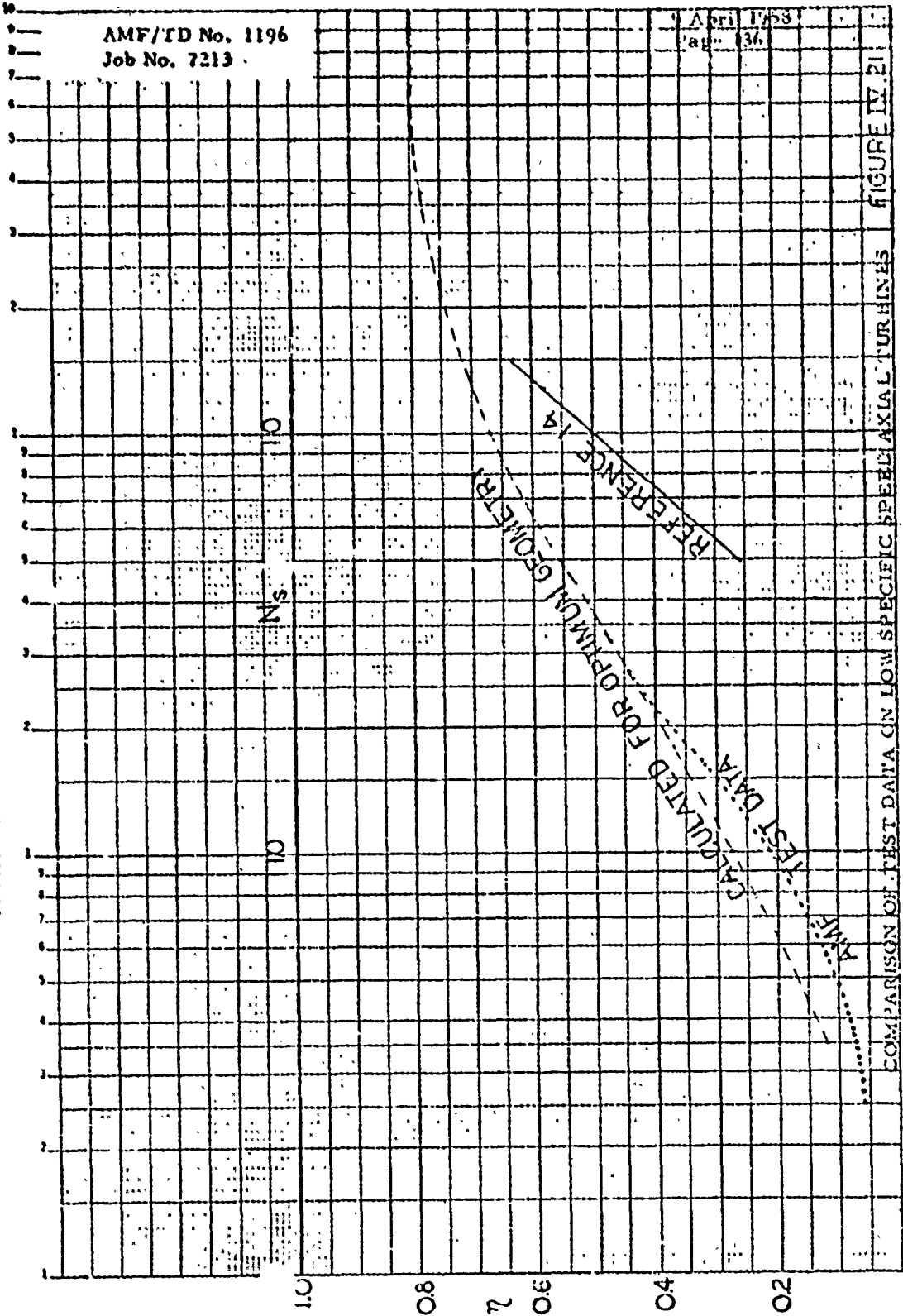
AMF TEST DATA

COMPARISON OF TEST DATA ON LOW SPECIFIC SPEED AXIAL TURBINES   FIGURE IV 21
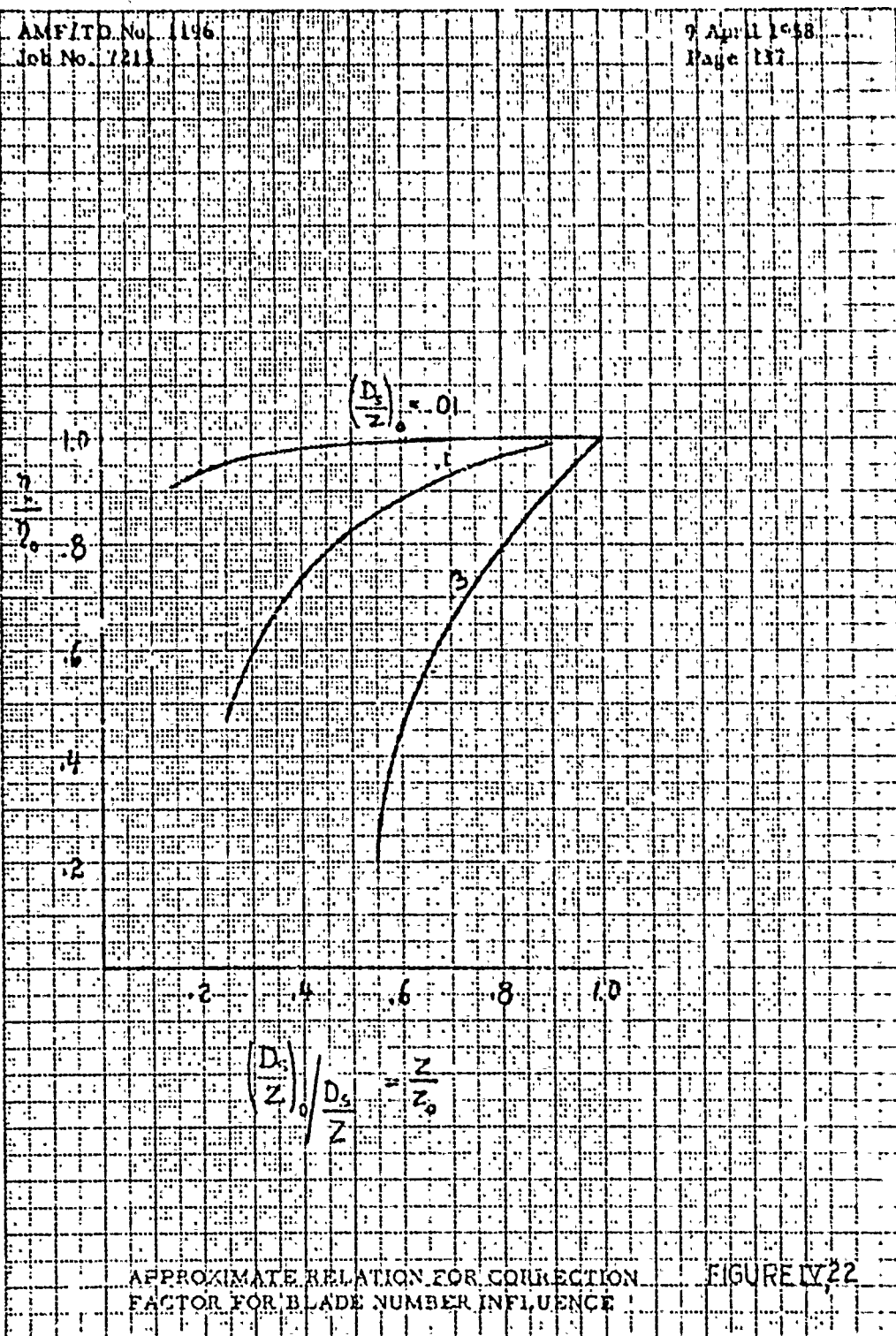
APPROXIMATE RELATION FOR CORRECTION
FACTOR FOR BLADE NUMBER INFLUENCE
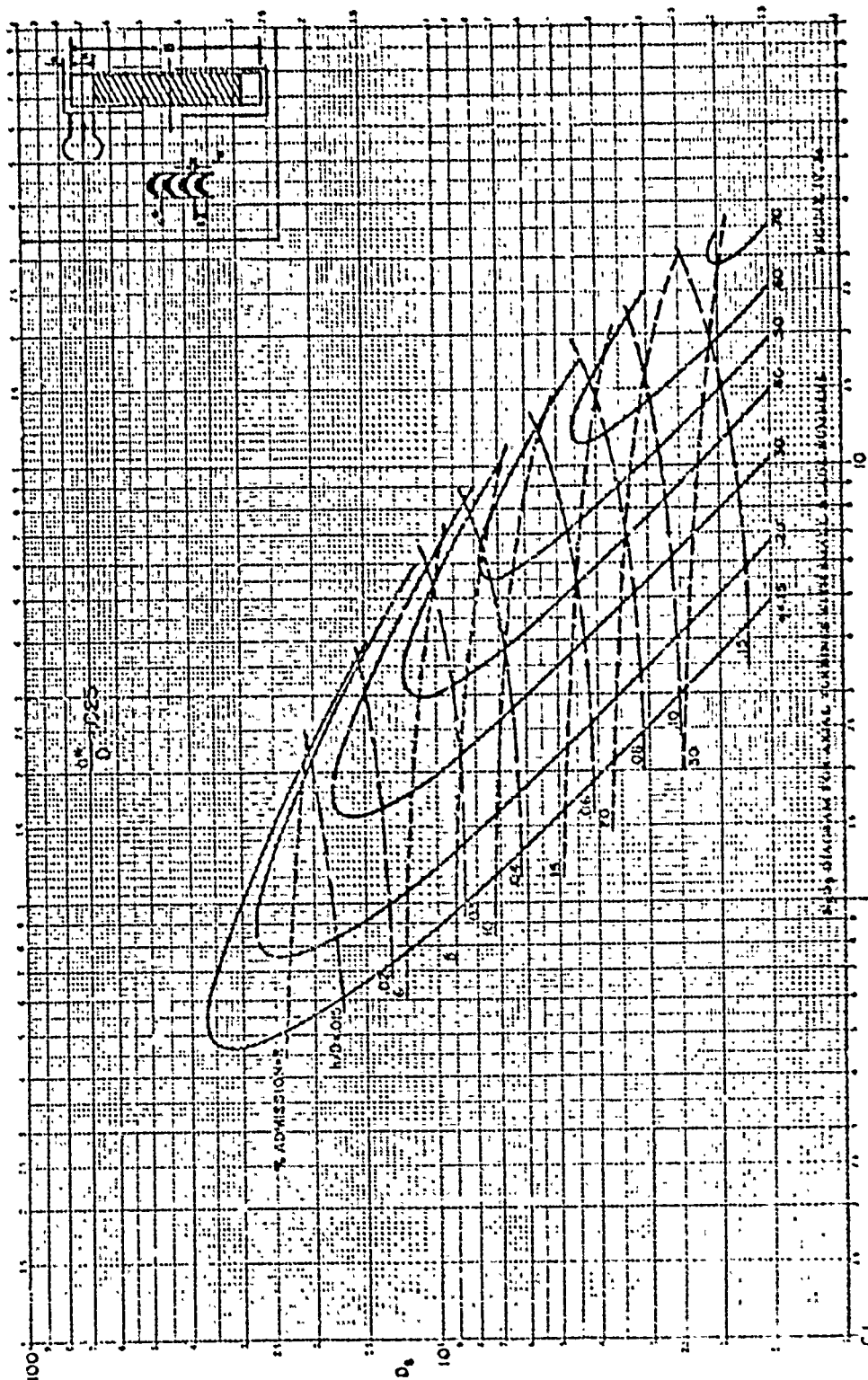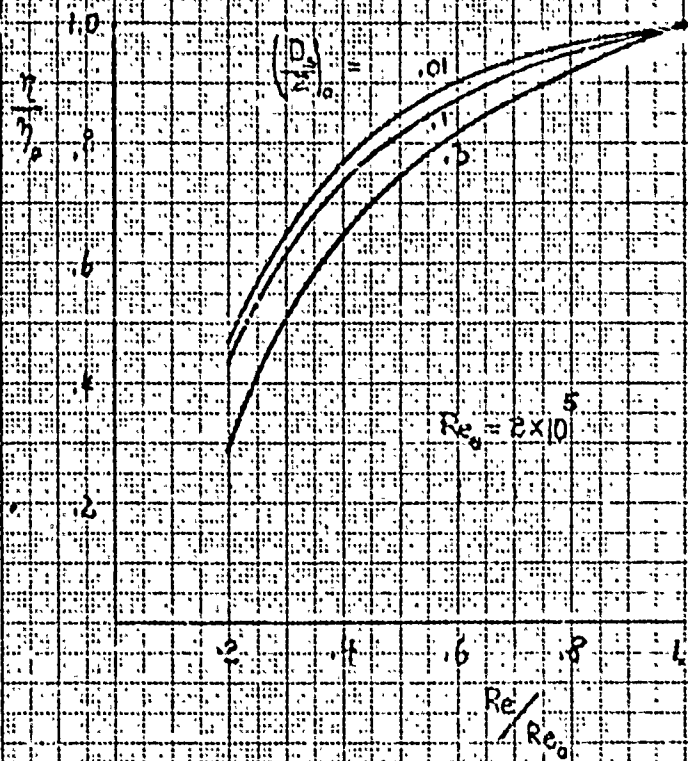
FIGURE IV-22

APPROXIMATE RELATION FOR CORRECTION
FACTOR FOR REYNOLDS NUMBER INFLUENCE FIGURE IV.25

FIGURE IV.26

APPROXIMATE RELATION FOR RIM CLEARANCE RATIO CORRECTION
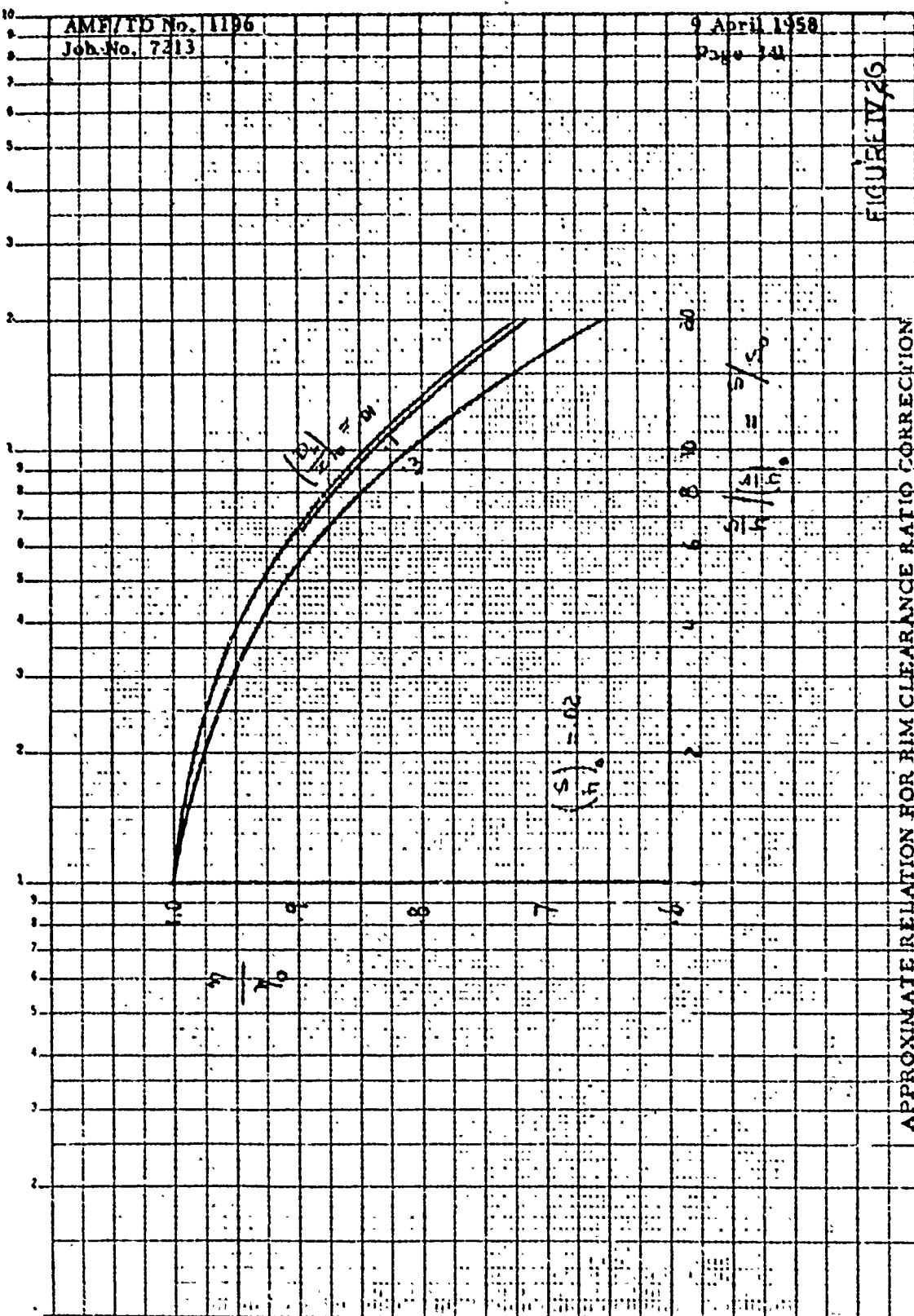
APPROXIMATE RELATION FOR TRAILING EDGE THICKNESS CORRECTION

NOZZLES

ROTOR→
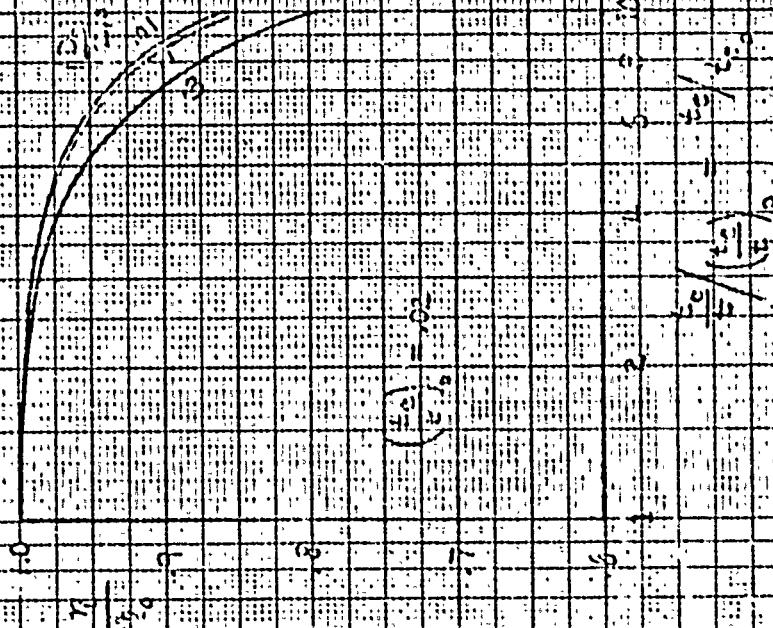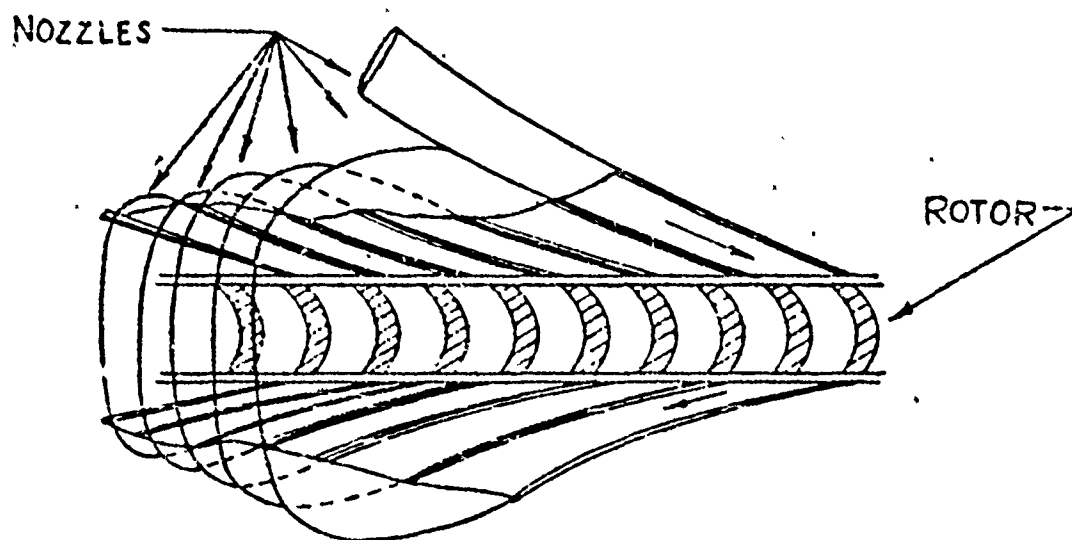
SCHEMATIC SKETCH OF AXIAL REENTRY
TYPE TURBINE

FIGURE IV.28

AMF/TD No. 1196

Job No. 7213

FIGURE 1723

EFFICIENCIES OF REENTRY-TYPE AXIAL TURBINES AS A
FUNCTION OF SPECIFIC SPEED AND SPECIFIC DIAMETER

SEMI-LOGARITHMIC   359·63
KEUFFEL & ESSER CO.   MADE IN U.S.A.
3 CYCLES X 140 DIVISIONS

9 April 1958
Page 115

FIGURE IV 30

EFFICIENCIES OF REENTRY-TYPE AXIAL TURBINES FOR
DIFFERENT STAGE NUMBERS AS A FUNCTION OF SPECIFIC SPEED.

N_s

2

4

8

16 NUMBER OF STAGES

η

1.00
.90
.80
.70
.60
.50
.40
.30
.20
.10

0.1   0.3   1.0   3   10   30
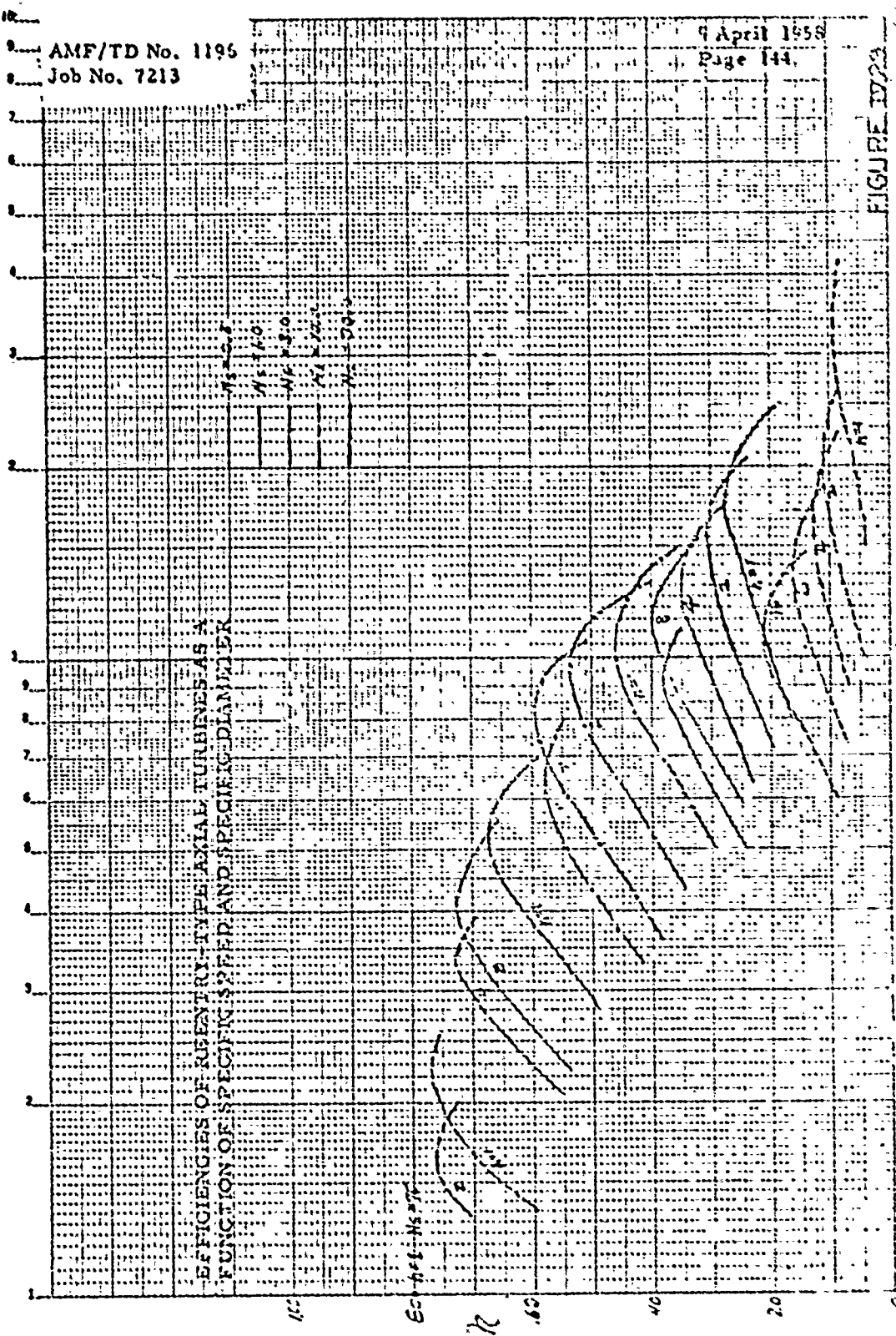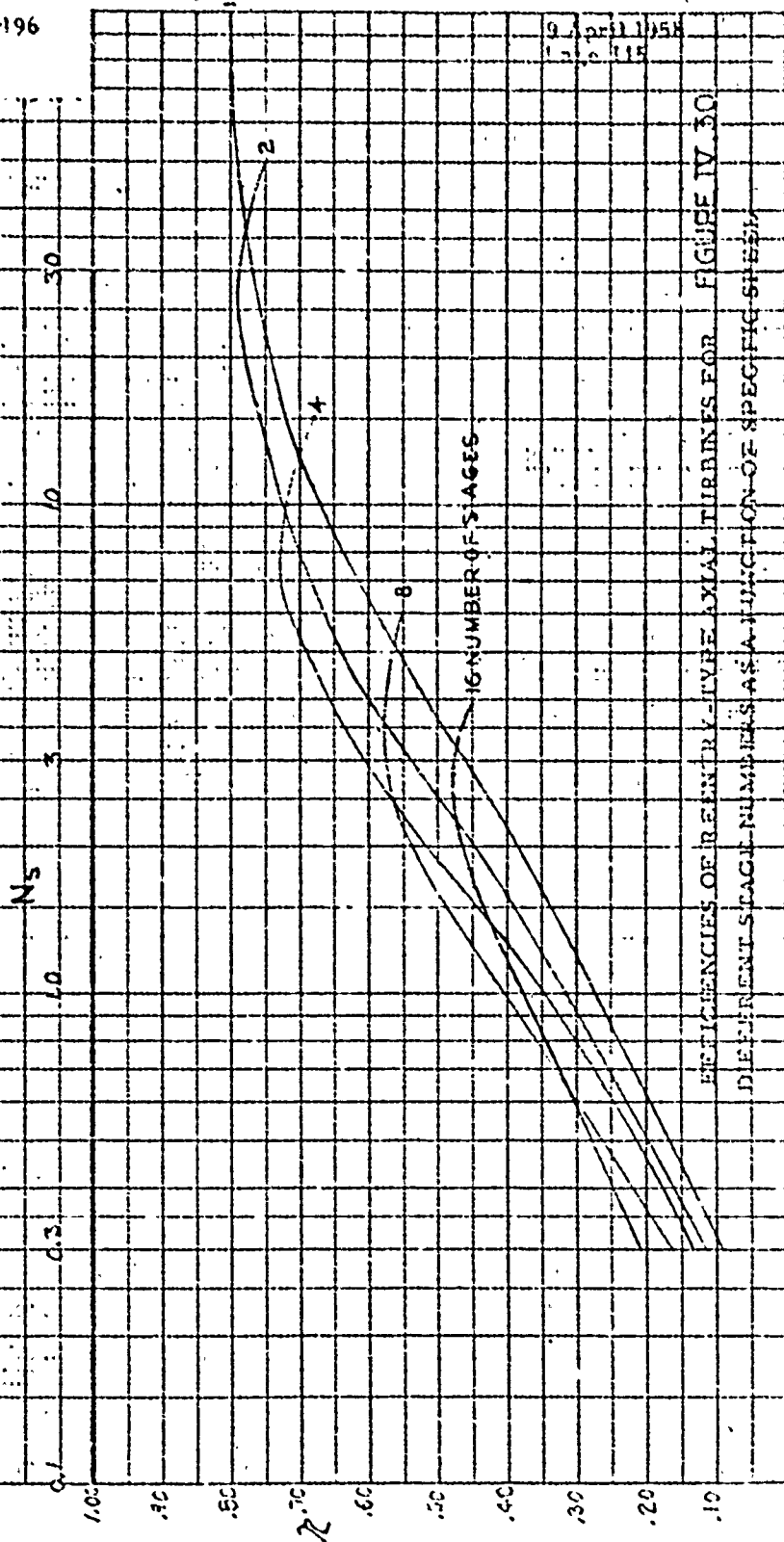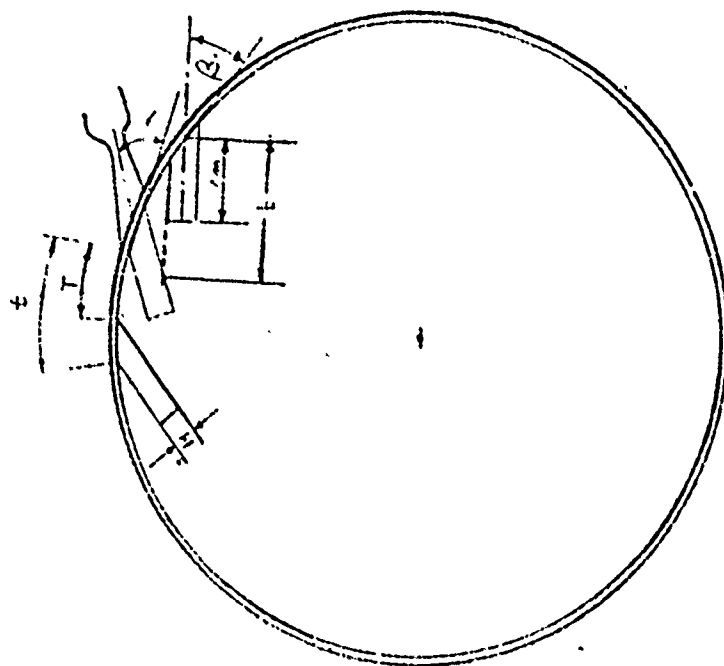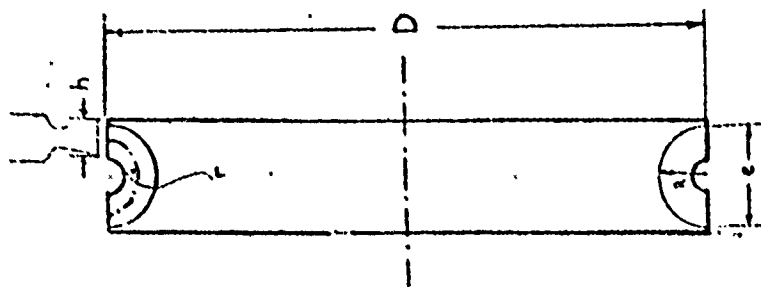
SCHEMATIC CROSS SECTION THROUGH A TERRY-TYPE TURBINE
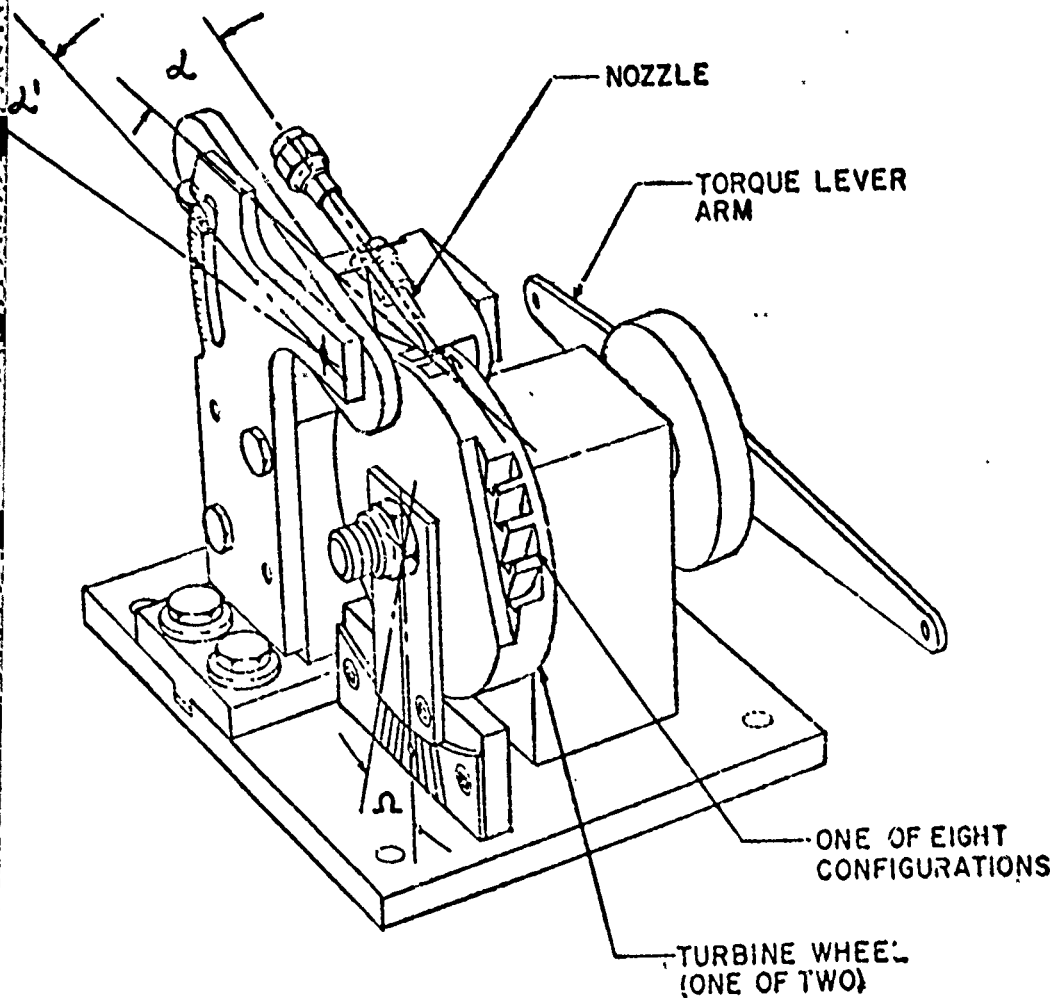
NOTE:
 1. ⍺' = NOZZLE ANGLE FROM HORIZONTAL
 2. ⍺ = NOZZLE ANGLE FROM TANGENT TO WHEEL
 3. Ω = WHEEL POSITION ANGLE

SCHEMATIC CROSS SECTION OF TERRY BUCKET TESTER   FIGURE IV,32

AMF/TD No. 1196
Job No. 7213

9 April 1958
Page 148

FIGURE 33

WIDE BLADE SPACING

NARROW BLADE SPACING

TORQUE INCH-OUNCES

70
60
50
40
30
20

WHEEL INDICATOR SETTING

-10 -8 -6 -4 -2 0 2 4 6 8 10
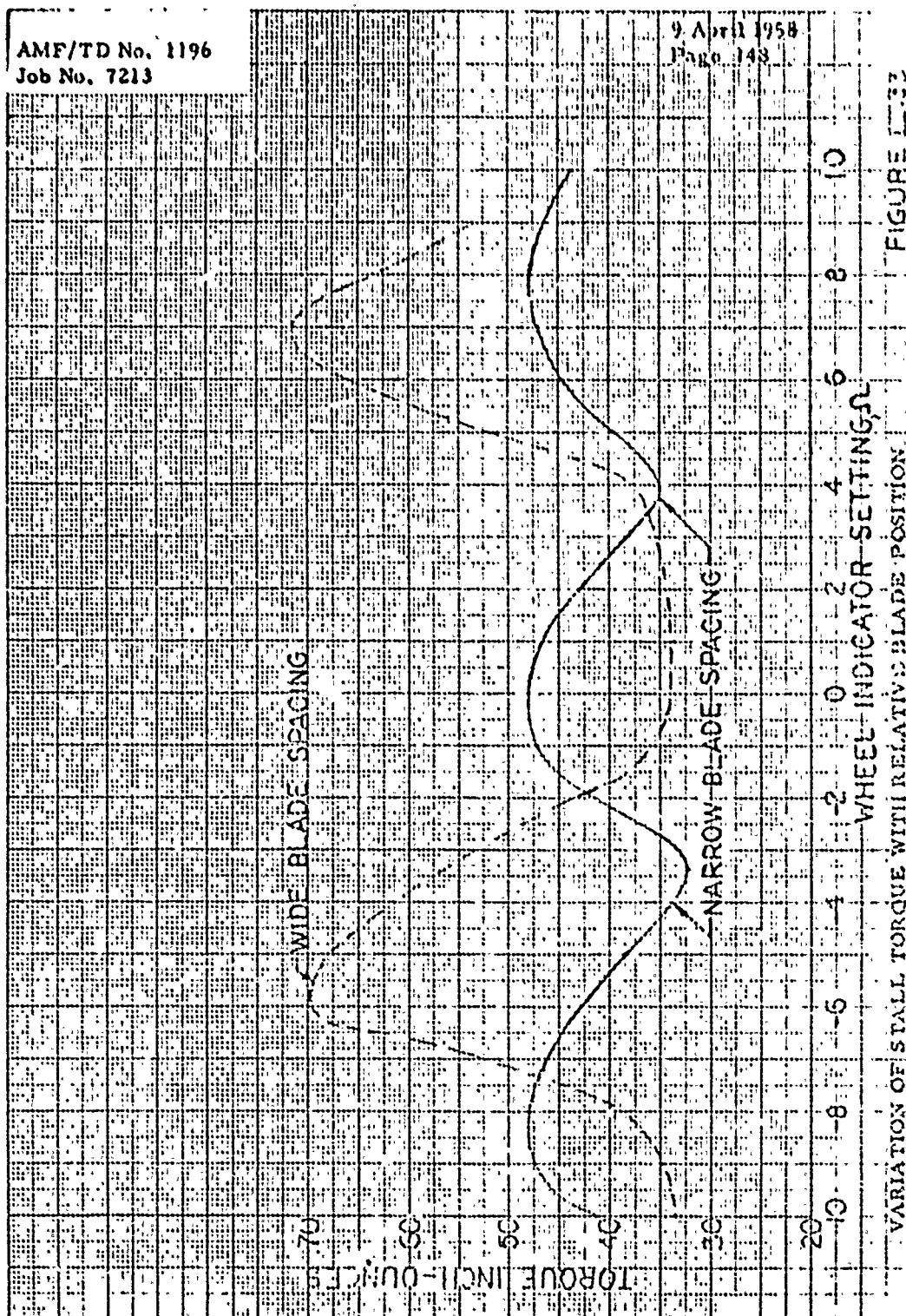
VARIATION OF STALL TORQUE WITH RELATIVE BLADE POSITION

K·E 10X10 TO THE CM   359·14G

FIGURE M.4

TERK: ROTOR COEFFICIENTS

ZERO INCIDENCE POINT
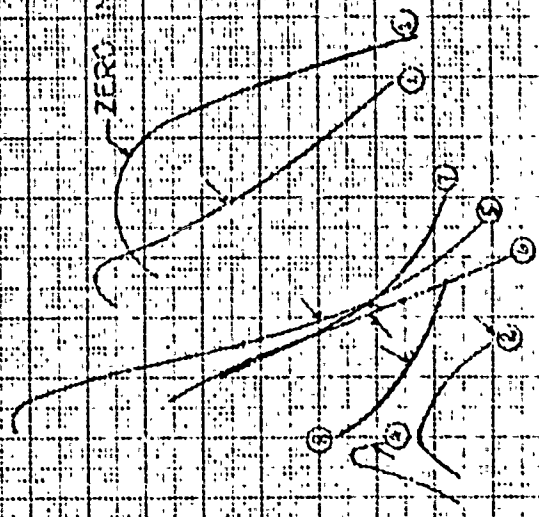
AMF/TD No. 1196
Job No. 7213

9 April 1958
Page 150

FIGURE IV.35

TERRY ROTOR COEFFICIENTS AS A FUNCTION OF GEOMETRY
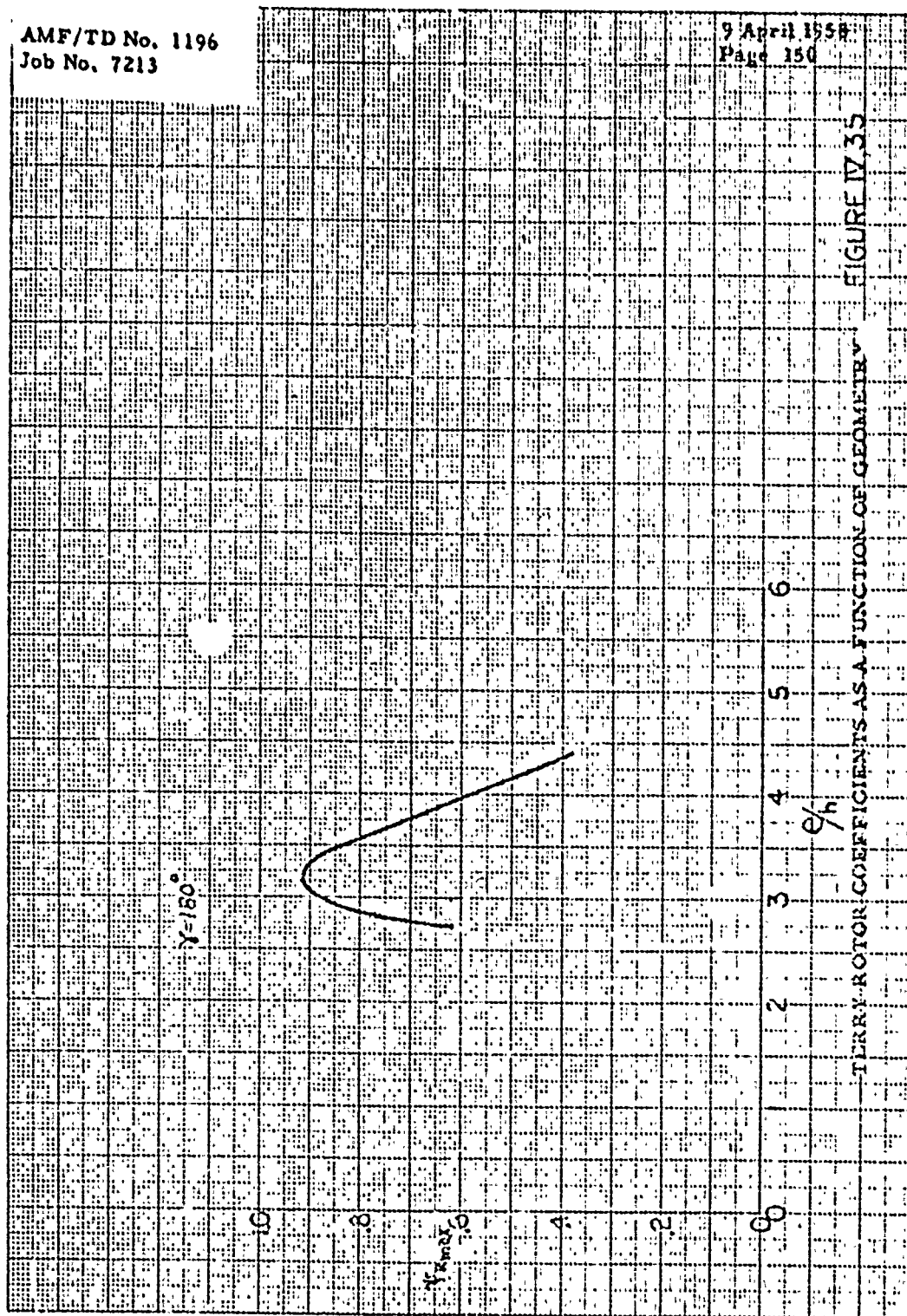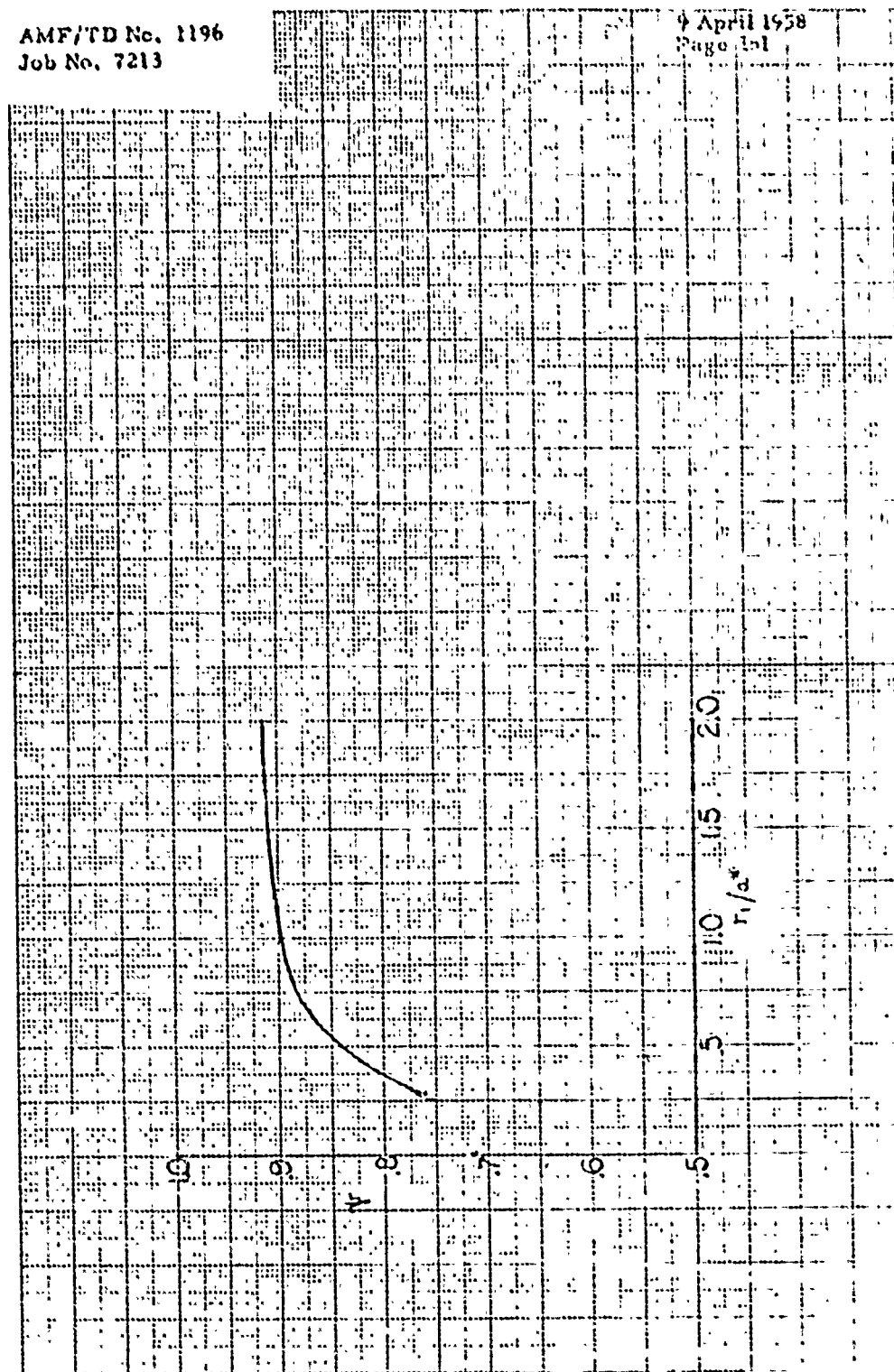
FIGURE 17

CASCADE LOSSES AS A FUNCTION OF TURNING RADIUS

r_1/d^*

AMF/TD No. 1196
Job No. 7213

9 April 1958
Page 152

$c/a = 3.22$ $\gamma = 180°$

B/X_{MEAN}

FIGURE IV, 7

TEN (X) ROTOR COEFFICIENT AS A FUNCTION OF GEOMETRY

K·E 10 X 10 TO THE CM   359-14G
KEUFFEL & ESSER CO.
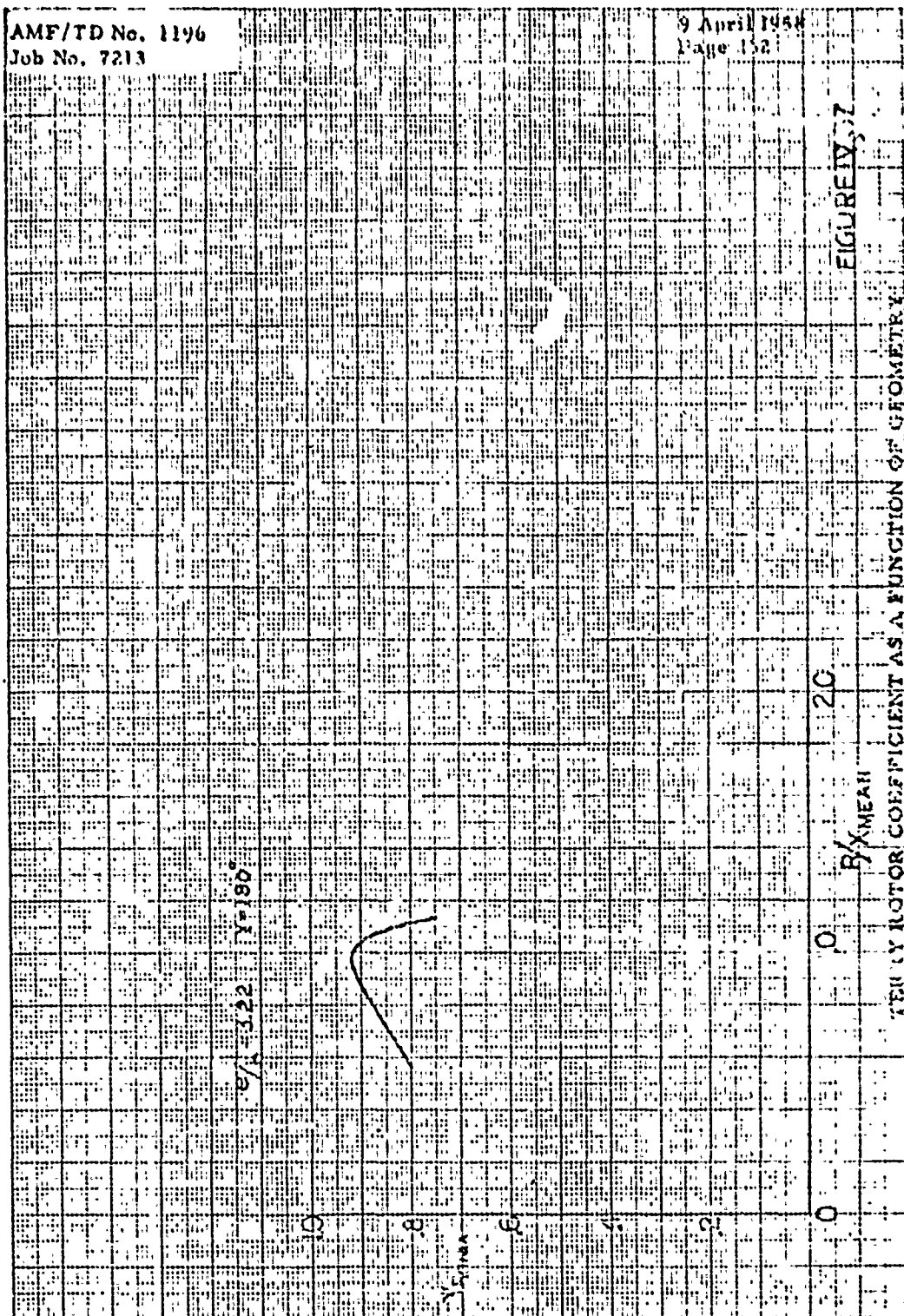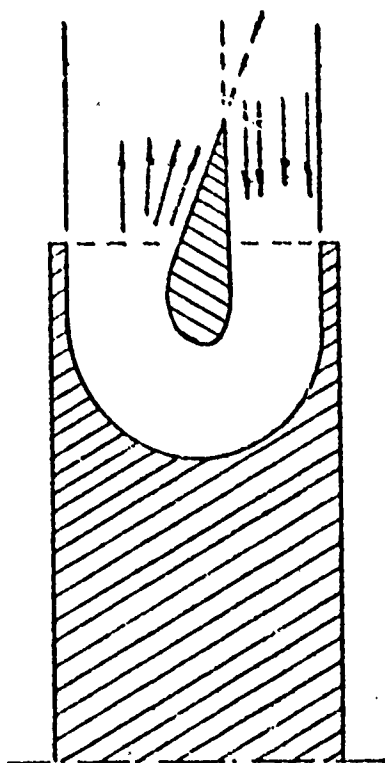
FLOW PATTERN IN TERRY BUCKET   FIGURE IV.38
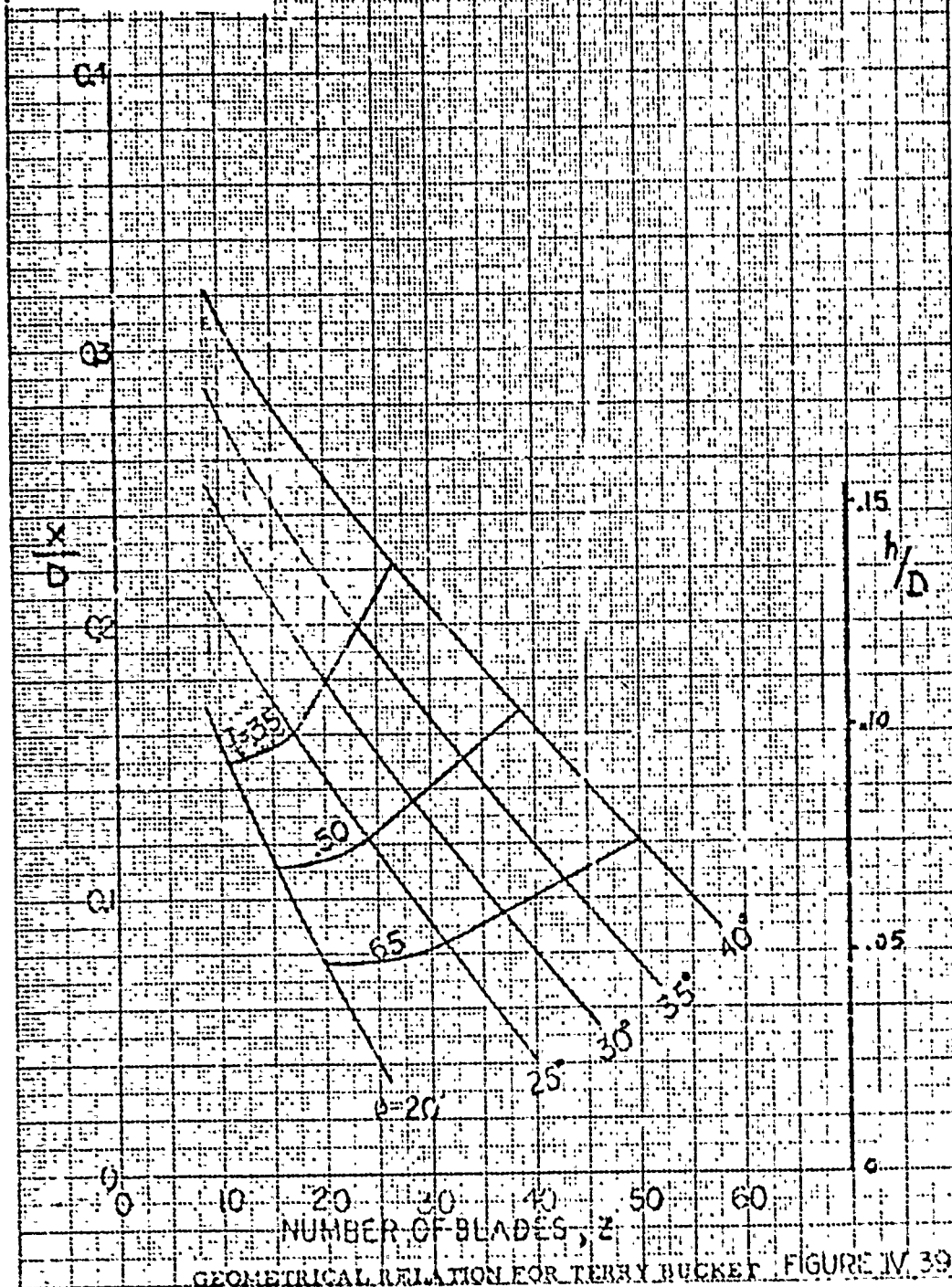
GEOMETRICAL RELATION FOR TERRY BUCKET   FIGURE IV 39
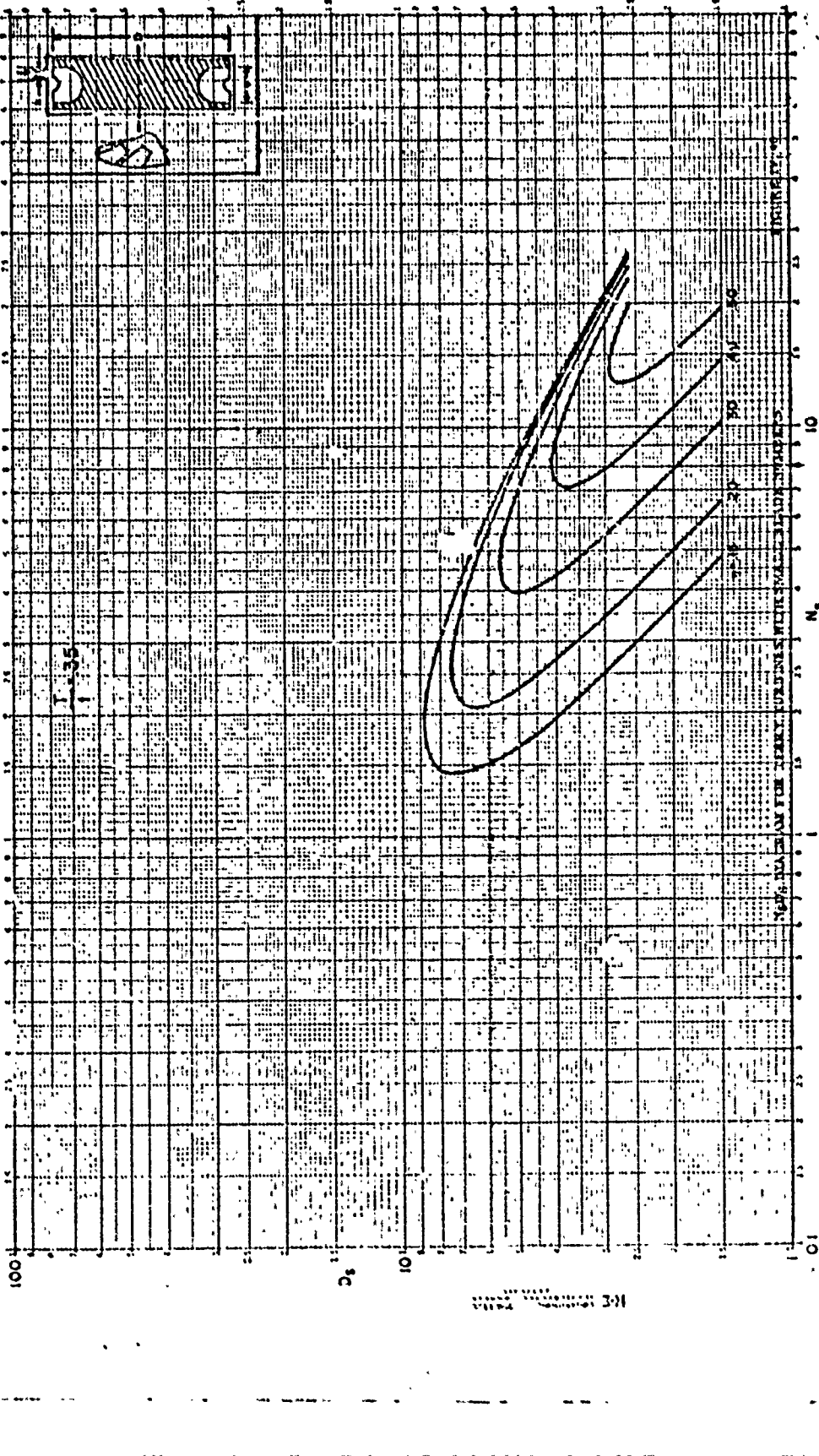
AMF/TD No. 1196
Job No. 7213

9 April 1958
Page 156
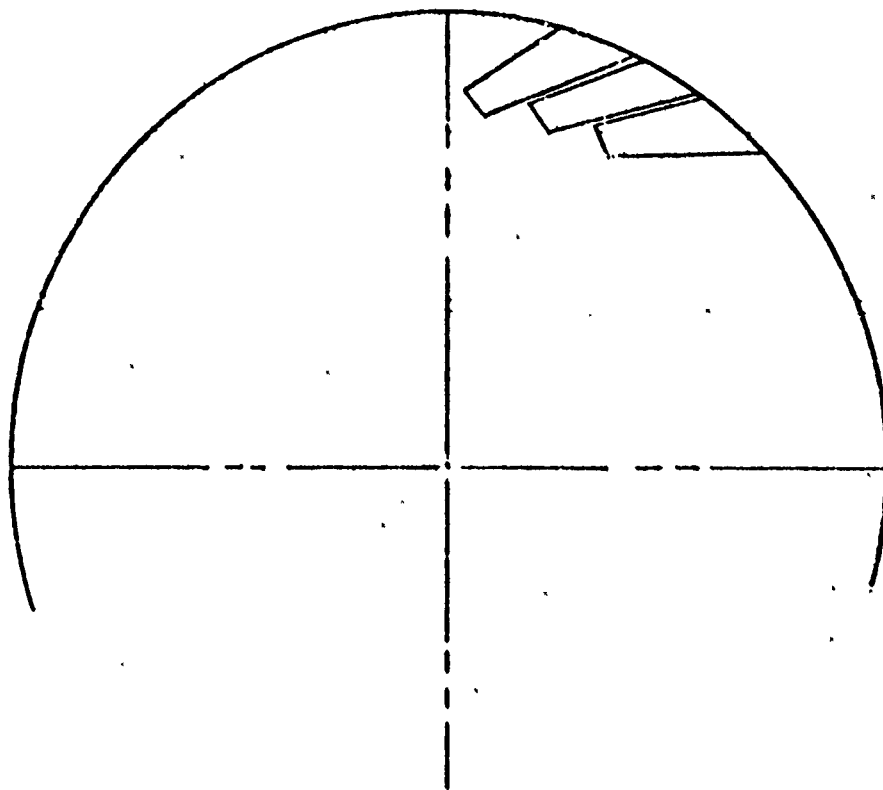
TERRY BUCKET GEOMETRY FOR LARGE BLADE NUMBERS   FIGURE IX,41

SINGLE NOZZLE
OPERATION

D_s

N_s
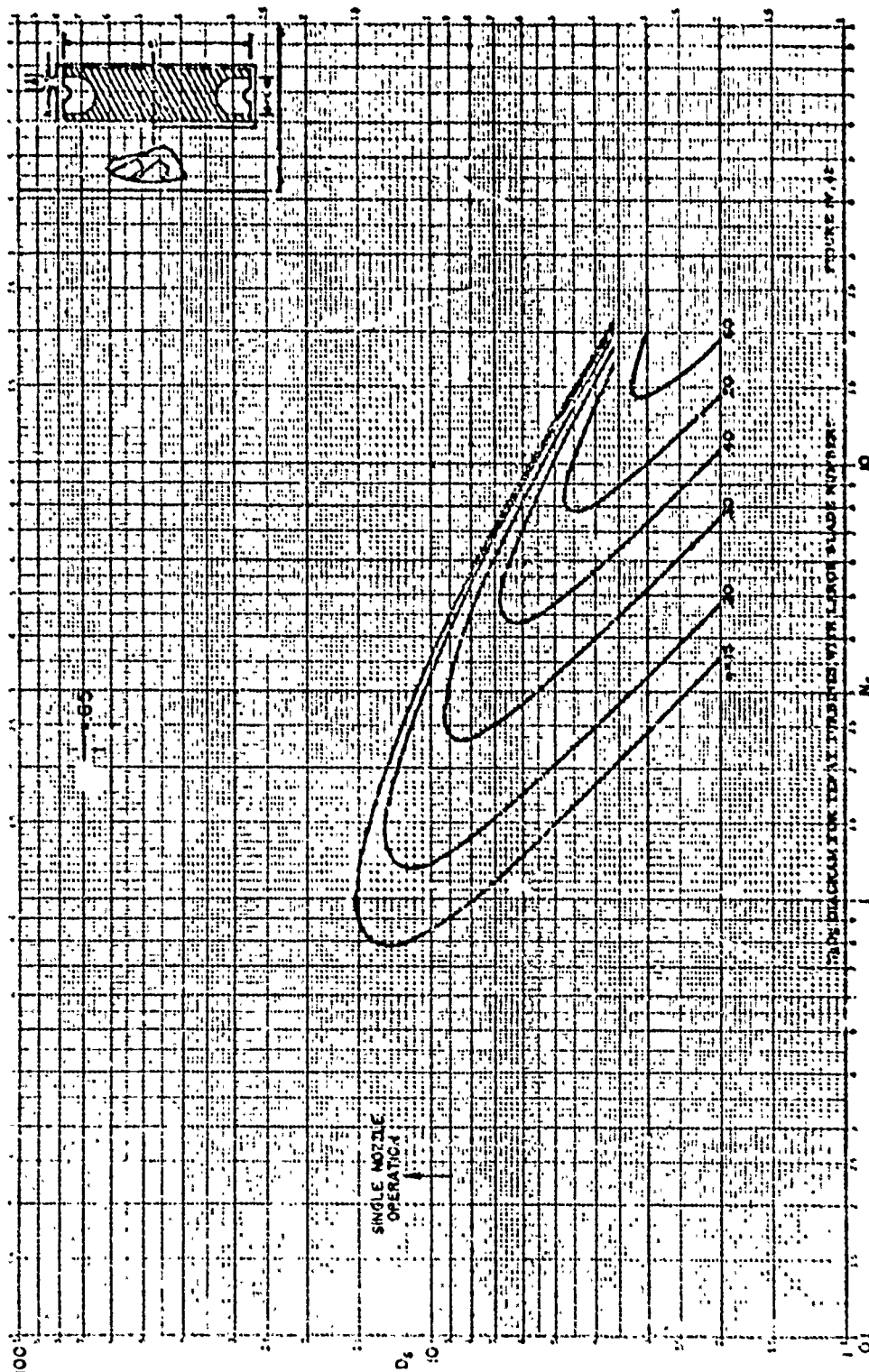
FIGURE IV.42

AMF/TD No. 1196
Job No. 7213

9 April 1958
Page 158
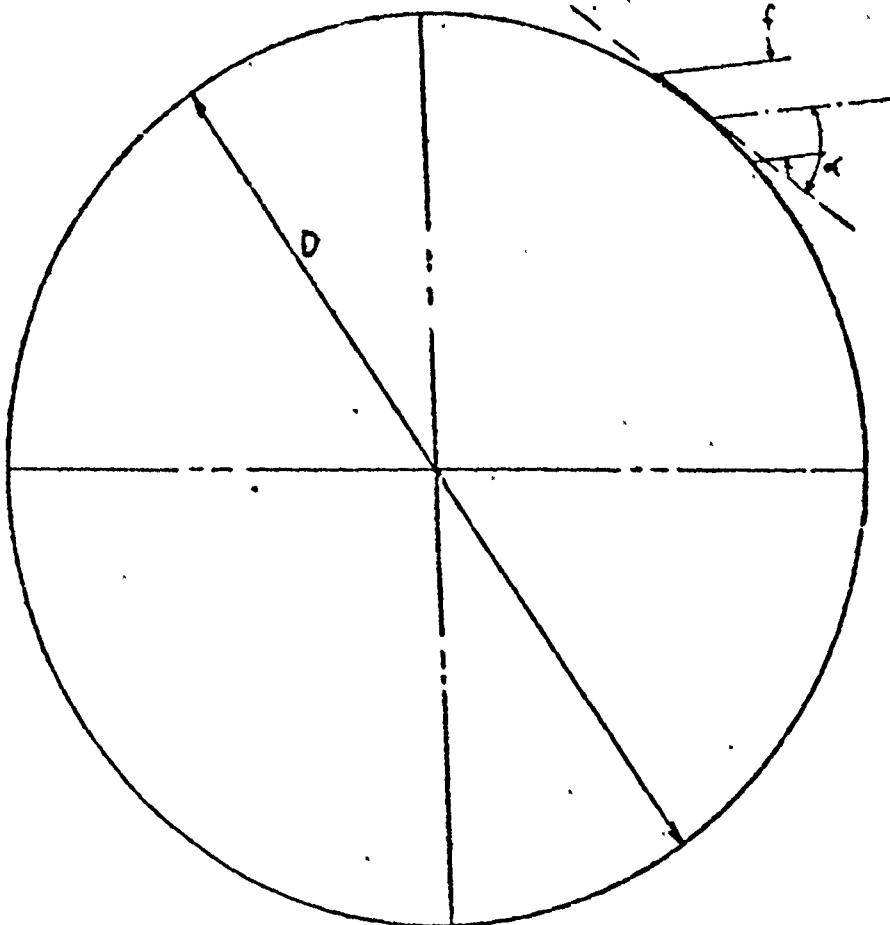
NOZZLE ARRANGEMENT IN TERRY TURBINES   FIGURE IV.43

MINIMUM NOZZLE ANGLE FOR SINGLE NOZZLE TERRY TURBINES.

FIGURE D.14

INFLUENCE OF DISTANCE BETWEEN NOZZLE AND ROTOR ON STALL TORQUE.

FIGURE IV-45

AMF/TD No. 1196
Job No. 7213
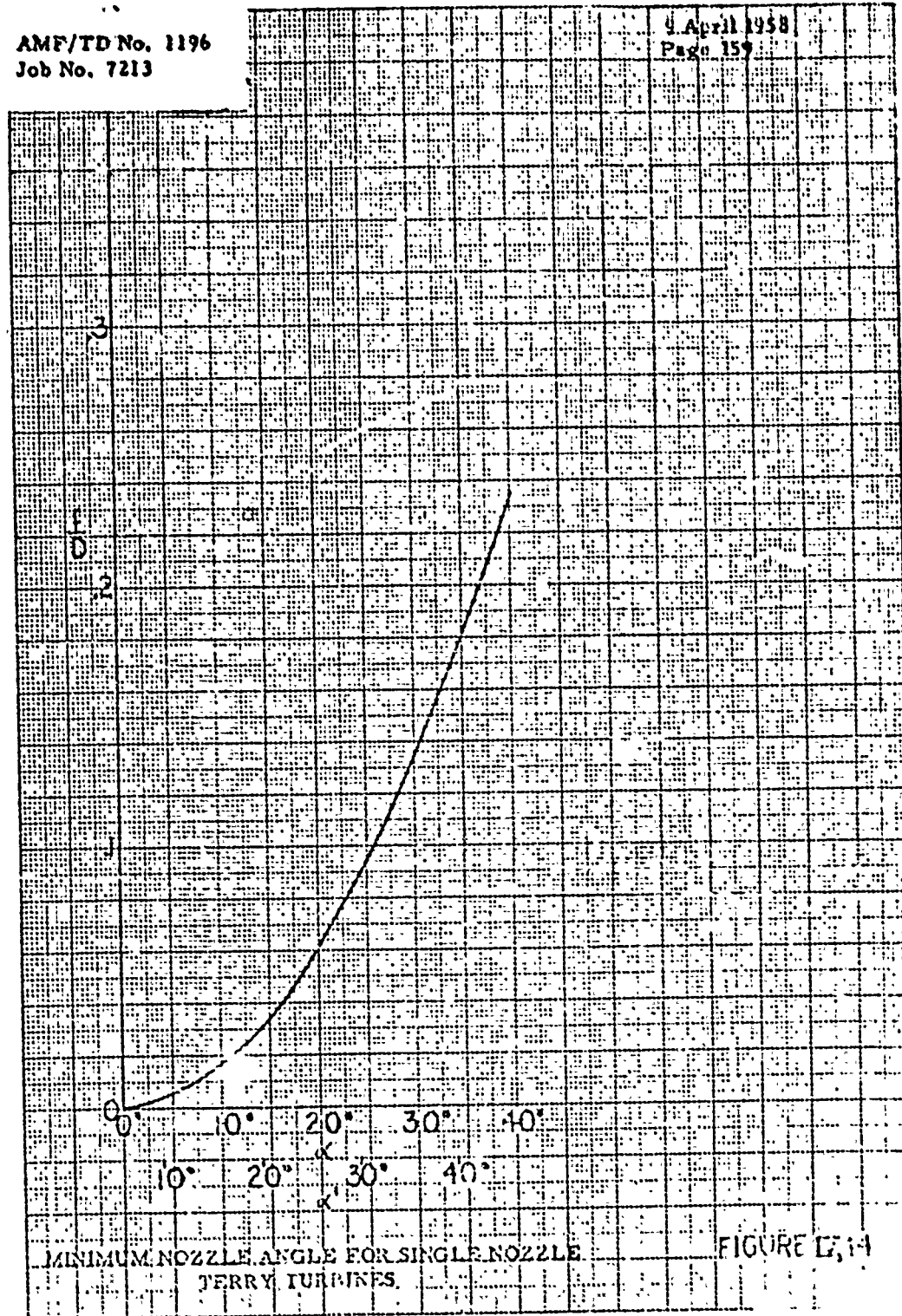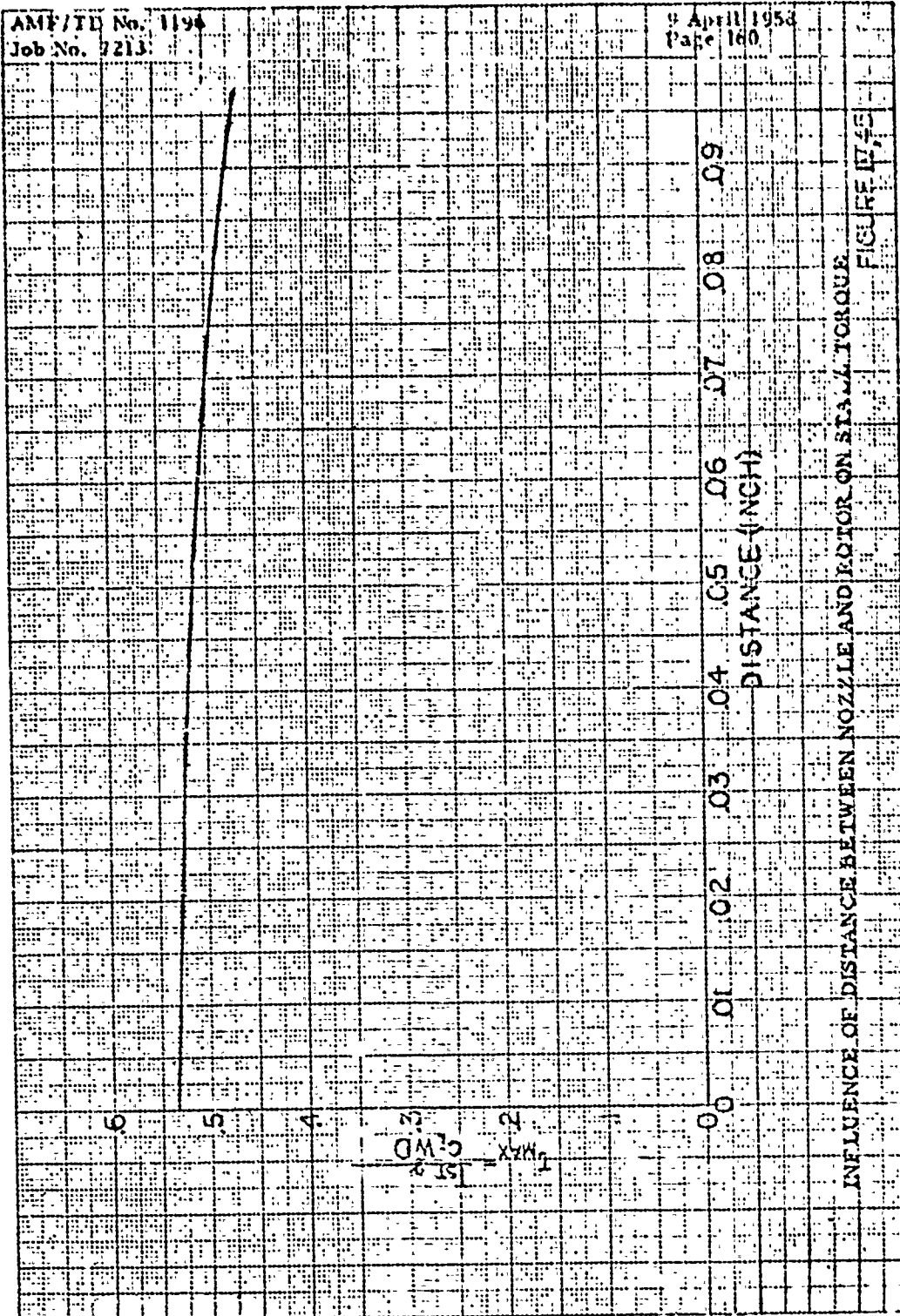
9 April 1958
Page 160

9 April 1958
Page 161

OPEN CHANNEL

SECTION A-A (ENLARGED)

ROTOR

SEAL

OUTLET

INLET

HOUSING

ROTOR

STREAMLINE
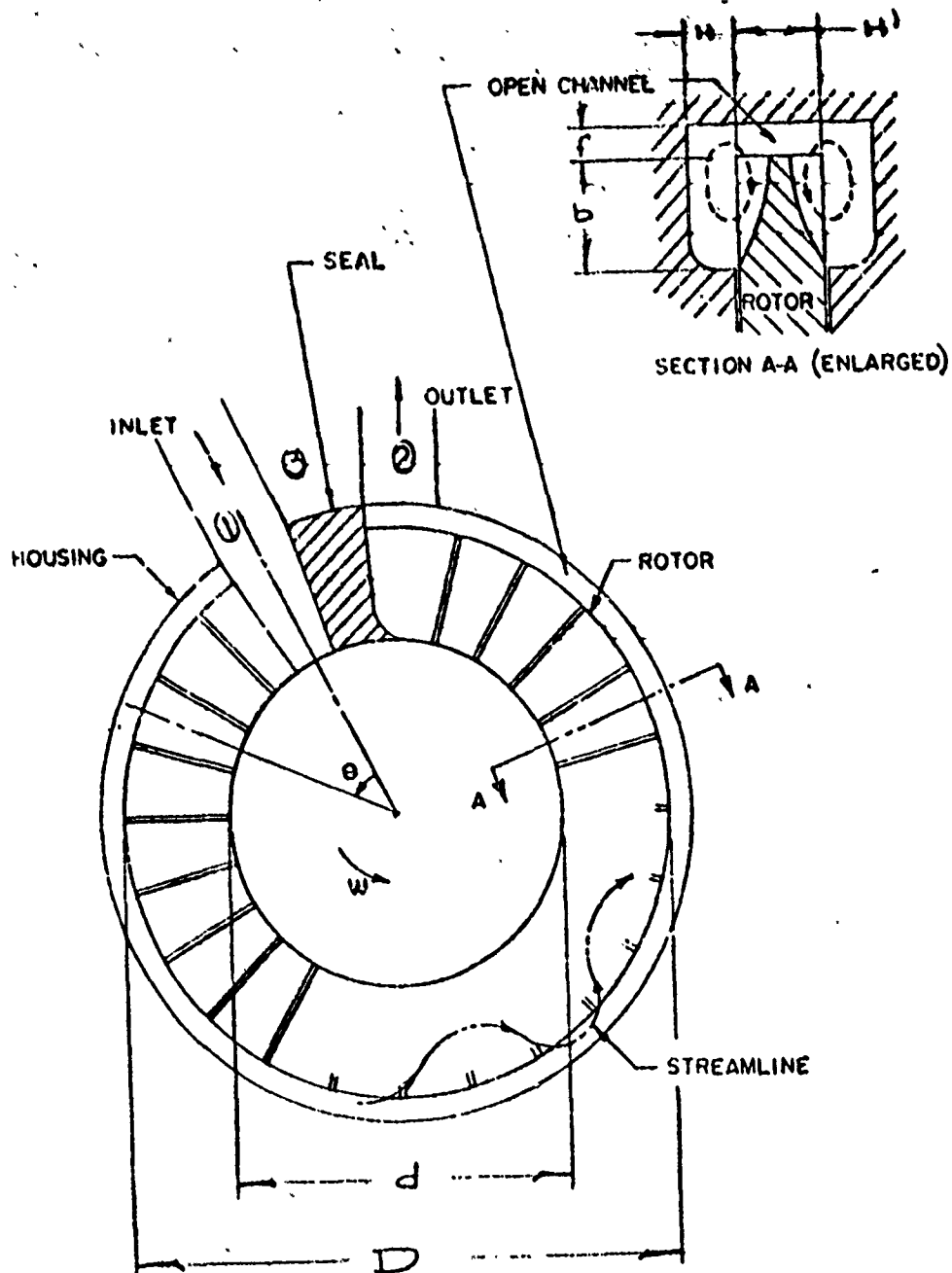
SCHEMATIC CROSS SECTION OF DRAG TURBINE   FIGURE VI.1
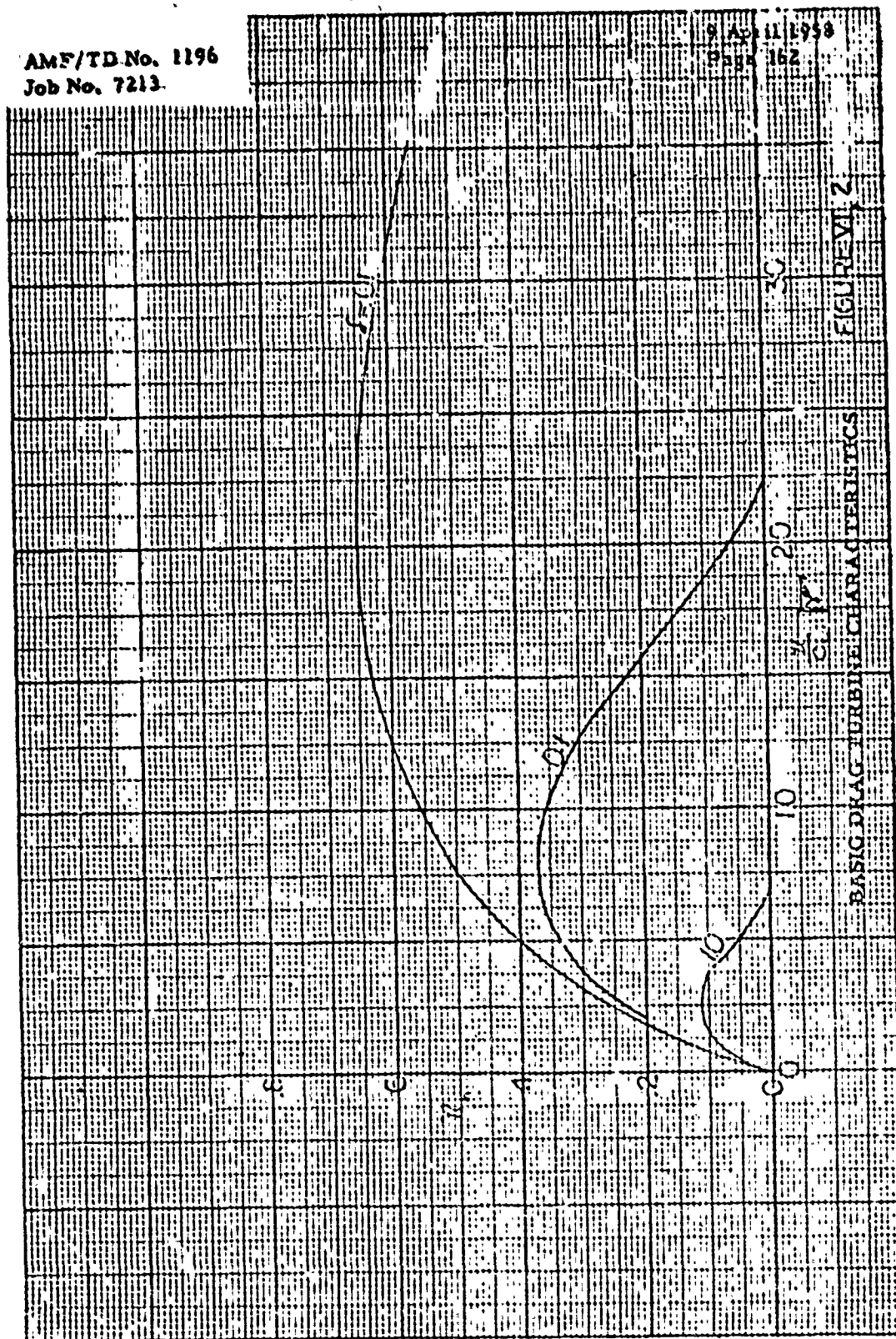
BASIC DRAG TURBINE CHARACTERISTICS

FIGURE VII-2
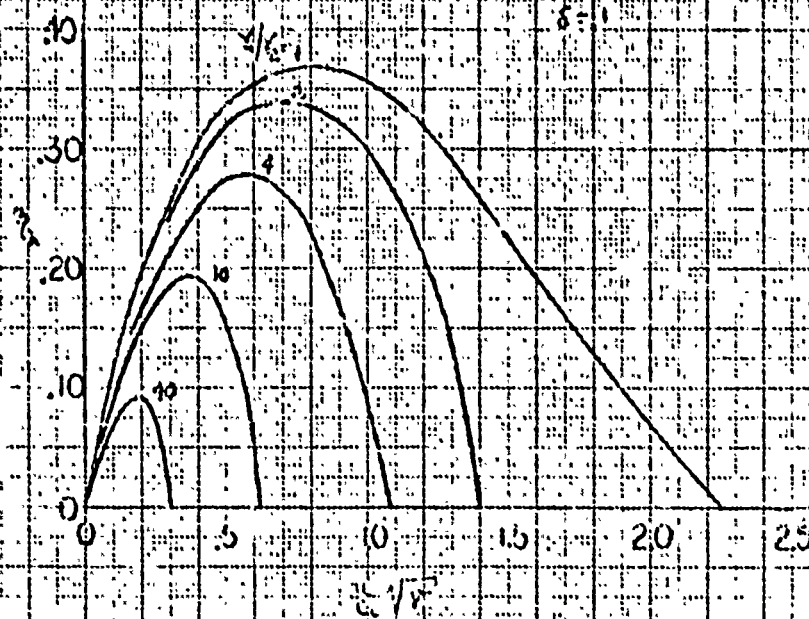
GENERAL DRAG TURBINE CHARACTERISTIC AS
A FUNCTION OF DENSITY RATIO (A = CONSTANT)   FIGURE VI.5

DRAG TURBINE CHARACTERISTICS FOR DIFFERENT CLEARANCES

FIGURE 21.4

$i=06$ $r=20$ $\lambda_w=06$ $h=.004$ INCH

DRAG TURBINE CHARACTERISTICS FOR
DIFFERENT CLEARANCES

FIGURE

$\delta = .08$ $n = 20$ $\lambda_w = .06$ $h = .015$ INCH

DRAG TURBINE CHARACTERISTICS FOR DIFFERENT CLEARANCES

FIGURE 1.14c

FIGURE VI 4d.

DRAG TURBINE CHARACTERISTICS FOR DIFFERENT CLEARANCES

CHANNEL NOTATIONS
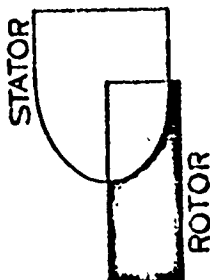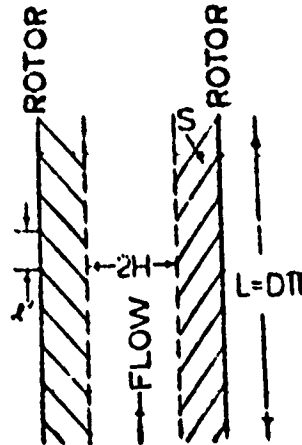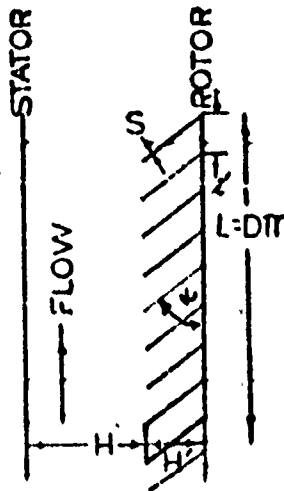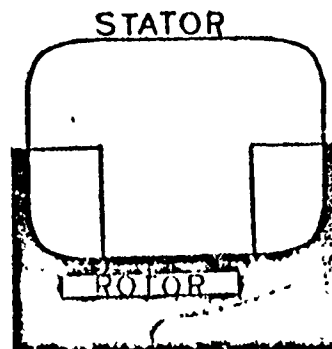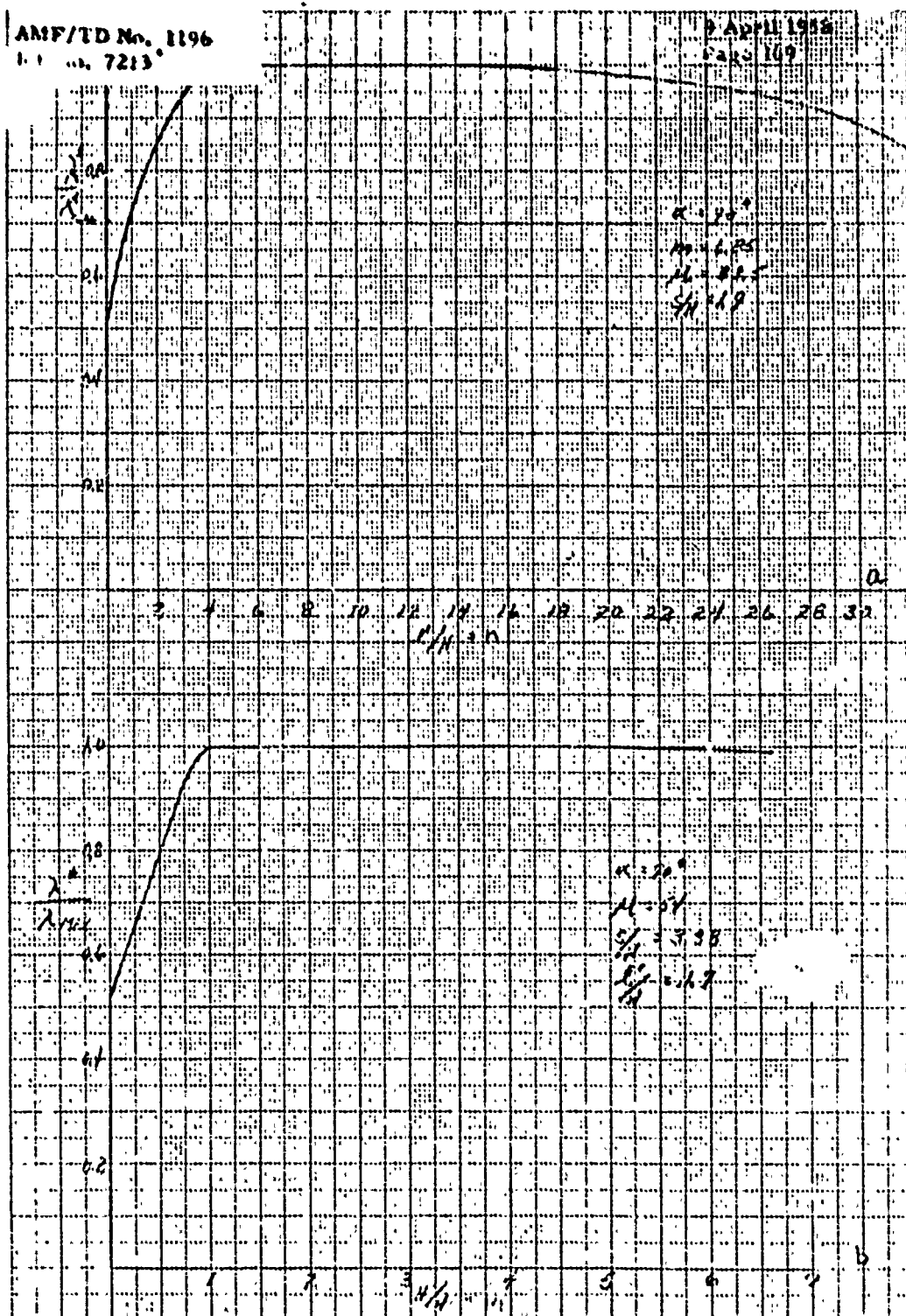
FIGURE VI.5

INFLUENCE OF BLADE SPACE AND
BLADE DEPTHS ON DRAG COEFFICIENT

FIGURE VI 6
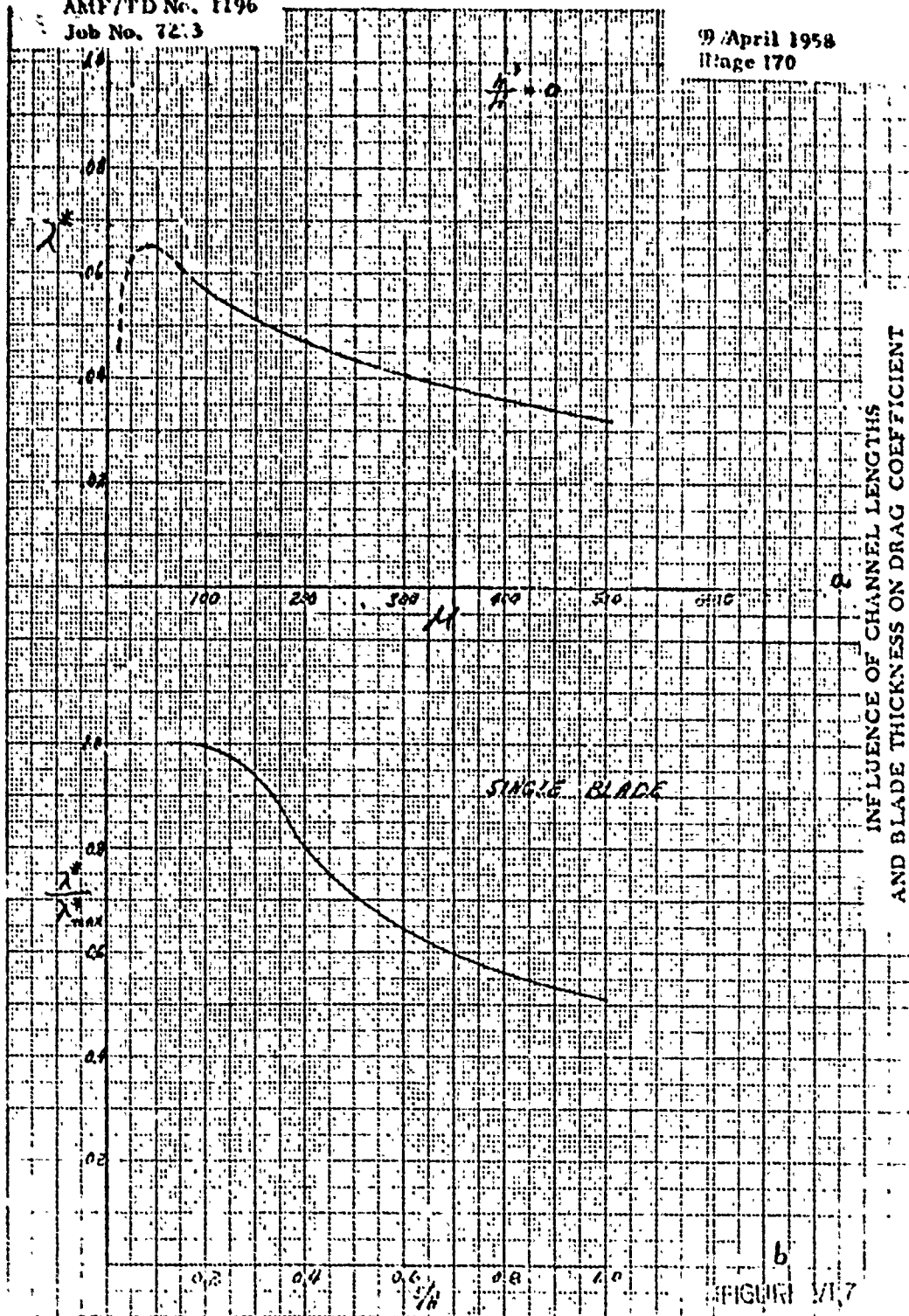
INFLUENCE OF CHANNEL LENGTHS
AND BLADE THICKNESS ON DRAG COEFFICIENT

FIGURE VI.7

INFLUENCE OF BLADE ANGLE ON DRAG COEFFICIENT   FIGURE 13
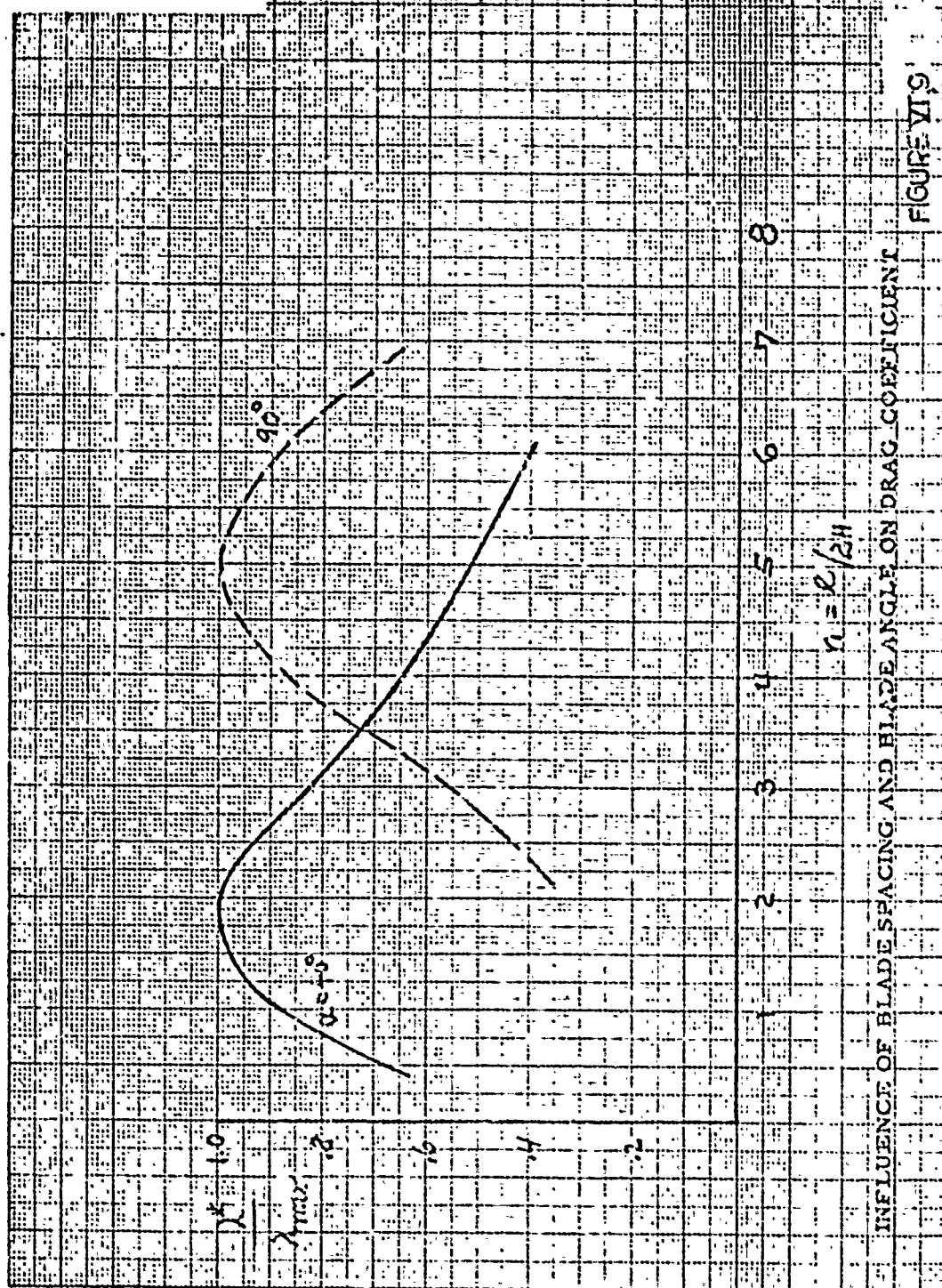
INFLUENCE OF BLADE SPACING AND BLADE ANGLE ON DRAG COEFFICIENT

FIGURE VI.9

u. April 1954
Page 173

Dimensionless β vs constants

$K = 5.17$

$M = 2.8$

$K = h/r$

$K = m$

FIGURE VI-10

INCIDENCE OF TYP. CHAIN. NO. BY k_yb D1 A4 CO·FD· CIENT

9 April 1956
Page 74

FIGURE VI.II

MAXIMUM DRAG COEFFICIENT AS A FUNCTION
OF THE RATIO ROTOR DIAMETER TO CHANNEL DEPTH

AMF/TD No. 1196
Job No. 7213

λ_{dr}
IDEAL

ALL VALUES FOR OPTIMUM n, ro AND f VALUES

Best Available Copy

NS DS DIAGRAM FOR DRAG TUP SIZES FOR LARGE PRESSURE RATIOS
AND CONSTANT CHANNEL GEOMETRY

SECTION A-A

FIGURE XI 15

OUTLET

SEAL

INLET

INLET

OUTLET

ROTOR

SEAL

ROTOR

SECTION B-B

A

A

SHROUD

INLET

SEAL

OUTLET

VIEW CC
(HOUSING OMITTED)

B

C

OUTLET

INLET

C

B

HOUSING
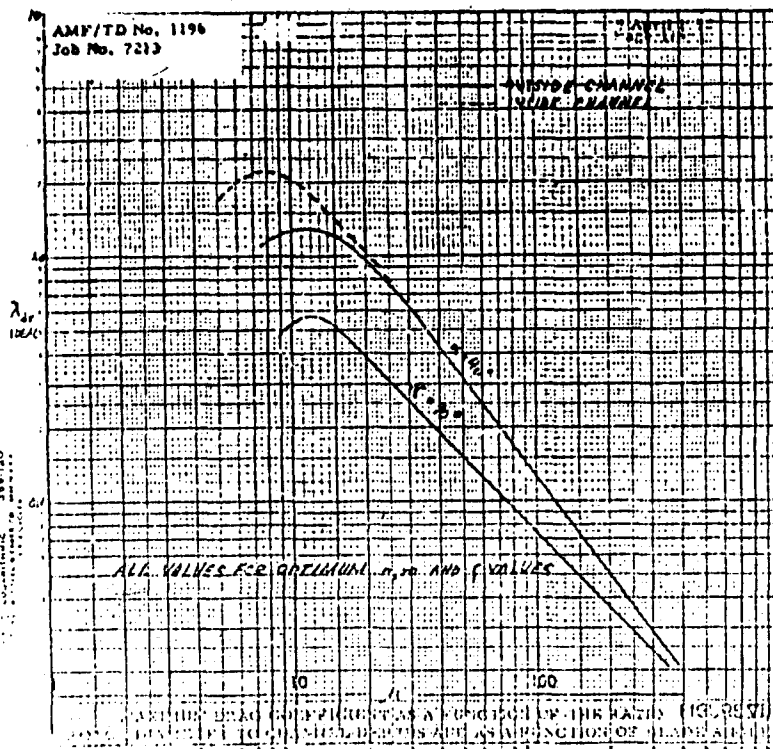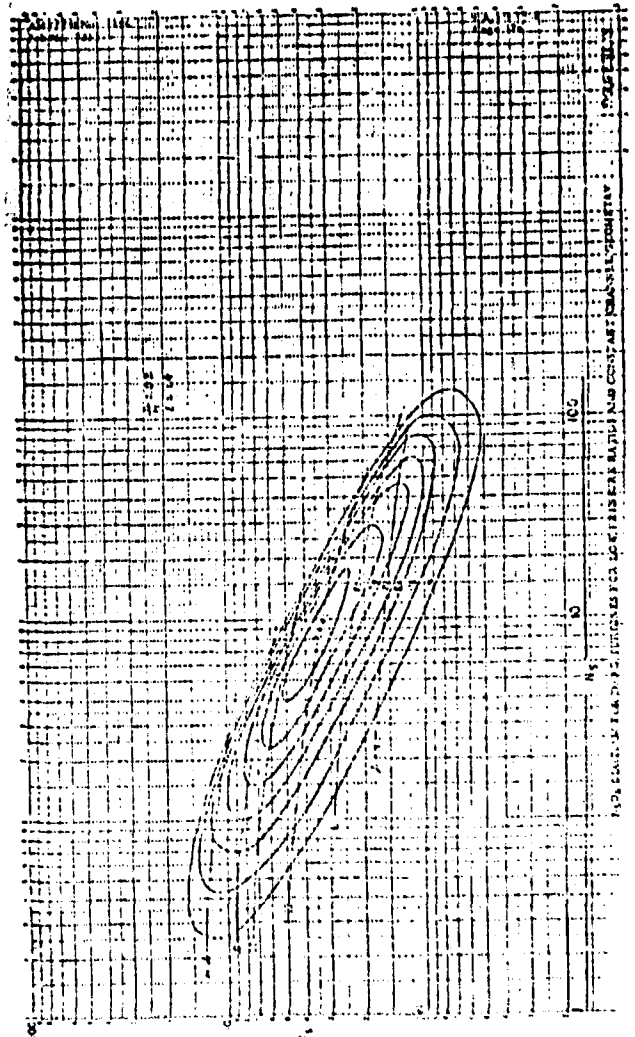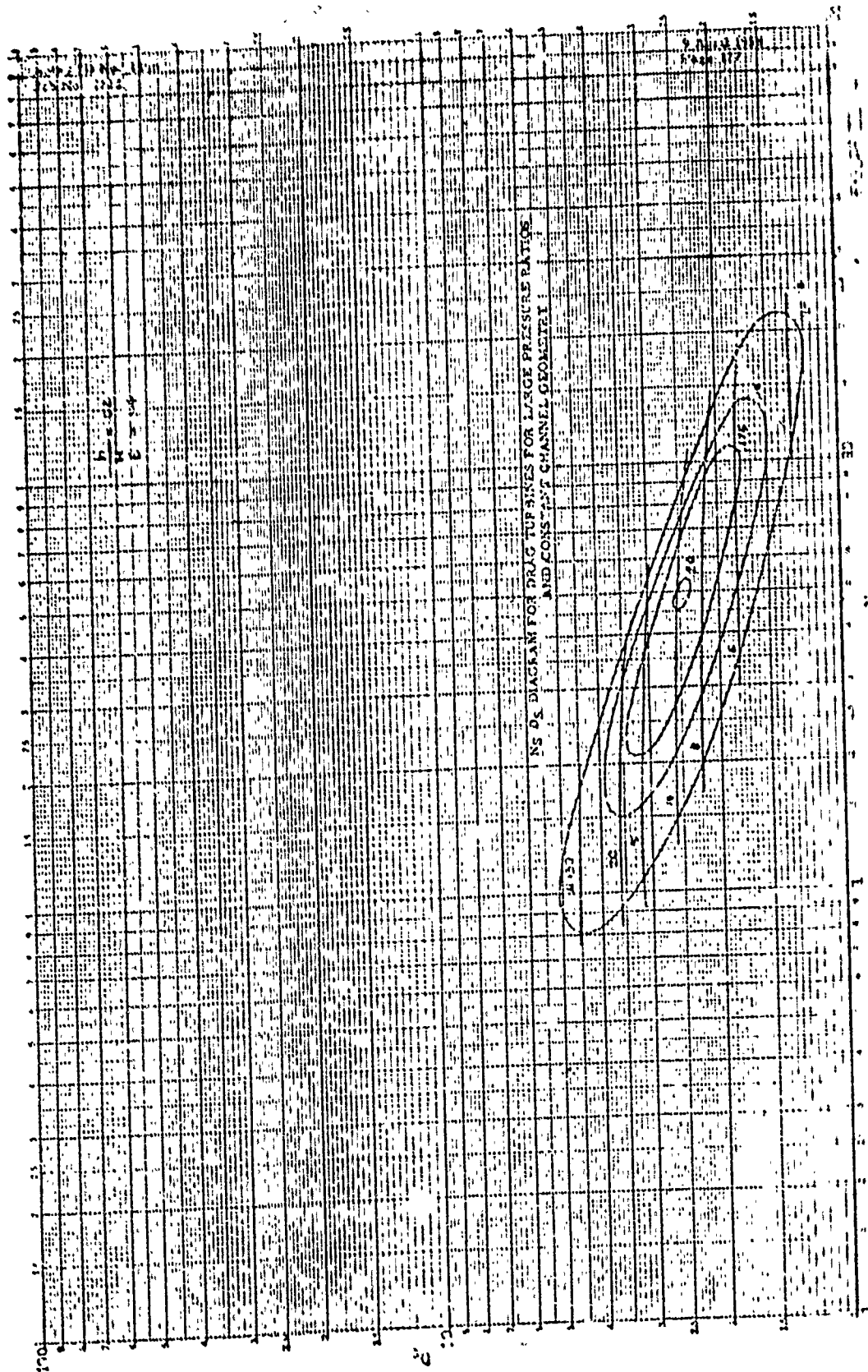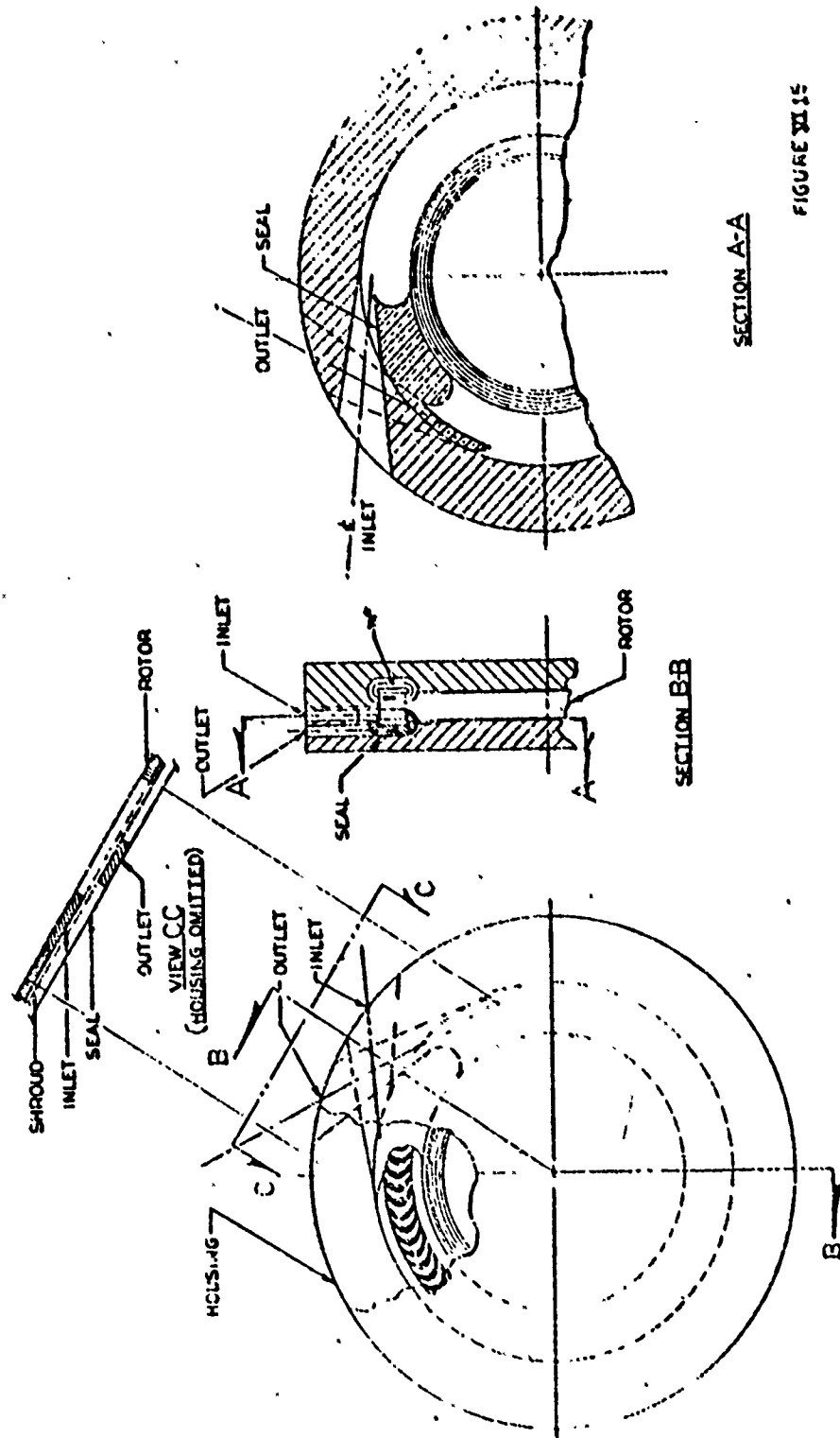
DRAG TURBINE DESIGN
FROM DYNAMIC CONSIDERATIONS
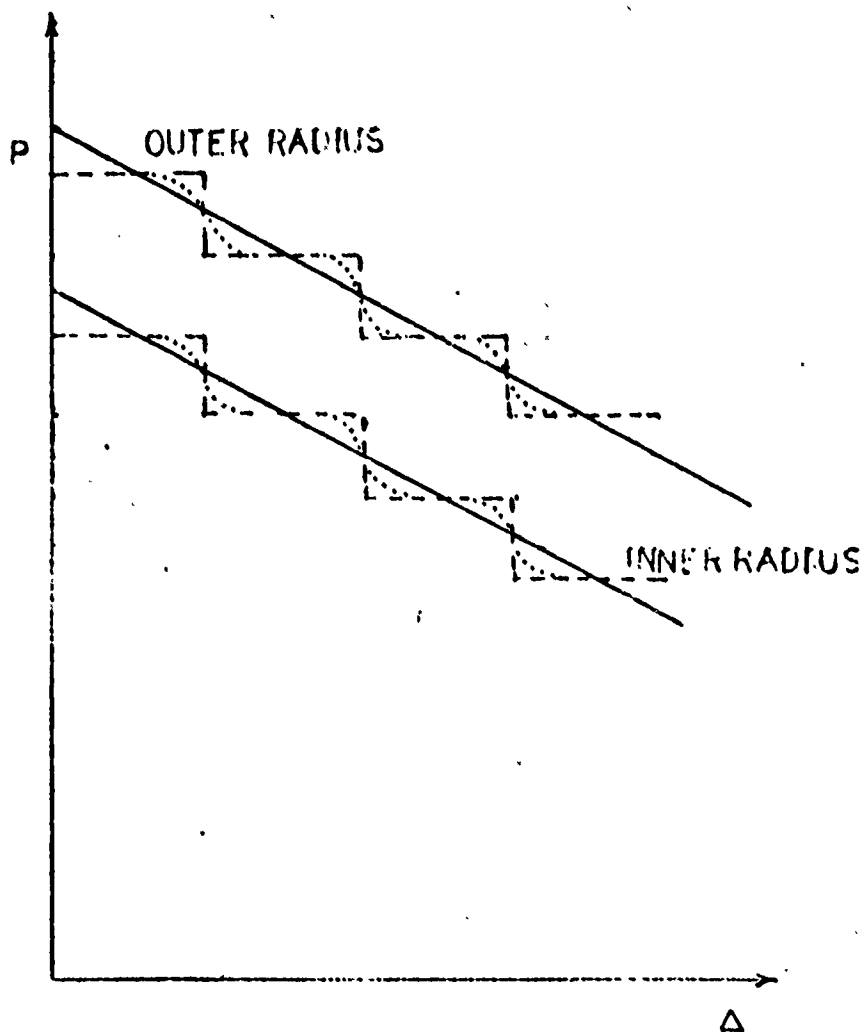
EXPECTED PRESSURE DISTRIBUTION IN DRAG   FIGURE VI.15a
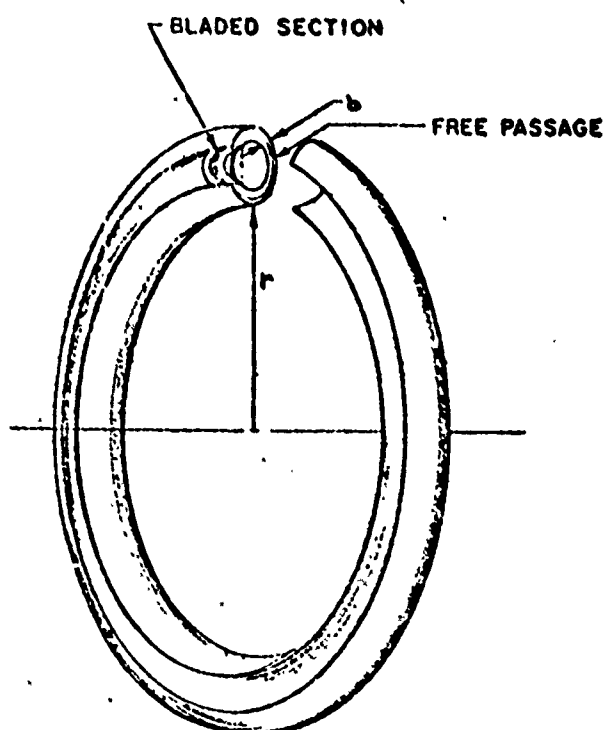TURBINE DESIGNS ACCORDING TO THE DYNAMIC FLOW CONSIDERATION

CALCULATED MAXIMUM EFFICIENCIES FOR DRAG TURBINES
DESIGNED FOR THE DYNAMIC FLOW THEORY
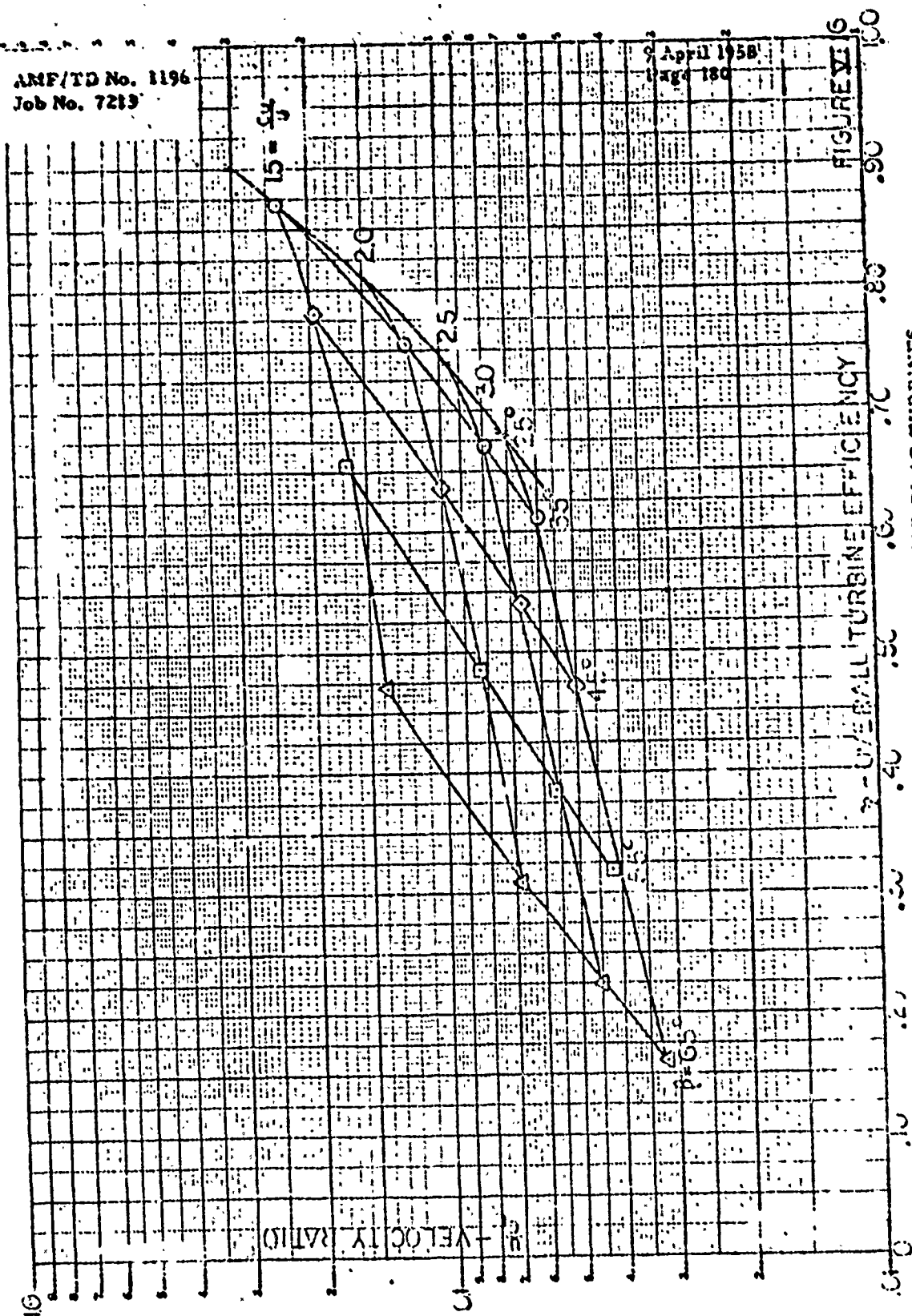
FIGURE VI

AMF/TD No. 1196
Job No. 7213

April 1958
Page 180

SCHEMATIC DRAWING OF DRAG TURBINE
FLOW PASSAGE

FIGURE VI 17